MATERIAL AND DESIGN CONSIDERATIONS FOR A PORTABLE ULTRA-VIOLET (UV) LIGHT EMITTING DIODE (LED) WATER PURIFICATION DEVICE

THESIS

Drew D. Gallucci, Captain, USAF

AFIT-ENV-MS-16-M-152

DEPARTMENT OF THE AIR FORCE
AIR UNIVERSITY

AIR FORCE INSTITUTE OF TECHNOLOGY

Wright-Patterson Air Force Base, Ohio

The views expressed in this thesis are those of the author and do not reflect the official policy or position of the United States Air Force, Department of Defense, or the United States Government. This material is declared a work of the U.S. Government and is not subject to copyright protection in the United States.

AFIT-ENV-16-M-152

MATERIAL AND DESIGN CONSIDERATIONS FOR A PORTABLE ULTRA-VIOLET (UV) LIGHT EMITTING DIODE (LED) WATER PURIFICATION DEVICE

THESIS

Presented to the Faculty

Department of Engineering and Management

Graduate School of Engineering and Management

Air Force Institute of Technology

Air University

Air Education and Training Command

In Partial Fulfillment of the Requirements for the

Degree of Master of Science in Engineering Management

Drew D. Gallucci, BS

Captain, USAF

March 2016

DISTRIBUTION STATEMENT A.
APPROVED FOR PUBLIC RELEASE; DISTRIBUTION UNLIMITED.

iii

AFIT-EN**V**-16-M-**152**

MATERIAL AND DESIGN CONSIDERATIONS FOR A PORTABLE ULTRA-
VIOLET (UV) LIGHT EMITTING DIODE (LED) WATER PURIFICATION DEVICE

Drew D. Gallucci, BS
Captain, USAF

Committee Membership:

Dr. Michael E. Miller, PhD
Chair

Dr. Alfred E. Thal Jr., PhD
Member

Dr. Willie F. Harper Jr., PhD, P.E.
Member

AFIT-ENV-16-M-152

Abstract

Department of Defense personnel often deploy to austere environments where clean water is not readily available. Ultraviolet (UV) radiation through the use of light emitting diodes (LEDs) in a portable device offers a potential method for expedient water treatment. This research studied the application of one diode, low power, UV LEDs and nine diode, high power, UV LEDs within a portable steel reactor and Teflon reactors of three different wall thicknesses. Reactor efficiency was determined through measuring and comparing the rate constants for Advanced Oxidation of hydrogen peroxide with yellow tartrazine as a witness dye. Experiments conducted with low power UV LEDs indicate that the medium thickness reactor has a statistically significant higher rate constant than the steel and thin cylinder reactors. All high power UV LED tests had rate constants ten times higher than the low UV LEDs, but exhibited no significant difference between materials or thicknesses. Additionally, this research examined the microorganism inactivation in the optimum reactor by exposing E. coli to UV radiation. The experiments demonstrated complete reduction of E. coli at a flow rate up to 15 mL/min, and a 2-Log reduction at 20 mL/min, thus demonstrating proof of concept for future portable UV LED disinfection units.

Table of Contents

List of Figures

List of Tables

MATERIAL AND DESIGN CONSIDERATIONS FOR A PORTABLE ULTRA-VIOLET (UV)
LIGHT EMITTING DIODE (LED) WATER PURIFICATION DEVICE

I. Introduction

General Issue

The United States Air Force (USAF) often deploys personnel to remote locations where

clean water may not be available. In those contingency environments, USAF civil engineers use

reverse osmosis water purification units (ROWPUs) to produce drinking water. ROWPUs are

transportable, but relatively large systems that require heavy equipment to position (AFH 10-

222, Vol 9 2011). They are designed to provide 1500 gallons of water per hour to multiple

people and require 35 kilowatts of power (AFH 10-222, Vol 2, 2012). However, there are

situations where USAF and other Department of Defense (DoD) personnel may encounter

emergency situations where the ROWPU may not be available or practical. Point-of-use

ultraviolet treatment (UV) is a method that could be implemented in those situations.

UV disinfection has been used to treat water since the 1800s (EPA, 2006). UV radiation

can inactivate bacteria and viruses by damaging their DNA, thus eliminating their ability to

reproduce (EPA, 2006). The traditional UV disinfection method uses mercury-vapor filled

fluorescent bulbs to produce UV radiation. These bulbs require a significant warm up time, are

inefficient, have short lifespans, and contain the toxic heavy metal, mercury. However, the last

few decades have seen a drastic advancement in light emitting diode (LED) technology. These

developments have included UV LED innovation within the last 15 years (Muramoto, Kimura, &

Nouda, 2014). Recent improvements to UV LED manufacturing have made it possible to mass-

produce them, thus enabling possibilities for cost effective and portable water treatment

applications (LG Innotek, 2015). A portable, point of use, UV water treatment system that can

treat any water source is of interest to the United States Air Force if it can be incorporated into an aircraft crash kit or used in other emergency situations. This research investigates the development of such a system to further the knowledge of the practicality of portable UV LED water treatment systems.

Problem Statement

Clean water is a necessity in emergency situations. USAF personnel in those situations may need to be constantly mobile, so portable methods for water disinfection are required. Portability considerations are weight, power, mechanical robustness and disinfection capability. UV LEDs were chosen because they have low (especially voltage) power requirements, are lightweight, and are more durable than compact fluorescent bulbs. However, the optimum material or design for a portable UV LED disinfection unit has not been determined. Material selection and thickness affects the weight of the unit, and certain materials reflect UV rays better than others. Therefore, reactor composition affects the performance and power efficiency of the reactor.

One such material, Polytetrafluoroethylene (PTFE), or Teflon, reflects UV radiation very well and may be suitable for the unit's construction (Ryer, 2000). PTFE also reflects light differently at different thicknesses, but dramatically increases in weight as thickness increases (Weidner and Hsia, 1981). There is little research on the use of UV LEDs in a small portable Teflon container for water disinfection purposes. This thesis seeks to research different possible configurations of portable UV water disinfection units and the factors that influence the efficiency of a small reactor.

Research Objective

The objective of this research is to examine the advance oxidation process (AOP) and

germicidal effectiveness of UV LED water reactors composed of varying materials to determine useful-characteristics of a portable water purification device.

Research Focus

The research focus for this thesis is measuring the germicidal effectiveness for different configurations of disinfection reactors that use small volumes of water. The intent is to apply the research to the development of a portable UV water treatment device capable of providing clean water to a single user.

Investigative Questions

This thesis investigates the following questions:

1) Will a Teflon, continuous flow, UV LED reactor be more effective in enabling an advance oxidation process (AOP) than a steel reactor of the same dimensions?

2) Does material wall thickness affect the efficiency of Teflon reactors?

3) Does the entry angle for water in the Teflon reactor affect mixing in a reactor?

4) Does the entry angle for water affect the efficiency of the portable reactor?

5) Can a continuous flow, portable, Teflon reactor disinfect water to EPA drinking water standards?

Methodology

The research methodology used in this thesis was modeling and experimentation. The first experimental set consisted of measuring the advanced oxidation process AOP, within Teflon reactors of different thicknesses and comparing it to a modified version of a steel reactor used in previous AFIT research. AOP was chosen as a way to measure reactor efficiency with regards to UV reflectivity. The research was divided into two sets of 24 experiments that tested the AOP of

high and low power UV LEDs. Tartrazine was used as a witness dye, responding to the creation of hydroxyl radicals formed from exposing hydrogen peroxide to UV radiation within the reactor vessel.

The low powered UV LEDs produced noisy AOP curves; so modeling was used to provide insight into mixing conditions within the reactor. Modeling in this thesis utilized the computational program COMSOL® multiphysics to understand the fluid characteristics of the reactors. The program generated water-flow velocity streamline plots that simulated the path of fluid particles from inlet to outlet through the reactors.

The second set of experiments measured the microbial inactivation ability of the most effective reactor determined from the first set of experiments. Two nine diode LEDs were used as the UV source. The microorganism measured was E. coli (ATCC 11229). To determine the inactivation ability, solutions containing the microorganism were pumped through the reactor and then placed on a culture plate. A colony count was performed after 24 hours.

Assumptions/Limitations

The experimentation was limited to three designed Teflon thicknesses. For the test with the steel reactor, the Teflon caps that were used for the thinnest walled Teflon reactor were used due to the unavailability of steel caps of the same design. Materials were also limited. Only one pair of high power UV LEDs were used for both the AOP and microbial inactivation experiments. The LEDs may have lost their optimal power output over the hours used in the AOP experiments, so they may not have been as powerful against the E. Coli as they could have been. Additionally, only one LED angle was used for each experiment, so the effect that Teflon has on UV reflectance within a small vessel was not fully investigated.

Implications

Teflon can reflect UV radiation more effectively than steel and aluminum, but it is a heavy material. If UV LED water reactors composed of thinner walled Teflon is able to treat water as well or better than the thicker material, it has potential to be used as a portable water purification device in field operations. If this research is successful, the DoD will benefit from a novel method of water purification that is portable and highly effective at disinfecting water.

Preview

Chapter II will discuss the available literature on the history of UV water disinfection, UV LED development, other methods of water treatment, and related Air Force Institute of Technology research. Chapter III will describe the methodology of this thesis experimentation and COMSOL® modeling. Chapter IV will report and analyze the results of the modeling and experimentation. Chapter V will state the conclusions of this study and identify potential future research.

II. Literature Review

The purpose of this chapter is to review the history of ultraviolet water treatment, the recent developments in UV LED technology, other methods of portable water treatment, and related Air Force Institute of Technology research.

History of Ultraviolet Water Treatment

Ultraviolet disinfection is a well-established form of water treatment. In 1877, Downs and Blunt (1877) discovered that sunlight exposure inhibited bacterial growth in their water samples. UV research progressed in 1901 when Peter Cooper Hewitt created the mercury vapor lamp. It was the first artificial UV light source when the lamp was coupled with a quartz sleeve (Linden, 1998). A few years later, a UV system was successfully applied to drinking water treatment in Marseille, France in 1910 (Lorch 1987). That same year, chlorine gas was discovered to disinfect water just as well as UV, but proved to be less expensive. As a result, UV water treatment was abandoned for the next few decades (Whitby and Scheible, 2004). Widespread use of UV water treatment was limited by the difficulty of creating the lamps. This problem was alleviated when the Westinghouse Company initiated the first mass production of low-pressure mercury UV lamps in 1938 (Whitby and Scheible, 2004). The first instance of commercial UV water treatment was in 1950, and it occurred in Switzerland and Austria (Percival, Yates, Williams, Chalmers, & Gray, 2013). Later in that same decade, the United States adopted UV water treatment in conjunction with a filtration and chlorine process, and it is in wide use today (Pontius, 2003). This series of unit operations was chosen because filtration reduces turbidity and materials that reduce the effectiveness of chlorine and UV treatment. Chlorination eliminates most bacteria and viruses, as well as provides a barrier to regrowth, and UV treatment effectively kills bacteria that are resistant to chlorine; this combination provides a

6

more thorough treatment down to viral inactivation than any of the processes can perform independently.

UV LED development

The basic composition of an LED is a semiconductor chip with a cathodic and anionic junction. Holonyak (1962) first developed traditional visible light emitting diodes while working at General Electric. They were composed of gallium, arsenic, and phosphorus, and emitted red light (Holonyak and Bevacqua, 1962). The next generation of LEDs was invented in the 1970s and emitted orange, yellow, and green light (Kovac, Peternai, Lengyel, 2003). Finally, Nakamura created a blue LED made from Lanthanum Gallium Nitride in the 1990s (Nakamura, Mukai, & Senoh, 1994), a feat that was recently acknowledged through the award of a Nobel Prize in 2015.

Alongside visible light LED development, ultraviolet LEDs were researched. At nearly the same time as the development of high energy blue LEDs, the first UV LEDs were created in 1992 (Schubert, 2005). Commercial UV LEDs took another 8 years to develop (Muramoto, Kimura, & Nouda, 2014). Visible light LEDs today are much brighter, mass-produced, and inexpensive as compared to their predecessors. They have followed a trend known as "Haitz law," which states that "every 10 years the amount of light generated by an LED increases by a factor of 20, while the cost per lumen falls by a factor of 10" ("Haitz's law," 2007). That same trend may occur for the UV LED market. LEDs that were once grown and handmade in the laboratory will soon be mass-produced, which will lead to dramatic decreases in price per unit.

Current Methods of Water Treatment

There are many methods to disinfect water. Some are more suitable for mass distribution and others for point of use. This section will review each of the methods and discuss its usefulness to a portable, point of use application.

The method of water treatment for this thesis is ultraviolet disinfection. UV is effective at inactivating vegetative and resistant bacteria (Morita et al., 2002). One of the four types of UV radiation, UV-C, encompasses germicidal wavelengths that exist from 100-280nm, and most low-pressure mercury lamps emit UV radiation at 254nm (EPA, 2006). Fortunately, LED output is not restricted to one wavelength. There are different diodes on the market that can produce UV in the 240-400 nm range. UV disinfection does not create harmful by-products as is common in chemical treatment using chlorine, but it has difficulty treating turbid water as particulates within the water will absorb the UV energy, thereby reducing the dose imparted to organisms within the water.

One company has already incorporated UV treatment into a portable point of use application. CamelBak® created a florescent UV treatment system which applies a compact UV fluorescent bulb positioned in the cap of a plastic container for disinfection (CamelBak, 2010). This apparatus requires approximately one minute to treat the volume of the container if the container is mixed properly and does not contain turbid water. This device with its container is bulky and contains a mercury UV bulb. UV LEDs could be incorporated in place of the mercury bulb, but other designs, such as the reactor device used in this thesis placed in line with a hydration pack, might prove to be more useful for emergency situations where weight and convenience are desired.

The longest established method of water treatment is boiling. Boiling water eliminates nearly all waterborne pathogens, but does little to treat chemical contamination (NY DOH, 2011). Boiling water requires an ignition source, combustible fuel, takes several minutes to reach 100˚C, and then up to 30 minutes to completely disinfect water (WHO, 2011). For military application, boiling water is an effective last resort method for water treatment. Boiling

is not advantageous in a expeditionary environment where fire is required and can reveal the location of an individual seeking to evade detection.

The most prevalent form of water treatment in developed countries is chlorine disinfection. Most drinking water and wastewater treatment plants integrate chlorine into their mass quantity disinfection process. It takes 1ppm of free chlorine at a pH of 7.5 and 25° C, approximately 1 minute to treat E. coli, but up to ten days to treat cryptosporidium (CDC, 2010). Chlorine also has the benefit of staying in water for days, thus providing residual treatment against microorganisms. According to the DoD, chlorine is the preferred bulk field water disinfectant, with calcium hypochlorite as its main chemical source (TB MED 577, 2010). Chlorine treatment has disadvantages. As noted earlier, chlorine is ineffective at killing cryptosporidium. Additionally, it can create hazardous by-products such as hypochlorous and hypobromous acid, which react with organic matter to cause more by-products, most notably chloroform, bromodichloromethane, dibromochloromethane, and bromoform (Rook, 1974). Those four by-products may cause long-term health problems from extended exposure (CDC, 2014). In military applications where a ROWPU is used, chlorine will damage the reverse osmosis membrane, so it can only be used after the reverse osmosis process (TB MED 577, 2010).

Another well-established disinfection method is iodine treatment. Iodine can easily be carried in the form of tablets. This technology is relatively cheap as well, with most bottles of 100 tablets priced around $10. Though it is effective at inactivating most bacteria and viruses, iodine has some drawbacks. First, iodine is not a good disinfectant against Legionella bacteria under certain conditions (Cargill et al., 1992). Next, iodine is temperature sensitive, so varying treatment times must be considered (Block, 2001). Also, iodine must be used in a dark container,

so for expedient situations, such a container must be carried. Additionally, there are consumption limits to iodine, and excessive iodine may cause goiter or other thyroid issues (Teng et al., 2006). Furthermore, some people are allergic to iodine, so they cannot use it as a water treatment method (Curtis, 1998). Although the allergy is rare, it is an elimination factor for a universal water treatment device. Finally, iodine-treated water does not taste good, which is not as much of a concern in emergency situations, but should still be a consideration when there are more pleasant tasting treatment methods.

Slow sand filtration is another form of water treatment that has existed for over 100 years. A typical filter consists of a container, a lid, diffuser plate, fine sand, course sand, gravel, and an outlet pipe (CAWST, 2012). Slow sand filtration has the advantage of no energy use and a relatively fast flow rate, approximately 0.6L/min (CDC, 2014). It is also made from easily attainable materials that filter nearly all bacteria and protozoa. Slow sand filtration's disadvantages are that it only eliminates a small number of viruses, and its materials are heavy, thus reducing its portability (CDC, 2014). Slow sand filtration would be a good alternative in an emergency environment if the individual can stay in one location for several days at a time.

Two widely applied commercial water treatment systems available today are granulated activated powder (GAC) and powdered activated carbon (PAC) systems. GAC is composed of pulverized carbon that has been ground into small porous granules. PAC is generally made from lower cost materials that make it less dense than GAC (Tuncel et al., 2015). The pores for both methods are capable of adsorbing soluble organic particles onto the granule (EPA, 2015). GAC and PAC systems filter natural organic compounds, some microorganisms, and are mostly used to improve the taste of water. The activated carbon systems cannot filter dissolved metals and can develop microbial growth after prolonged use (EPA 2015). Activated carbon filtration is not

a good stand-alone method for water treatment, but it may work well in combination with UV treatment. The carbon can reduce water turbidity, which will increase the effectiveness of UV disinfection.

Reverse osmosis water treatment eliminates nearly all of microorganisms in water. A reverse osmosis filter has 0.0001-micron pore size, which is effective in removing all pathogens, including smaller viruses (CDC, 2012). It works so well that it strips the water of electrolytes. While these electrolytes can be replaced in large installations through remineralization, this process is not convenient in emergency situations. As discussed before, the DoD incorporates ROWPUs into expeditionary locations, but they are large machines and not suitable for emergency point of use applications. There are portable reverse osmosis systems on the market, but they are relatively bulky, with the average system taking up about as much room as a car battery.

In 2005, the Vestergaard company developed a promising new form of water treatment, the Lifestraw®. It is a portable, 9"x1" device that can filter water to 0.2 microns (Vestergaard, 2014). At that level, it is able to remove most microorganisms, including cryptosporidium, which as noted earlier, chlorine is ineffective against. However, the Lifestraw® cannot eliminate viruses from water. A useful water treatment system might combine the filtration capabilities of the Lifestraw® with the viral disinfection ability of a UV LED system. Another disadvantage of the Lifestraw® is that it requires a large pressure differential to pull water through the filter, meaning that a physical burden has been placed on the user to suck water through the straw.

As of 2015, a new method of water treatment has been developed for third world countries. It is known as the "drinkable book" and uses slips of paper coated with silver nanoparticles (AgNPs) to kill microorganisms in water (Water is Life, 2014). Dankovich and

Gray (2011) performed the original tests for this technology. They determined that a page with a silver content of 6-mg/G of paper and nanoparticles 7.1±3.5nm in size could cause a Log-7 reduction in E-coli after an average of 10 minutes of filtration (Dankovich and Gray, 2011). For a DoD emergency situation, one page from this book would be useful. It would be portable, useable for a month upon opening the package, and not require a power source. A major disadvantage to this system is that the viral inactivation capabilities of the drinkable book have yet to be tested. It is unclear if the book contains enough silver to kill a virus. One study showed that 100 mg/L of AgNPs can deactivate a viral bacteriophage (Shao, 2014). Another study found that a 440-910 mg/L concentration of silver nanoparticles could inhibit 50% of HIV infectivity (Lara, Ayala-Nuñez, Ixtepan-Turrent, & Rodriguez-Padilla, 2010). A page from the drinkable book does not provide that dose of AgNPs to water, and so it has the same limitations as the Lifestraw®. Another disadvantage to the drinkable book is that silver can be toxic if too much is ingested. At its current dose of AgNPs, each page does not leech enough silver to be a problem, but if more is needed to eliminate viruses it may become an issue. Overall, this technology has the potential for emergency water disinfection, but more studies on viral inactivation are needed. Like the Lifestraw®, this technology may be more useful if combined with UV disinfection.

Each method of water treatment discussed above has advantages and disadvantages. There is not a current, portable, emergency point-of-use water disinfection unit that eliminates all microorganisms. The combination of a filter with the UV reactor may provide a suitable solution.

Relevant Research

Spencer (2014) created the first UV LED reactor at AFIT in 2013. His thesis first focused on the construction of a reactor, then concentrated on measuring the UV LED output

angle in water.   Spencer constructed the reactor using stainless steel, and placed seven LEDs

perpendicular to the water flow. He built three reactor vessels and two electronics boards

through the course of his research. Captain Spencer concluded that there are seven

characteristics that should be considered for UV LED water-reactor vessel design: LED

wavelength, UV dose requirements, dispersion geometry, LED placement, optical path, vessel

material, and LED control components. He also determined that a flat window LED produces

nearly a 45-degree angle in water (Spencer, 2014). During Spencer's time as a student, fellow

AFIT graduate students, Kelsey Duckworth, John Richwine, and Tho Tran used his reactor for

their own research.

Duckworth (2014) was the first AFIT researcher to use UV LEDs and a witness dye to

measure the advanced oxidation process (AOP). She used 240 nm UV LEDs, and a hydrogen

peroxide solution with methylene blue as the witness dye. She performed her tests in one of

Spencer's steel reactors. Her experiments showed that hydroxyl radicals are produced when

hydrogen peroxide is exposed to UV LEDs under different duty cycle conditions. She ultimately

concluded that continuously driven, or 100% duty cycle, UV LEDs caused higher levels of

witness dye degradation but were not as energy efficient as the short-pulsed cycles (Duckworth,

2014). The AOP process in this thesis is modeled after Duckworth's procedures of applying

hydrogen peroxide and a witness dye to evaluate differences in reactor performance as a function

of reactor design attributes.

Richwine (2014) focused on simulation and modeling of UV LEDs as an energy source

in an effort to predict the efficiency of different reactor vessel geometries. He created a model

that could provide insight into design considerations for reactors that have a primary AOP

purpose as well as considerations for reactor design for germicidal applications. His model also

evaluated different arrangements and numbers of LEDs within a reactor. It showed that a single UV LED will not reflect off of the walls in a three-inch pipe vessel but a configuration of seven LEDs will (Richwine, 2014). This information was applied in the design of the reactor for the current research.

Tran (2014) acquired Spencer's reactor and applied it to a germicidal function. Tran's experiment also ran UV LEDs under pulsed and continuous conditions, but instead of measuring AOP, the experiments measured the inactivation of *Baccillus globigii* spores. Contrary to Duckworth's AOP trials, Tran found that pulsed UV LEDs were 1.5 times more effective at inactivating spores than continuous cycles (Tran, 2014). This information may be useful for future research of pulsing higher power UV LEDs in the 1-inch diameter reactor vessel against another microorganism.

While Tran tested the germicidal functions and AOP in UV LED reactors, Bates (2014) researched the optical power of various UV LEDs independent of a vessel. He used a Labsphere (North Sutton, NH) shutter device in air and water to test the output of 240 nm, 260 nm, 265 nm, and 270 nm UV LEDs. He determined that there is a linear relationship between optical power and current for air measurements, but due to time constraints and the optical losses that occur in water, was not able to collect useful measurements of LED performance in water (Bates, 2014).

Mudimbi (2014) was the first AFIT researcher to use tartrazine dye in UV LED experiments. Like Duckworth and Scott, he studied the effects that pulsing has on AOP. He measured tartrazine degradation for 0%, 5%, 10%, 20%, 30%, 50%, 70%, and 100% duty cycles in Spencer's steel reactor. Mudimbi found that tartrazine degradation increased with increased duty cycles. He was also concerned about mixing characteristics within the reactor, so he performed the tests at flow rates of 1.4mL/min and 0.7mL/min, as well as applied a mechanical

stirrer. His results indicate that the reduced flow rate increased data scatter, and the stirred reactor decreased the data scatter observed from a non-mixed reactor (Mudimbi, 2014). The concentrations of tartrazine and hydrogen peroxide used in this thesis were based upon Mudimbi's research.

Scott (2015) investigated UV LEDs in an advanced oxidation process using Brilliant Blue FCF as the witness dye and compared it to experiments that used methylene blue and tartrazine. He used the reactor designed by Spencer, and performed tests that were driven at lower duty cycles of 10% and 5%. He determined that the lower duty cycles were almost twice as efficient at driving AOP than LEDs at a 100% duty cycle. Scott also noted that Brilliant Blue had degradation rate constants up to 15 times greater than the tartrazine rate constants in Mudimbi's research (Scott, 2015).

Fyda, Godby, Almquist, Harper, and Miller (2014) were the first at AFIT to use a smaller UV LED reactor. They set up a 1" diameter cylindrical steel reactor where LEDs were placed in silicone plugs at each end. The LEDs produced a wavelength of 245nm and had an average of .35 mW output. They measured the AOP of a methylene blue and hydrogen peroxide solution at a flow rate of 1.4 mL/min. They concluded that methylene blue degradation increases linearly with pulsed power settings, and that the small reactor had a higher degradation rate constant at 100% duty cycle than the larger reactor (Fyda et al., 2014).

Duckworth (2014), Mudimbi (2014), and Fyda et al. (2014) used the advanced oxidation process to quantify the efficiency of the UV LED reactor they were testing. They tested three different chemicals, two quantities of LEDs, and two types of reactors using a flow rate of 1.4 mL/min. The efficiencies were defined by the AOP degradation rate constant, and Table 1 summarizes what they found at 100% duty cycle for the reactor and LED configuration used.

Table 1: Summary of AFIT Research for 100% Duty Cycle Degradation Rate Constants

Researcher	Chemical	Reactor	# of LEDs	Mean Rate Constant/Min
Duckworth	Methylene Blue	Large	7	0.011
Fyda Et. Al	Methylene Blue	Small	2	0.008
Mudimbi	Tartrazine	Large	7	0.0013
Scott	Brilliant Blue	Large	7	0.0145

Table 1 shows that Scott's (2014) rate constants for brilliant blue were slightly higher than methylene blue and tartrazine. Fyda et al. (2014) demonstrated that a smaller reactor using only two UV LEDs can produce a similar efficiency to the large, seven LED counterpart. Mudimbi (2014) found a mean rate constant for the large, seven LED reactor, and this thesis will be able to compare the degradation of tartrazine in a small, two LED reactor to his research.

Researchers outside of AFIT have also conducted water disinfection studies using UV LEDs. In 2009, Chatterly and Linden (2010) compared 265nm UV LEDs to mercury lamps and determined that they provide an equal level of treatment when inactivating E. coli. Two years later, researchers made another comparison to UV LED effectiveness versus mercury lamps. Bowker, Shatalov, and Ducoste (2011) developed a collimated beam apparatus that compared UV-Fluence responses of E-coli, MS-2, and T7. They used both 275nm UV-LEDs and mercury lamps. They determined that the 275nm LED was more effective at inactivating E-coli and T-7, and equal in germicidal capability to the mercury lamp for MS-2.

Jenny, Jasper, Simmons, Shatalov, and Ducoste (2015) evaluated a new design paradigm for a point of use UV-LED reactor. They tested the inactivation of E. coli in their own designed

continuous flow reactor through numerical modeling using COMSOL® coupled with another

program called ModeFrontier™. The reactor was composed of an inlet and outlet pipe

connected to a steel box that used 30, 254nm, UV LEDs. The water flow rate for the reactor was

109mL/min. COMSOL® provided complex fluid dynamic models and UV-LED spatial

arrangement options. The modeling design predictions they developed with COMSOL® agreed

with previous E. coli inactivation experiments that they had performed. Jenny et. al (2015)

concluded that the modeling was an effective way to reduce an engineer's design decisions for

an optimal UV-LED reactor.

Most recently, Oguma, Rattanakul, and Bolton (2015) developed a device that

incorporated a ring of 285nm UV LEDs to expose E-Coli, QB, MS2, and adenovirus to UV

radiation in water. The device used 20 UV LEDs with a 20mA current at 8.0V, and output

1.3mW of power per LED. Oguma et. al (2015) determined the inactivation rate constants for E-

Coli, QB, MS2, and adenovirus, and demonstrated that 285nm UV LEDs are a viable option for

adenovirus inactivation in water.

Summary

Many methods of drinking water treatment are available for commercial use today. Most

portable means eliminate bacteria but not viruses. A combination of a pre-filter and UV LEDs

may offer the most effective alternative. Various studies have shown that UV LEDs can

inactivate multiple bacteria and viruses as well as their mercury lamp counterparts and are

suitable for purification device incorporation. AFIT has conducted research on different

configurations for UV LED reactors. Each of the three chemicals yields similar rate constants

under the same experimental conditions, and the rate constants of the large versus the small

reactors have similar results. AFIT research has demonstrated a method to measure reactor

efficiency and may be close to developing a fully functional, portable, decontamination device.

III. Methodology

The purpose of this chapter is to review the methods used to answer the research questions posed in Chapter I. Two sets of experiments were conducted to answer research questions 1-4. The experiments collected observations of changes in the hydroxyl radical production from ultraviolet exposure of hydrogen peroxide, as measured using tartrazine as a witness dye, within four different reactors. These experiments measured the rate at which tartrazine was decolored over time as the dye was oxidized by hydroxyl radicals produced from UV reaction with peroxide. The data from the advanced oxidation process experiments had noisy results, especially the low power tests, so a tracer test and computational modeling was performed to gain insight into the fluid flow characteristics within the reactors. The final set of experiments attempted to answer research question 5 by observing the effects of UV dosage from two nine diode UV LEDS on a microorganism, using the most efficient reactor that was determined from the AOP experiments.

Theory

This research studies the concept that the thickness of Teflon reflects UV light differently as it increases; therefore there is an optimum Teflon wall thickness within a UV LED disinfection reactor. Weidner and Hsia (1981) reported that Teflon with 0.8 g/cm^3 density exhibited increasing UV reflectance as it increased in thickness. They found that 1mm thick Teflon exhibited a UV reflectance of 0.991, 4mm had 0.995, and 6-10mm had 1.0 reflectance (Weidner and Hsia, 1981). That is a small range for near perfect UV reflectance, and as stated earlier, Teflon greatly increases in weight as thickness increases, so there are portability versus efficiency considerations. Next, stainless steel is known to reflect approximately 30-60% of UV light, depending on its composition (Coblentz and Stair, 1929). A steel reactor of same

dimensions as a Teflon reactor should not be as efficient at reflecting UV. The optimum reactor design should be selected and used to test the germicidal capabilities of the UV LED system.

The advanced oxidation process was used to determine the efficiency of each reactor. As hydroxyl radicals are produced from the interaction of hydrogen peroxide and UV radiation, the witness dye degrades (Scott, 2015). Equation 1 shows the AOP formula.

$$H_2O_2 + UV \rightarrow 2 \cdot OH^- \qquad\qquad (1)$$

Materials, Equipment, and Methods

Low Power UV LED Experiments

The 2mm, 6mm, and 12mm thick Teflon reactors, and their accompanied caps were composed of McMaster-Carr brand Polytetrafluoroethylene (PTFE), and machined to shape by the AFIT machine shop. Each reactor is shown in Figure 1. Two types of caps were also created by the machine shop. The first type of cap positioned the water inlet/outlet directly facing to the LED housing, while the second one introduced water at about a 30˚ angle to the housing in an attempt to "swirl" the water. The two caps are shown in Figure 2. Each assembled reactor was attached to a support stand, and oriented vertically to where the inlet cap was on the bottom, and outlet cap on the top. An example of the reactor assembly is shown in Figure 3.
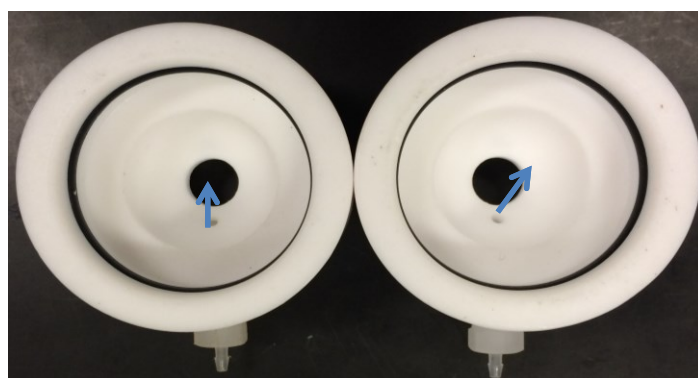
Figure 1: Reactor Materials

Figure 2:"Across LED" and "Swirl" Caps

Figure 3: Example of Reactor Assembly

The two-diode and nine-diode LEDs were manufactured at Sensor Electronic

Technology, Inc. (SETi). The LEDs power and peak wavelength were measured using a

Labsphere® (North Sutton, NH) integrating sphere and spectral radiometer that was calibrated

with a D2 Deuterium lamp (S/N 667329) and Illumia® Pro software. The wavelengths and

power outputs are shown in

Table 2. Spencer (2014) built the board that powered the LEDs. The board had two

20mA semi-conductor resistors (DynaOhm 4006-020 1338, Randolph, VT) that provided a

constant current of 40mA to each of the LEDs, which were connected in series to the constant

current source.

Table 2: UV LED Wavelengths and Power Outputs

UV LED	Identifier Code	Wavelength (nm)	Power Output (W)
LP Top	G38	264	0.002779
LP Bottom	X22	264	0.002728
HP Top	G3	254	0.002928
HP Bottom	G6	254	0.003003

A solution of 26.7 mg/L of yellow tartrazine dye (85% dye, Sigma- Aldrich, St. Louis,

MO) and 2.88g of 30% in water hydrogen peroxide (Fisher Scientific, Pittsburgh, PA) was

pumped through Masterflex 14 tubing using a Masterflex pump (model 77200-50, Cole-Parmer,

Gelsenkirchen, Germany). The dye was pumped through the reactor from bottom to top at 1

mL/min and then through an Agilent Technologies Cary 60 UV- Vis Spectrophotometer (Santa

Clara, CA). The Cary 60 measured the absorption of the 430nm wavelength light, the absorbent

peak for yellow Tartrazine dye, every minute, for 180 minutes. Each combination of reactor and

type of cap was tested in triplicate. The experimental setup is shown in Figure 4.
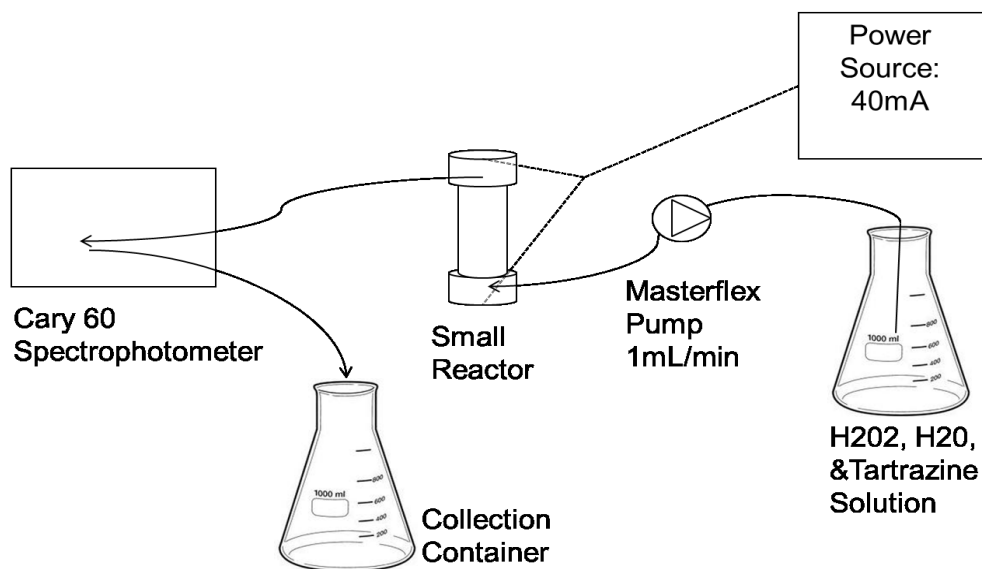
Figure 4: Experimental Setup

High Power UV LED Experiments

The second set of experiments used the same combination of reactors and caps as the first set but used the nine-diode UV LEDs in place of the low powered ones. The high-powered LEDs also required a different circuit board than the low powered LEDs. The board consisted of eight Luxdrive resistors (DynaOhm 4006-020 1338, Randolph, VT) connected in parallel to provide a current of 200mA, which was five times greater than the low power tests. A BK precision Triple output DC power supply (1651A) set to 15V powered the board and LEDs. The second experimental setup included the same procedures from the first set for another 24 experiments.

Tracer Test

The low power UV LED experiments yielded noisy data with respect to the expected

tartrazine degradation. Fluid mixing was suspected, so to research the flow characteristics of the

reactor setup, a tracer test was conducted. The 6mm thick reactor was assembled with swirl caps

and attached to the Masterflex pump and Cary 60. The reactor was filled with reverse osmosis

water and was pumped through the setup at 1 mL/minute for 36 minutes. At 36 minutes, the

pump was stopped, and the water was replaced with the Tartrazine solution used in the first set of

experiments. It was pumped through the reactor for an additional 36 minutes and then replaced

with water. Water cycled through the reactor for 332 minutes. The Cary 60 took readings at 430

nm every minute throughout the tracer test. The test was repeated using across LED caps and the

same reactor thickness. At the end of each trial, the reactor was drained and the remaining

solution was sent through the Cary 60 as well. That solution was then compared to the last

reading taken when the tartrazine was pumped through the reactor.

Multi-Physics Modeling

The multi-physics modeling program COMSOL® (COMSOL Inc., Burlington MA) was

used to model the fluid flow path through the reactor. The software was used to create the

geometry and mesh of the reactor, and COMSOL®'s complex fluid dynamics (CFD) module

was used to calculate the fluid flow physics. The reactor geometry was designed in the program

to represent the inner dimensions that all four reactors shared. The flow domain was specified to

represent water within Teflon material with boundary conditions set as no-slip inner walls. The

mesh was set to coarse, and the initial flow rate was set to1 mL/min at the inlet and outlet.

COMSOL® solved for single phase, laminar flow using the incompressible Navier-Stokes

equation in the laminar flow interface (COMSOL®, 2015). The Navier-Stokes laminar flow

equation solved for is:

$$\rho(u \cdot \nabla) = \nabla \cdot [-p\mathrm{I} + \mu(\nabla u + (\nabla u)^T)] + F \qquad (2)$$

where:

ρ= Density

u= Flow Velocity

p=pressure

∇=del operator

I=Identity Matrix

COMSOL® also calculated the Navier-Stokes equation at the inlets and outlets using Equation 3

(COMSOL®, 2015).

$$L_{exit}\nabla_T \cdot [-\rho 2\mathrm{I} + \mu(\nabla_t \mathrm{u}2 + (\nabla_t \mathrm{u}2)^T)] = -p_{exit}n \qquad (3)$$

Once the model for 1 mL/min was created, COMSOL® was used to develop models for

2, 10, 20, and 100mL/min, as well as 1L/min. An additional theoretical reactor design was tested

using equations 2 and 3. It also modeled the flow through two inlets and outlets under the same

conditions and increasing flow rates as the first model.

Microorganism Inactivation

Escherichia coli (ATCC® 11229TM), strand AMC 198, from Castellani and Chalmers, is a gram negative, rod shaped bacterium used for testing disinfectants and sanitizers. E. Coli is an indicator of fecal pollution in drinking water and has been used to analyze drinking water safety since the 1890s (Edberg, Rice, Karlin, & Allen, 2000).

The E. coli was prepared from freeze-dried pellets that were crushed into a 0.5 mL sterile water solution and then grown on auger cultures for 48 hours. The colonies were then transferred to a nutrient broth where they were incubated for 7 days. Two sets of experiments were performed from the nutrient broth.

The first set of experiments compared two flow rates of non-chlorine treated E. coli solutions with chlorine treated solutions. Three types of solutions were prepared. The first solution contained only water and the E. coli nutrient broth. The second and third solutions contained 1ppm chlorine and 2ppm chlorine, respectively. The E. coli only, and 2ppm chlorine solutions were diluted using an Fisherbrand Elitie 10-100 µL HJ1554 (Finpipette by Fisherbrand® Pittsburgh, PA) to contain $1*10^{-5}$ colony forming units (cfu) of E. coli/mL. The 1ppm solution contained the same amount of E. Coli, but was collected using a Fisherbrand® Elite 1-10 µL pipette (Finpipette by Fisherbrand® Pittsburgh, PA). All solutions were given a 5-day residual time before being testing, and had a magnetic stirrer inserted into its 500mL container.

The solutions were placed upon a Corning Model PC-210 laboratory stirrer (Cole-Parmer, Vernon Hills, IL) and pumped through the medium thickness reactor with swirl caps into a collection container at 1mL/min and 10 mL/min, respectively. The medium thickness swirl cap reactor was chosen because it had the highest average rate constant for both high and low power

26

UV LED AOP trials. The reactor was first filled with the experimental solution to its 35.7 mL

volume. Then, the high-power UV LEDs were activated at the same time as the pump. The

1mL/min solutions were run for 35.7 minutes to achieve their residence time, and the 10-mL/min

solutions for 3.57 minutes. Ten milliliters of the effluent solution were pumped into a 50 mL

beaker, and samples were collected using a 20-200 μL Finnpipette II F149982 pipette (Finpipette

by Fisherbrand® Pittsburgh, PA) upon exiting the reactor and placed on a culture dish in

triplicate. The reference sample was collected from the 500 mL container, and not pumped

through the reactor. The dishes were incubated for 24 hours, and a colony count was recorded.

The second set of experiments had solutions diluted to $1*10^{-5}$ cfu/mL, but did not receive

a 5-day residual time before being sent through the reactor. This set observed the inactivation

ability of the reactor at a wider range of flow rates. The rates were 5, 10, 15, 20, and 25 mL/min.

The residence times were also adjusted for the flow rates, and are shown in Table 3: E. coli

Solution Flow Rates.

Table 3: E. coli Solution Flow Rates

Flow Rate (mL/min)	Residence Time(min)
1	35.7
5	7.14
10	3.57
15	2.38
20	1.79
25	1.43

The same collection procedures and equipment from the first set were used for the

second. To determine the inactivation capability of the reactor, the log reduction value (LRV)

equation was used for both sets of experiments (Bennett, 2008). That equation is:

$$LRV = log_{10}\left[\frac{Influent\ Pathogen\ Conentration}{Efflluent\ Pathogen\ Concentration}\right] \qquad (4)$$

High and Low Power UV LED Tartrazine Degradation Modeling

The oxidation reaction responsible for the degradation was modeled using the mass balance equation for an assumed complete mix reactor. It is the same model used by Duckworth (2014), Fyda et al. (2015) Scott (2015), and Mudimbi (2015) for the methylene blue, brilliant blue, and tartrazine research.

Mass accumulated = Mass In – Mass Out + Mass Produced – Mass Consumed   (5)

$$\frac{C_T}{C_{T0}} = \left(\frac{1}{1+\tau k}\right)\left(1 = \tau k e^{-\left(\frac{1}{\tau}+k\right)t}\right) \qquad (6)$$

where:

C_T = final concentration of Tartrazine

C_{T_O} = initial concentration of Tartrazine

τ = residence time

k = apparent first-order rate constant

t = reaction time

The Residence time (τ) was calculated as volume (V) divided by flow rate (Q):

$$\tau = \frac{V}{Q} = \frac{35.7\ mL}{1.0\ mL/min} = 35.7\ min \qquad (7)$$

Summary

Research on UV LEDs in a portable disinfection unit consisted of multiple experiments. Two sets of AOP experiments used hydrogen peroxide and tartrazine as a witness dye. Flow

characteristics were tested using a COMSOL® modeling and a tracer test. Finally, the microbial

inactivation capability of the UV LEDs was tested using E. coli as an indicator organism.

IV. Results and Analysis

Chapter Overview

 This chapter will report and discuss the results from the advanced oxidation process experiments (AOP), tracer test, COMSOL® modeling, and microbial inactivation experiments. The complete set of relative concentration measurements as a function of time for the 48 AOP experiments is shown in Appendix B.

AOP Control

 The AOP experiments began with a control experiment. It was performed to show that the hydrogen peroxide required UV from the LEDs to produce hydroxyl radicals in the AOP for tartrazine. A solution of tartrazine and peroxide mixed as described in Chapter III was pumped through the steel reactor with Teflon across LED caps. Its dye concentration at the 430 nm wavelength was recorded every minute for 180 minutes using the spectral photometer. The results show that the concentration of the dye did not change over time, thus no AOP had taken place. The control experiment is shown in Figure 5.
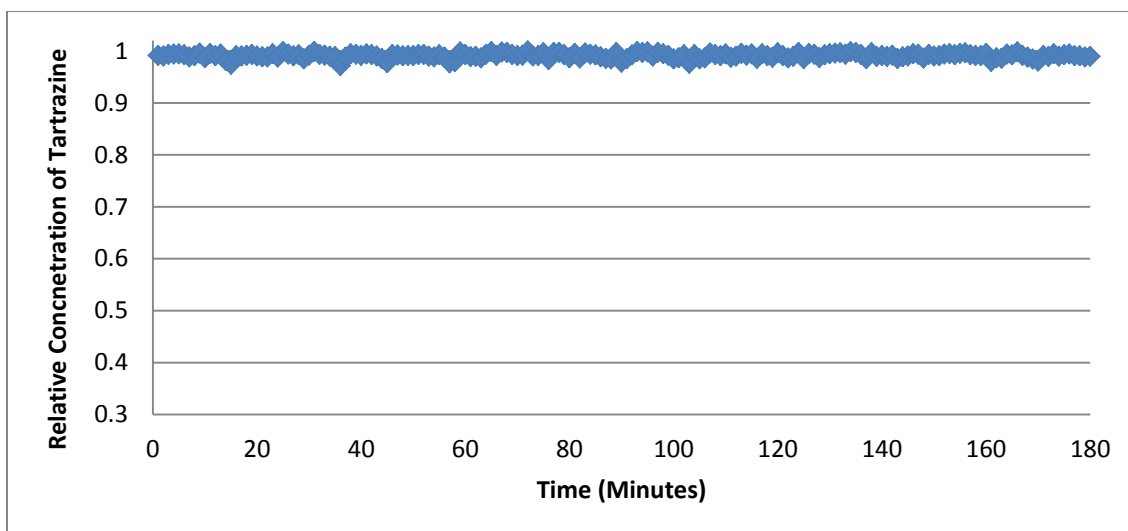
Figure 5: Relative concentration of tartrazine as a function of time in the AOP Control
Experiment

Results of Low Power AOP Experiments

The 24 low power experiments consisted of testing each material with either the swirl cap

or across cap configuration in triplicate. The spectral photometer recorded the absorption of

Tartrazine at 430 nm every minute of the 180 minute trials. Absorption data was translated into

concentration data using a five-point regression calibration curve generated in Microsoft®

Excel™ 2007. The five calibration points were unique to each experiment, and they consisted of

0%, 25%, 50%, 75% and 100% dilutions of the tartrazine and peroxide solution. Figure 6

illustrates an example of the calibration curve used in the degradation experiments.
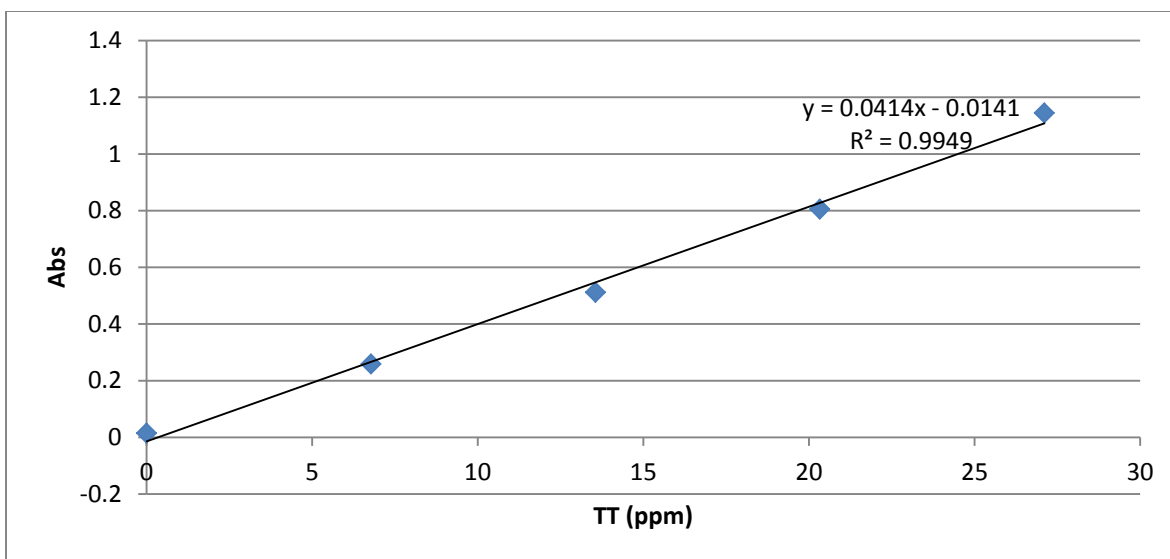
Figure 6: Calibration Example (Thin Teflon with Across Caps Trial 3)

The low power experiments yielded approximately 15-25% tartrazine concentration degradation after three hours. All three materials produced degradation curves similar to the example shown in Figure 7.
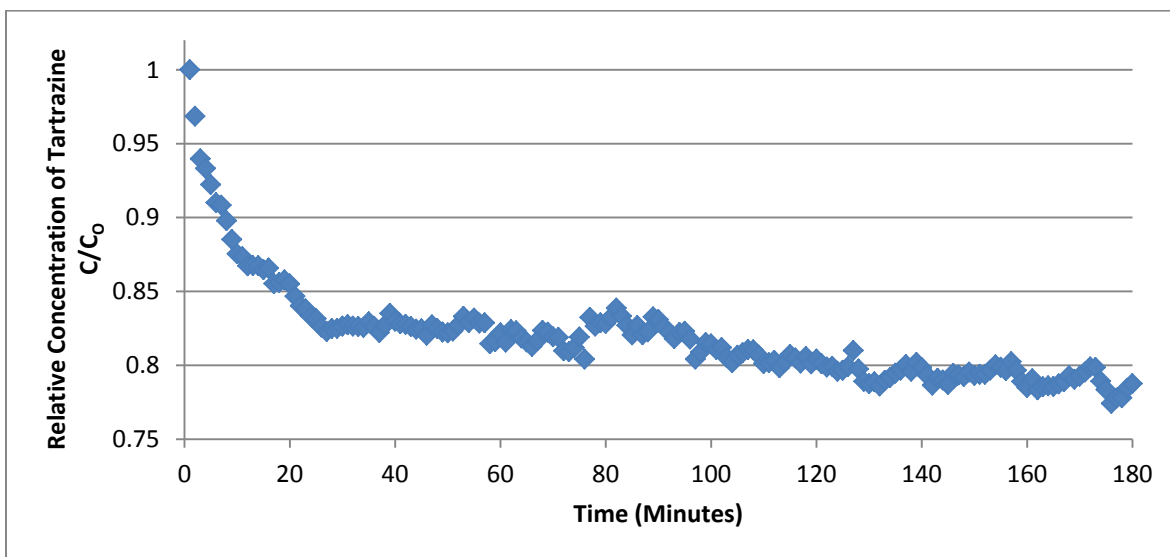

Figure 7: Example of Low Power UV LED Tartrazine Degradation Curve (Thin Teflon with Swirl Caps, Trial 3)

The curves plotted relative concentration of tartrazine as a function of time. An initial

sharp drop in concentration up to about the 35-40 minute range, followed by fluctuations in the

concentration with an overall decrease was observed for all tests. Some trials produced noisier

fluctuations than others. The complete set of low power UV LED tartrazine concentration

curves can be found in Appendix B.

After data collection and translation, each experiment was fit with a model using the

statistical program MATLAB®. The program minimized the sum of squares difference between

the experimental data and Equation 5 model line, and solved for the first order rate constant (k_{st}).

The low power rate constants and their associated R^2 values are shown in Appendix C.

Results of High Power AOP Experiments

An additional 24 AOP experiments were completed following the same procedures as the

low power UV LED tests. The only change was that the higher power, nine-diode, UV LEDs

were used instead of the single-diode LEDs. The 24 experiments' data were collected, and each

trial of tartrazine concentration over time was plotted in Microsoft® Excel™ 2007. All tests

were calibrated using the five-point method described in the low power UV LED results section.

Each run was also modeled using Equation 5, and had its rate constant determined. An example

of a high power UV LED AOP experiment is shown in Figure 8, and the calculated rate
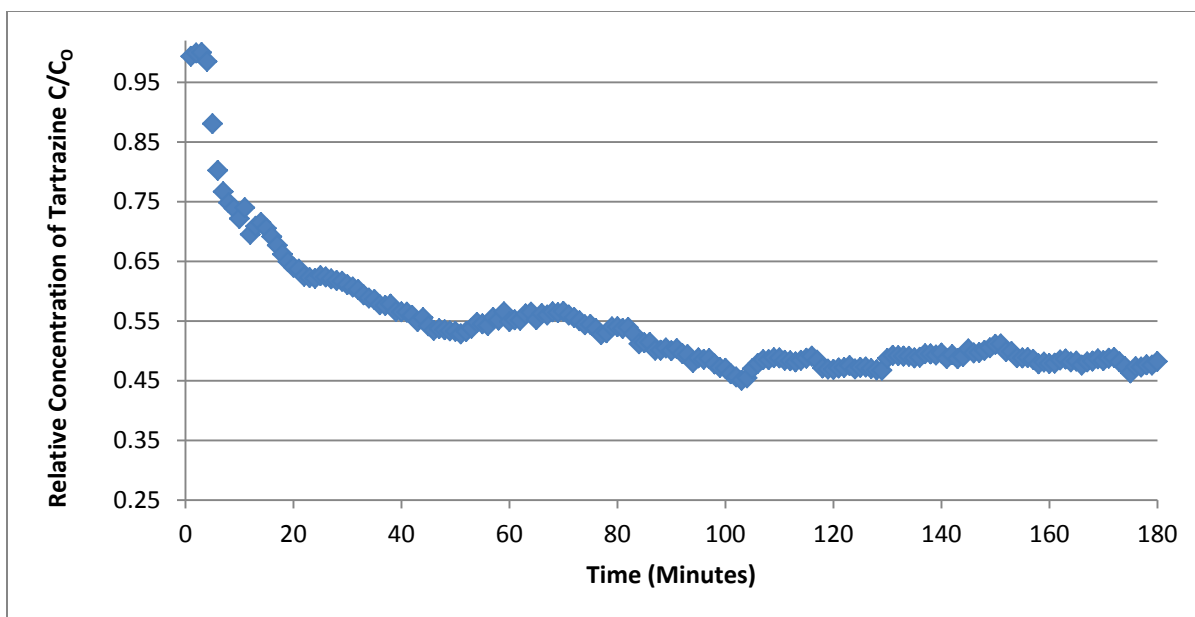
constants are shown in Appendix C.

Figure 8: Example of High Power UV LED Tartrazine Degradation Curve (Thin Teflon with Swirl Caps, Trial 3)

Although the high power AOP experiments yield similar looking curves to the low powered ones, the high-powered experiments yielded tartrazine levels that were nearly 40% lower in each case. The lowest relative tartrazine concentration recorded in the low power tests was 73.37%, which was exhibited by the thick Teflon reactor with across caps in its second trial. In contrast, the lowest concentration for the high power tests was 32.96%, which was exhibited by the thin Teflon with the across caps in its first trial. All high power tests degraded beyond the 73.37% concentration within nine minutes. The high power curves also fit Equation 5 with less noise. The average R^2 value for the high power rate constants was 0.879 versus 0.778 for the low power rate constants. Figure 9 illustrates the difference between the high and low power AOP experiments. It graphs the average run for each reactor experimental setup. The complete set of high power UV LED AOP tartrazine concentration curves can be found in Appendix B.
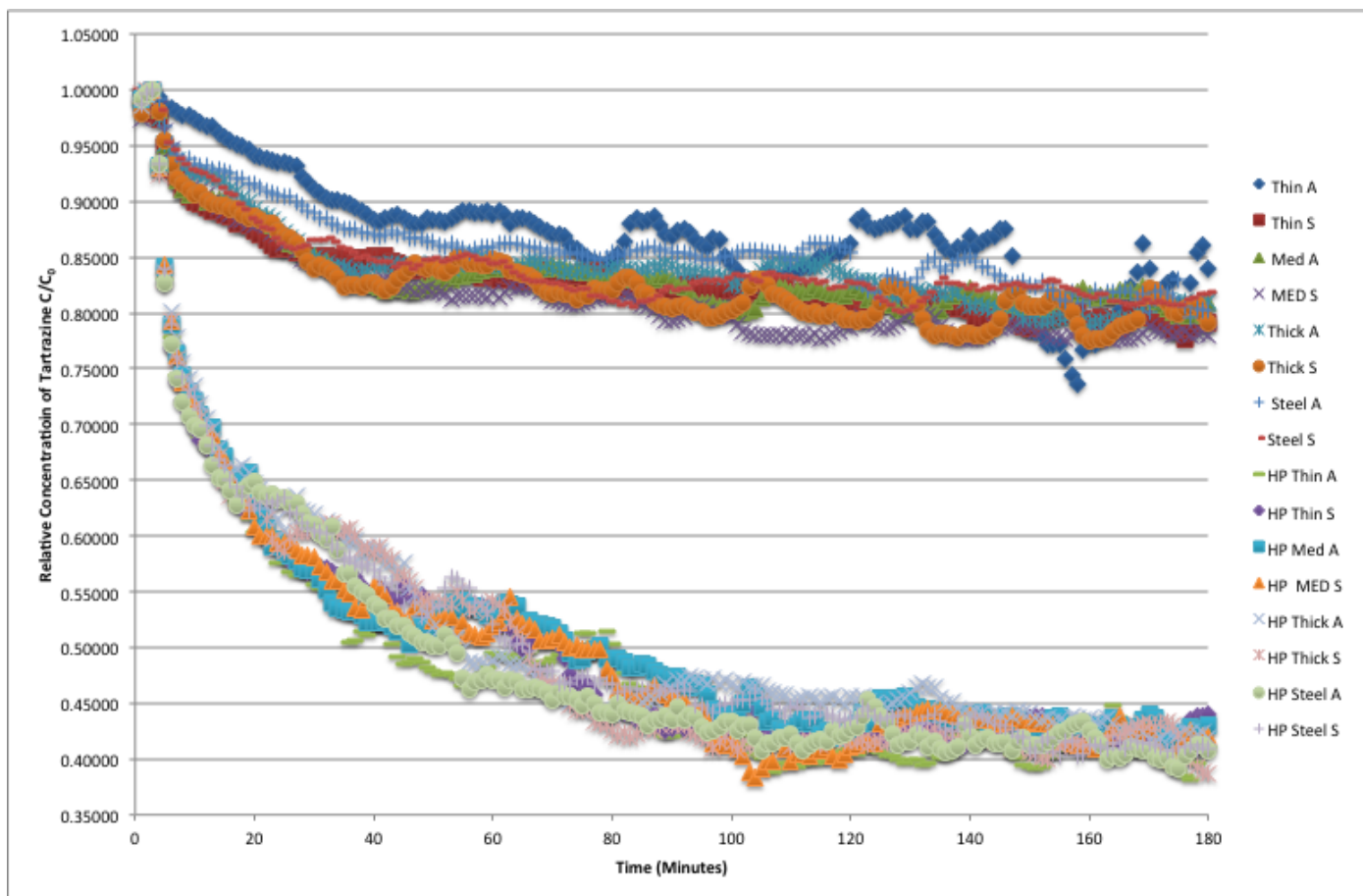
Figure 9: Average Trial for Low and High Power AOP Experimental Designs

Results of COMSOL® Modeling

Ten models were created using the COMSOL® CFD module. The primary model of concern was the streamline conditions under the experimental conditions used for the AOP experiments. COMSOL® was set to solve for laminar flow, and to plot 100 streamlines that change from blue to red as velocity increases. The tolerance for calculation was set to 0.1, and COMSOL® found a converged solution. Figure 10 shows the COMSOL® plotted the fluid path streamlines through the reactor from the bottom inlet, shown on the right, to the top outlet, shown on the left. The initial vortex shown Figure 10 indicates that mixing is not occurring

35

throughout the entire reactor but occurs primarily near the inlet of the reactor; this phenomenon may be contributing to the fluctuations seen in the low power experiments.
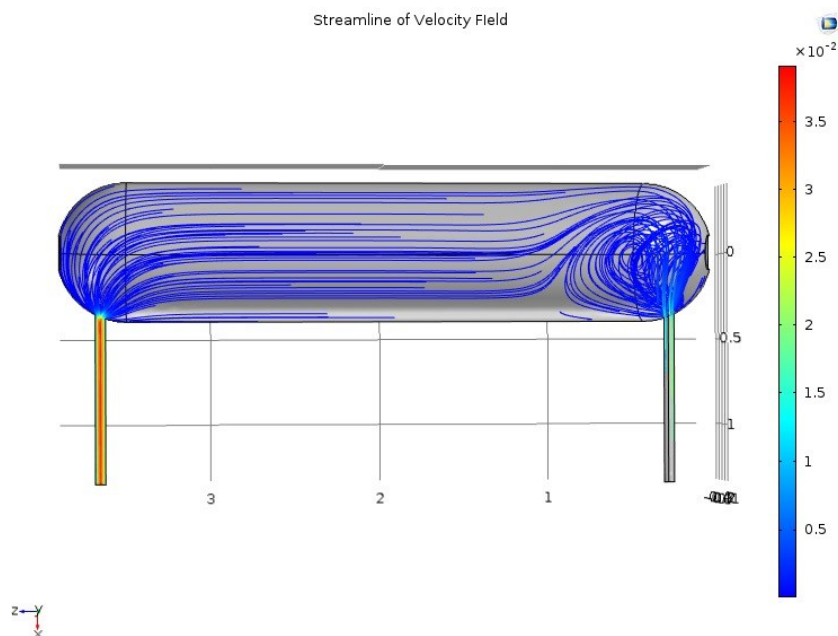

Figure 10: Streamline Model of Experimental Reactor

Additional COMSOL® models were created to provide insight into the mixing conditions for faster flow rates and a theoretical smaller diameter reactor. The same laminar flow equations were solved for, and streamlines were created for 2mL/min, 10 mL/min, 100 mL/min, and 1 L/min. COMSOL® found converged solutions up to 10mL/min. This suggests that the flow conditions in the reactor may be turbulent at a flow rate of 100 mL/min. The 10 mL/min and faster streamline graphs suggest that the reactor may have more distributed mixing at higher flow rates. Each streamline is shown in Appendix D.

The smaller theoretical reactor was created out of the same materials, but had a diameter of 8.2 mm, which is the same diameter of the UV LEDs used in the AOP experiments. COMSOL® generated a 100 streamline model set at 1 mL/min, shown in Figure 11. The same

flow rates used in the regular sized model above were used to plot additional models showing

100 streamlines. Under the same conditions as the large, the small diameter reactor shows that

the streamlines also produce an initial vortex upon entering the reactor. The vortex also does not

extend as far into the reactor tube as the experimental vortex did. The smaller design reactor

vortex only reaches about half way to the 1-inch mark, while the experimental reactor vortex

extends nearly to the 1-inch mark. Finally, the vortex has a higher velocity and the streamlines

are more closely distributed, which may indicate more complete mixing than is present in the
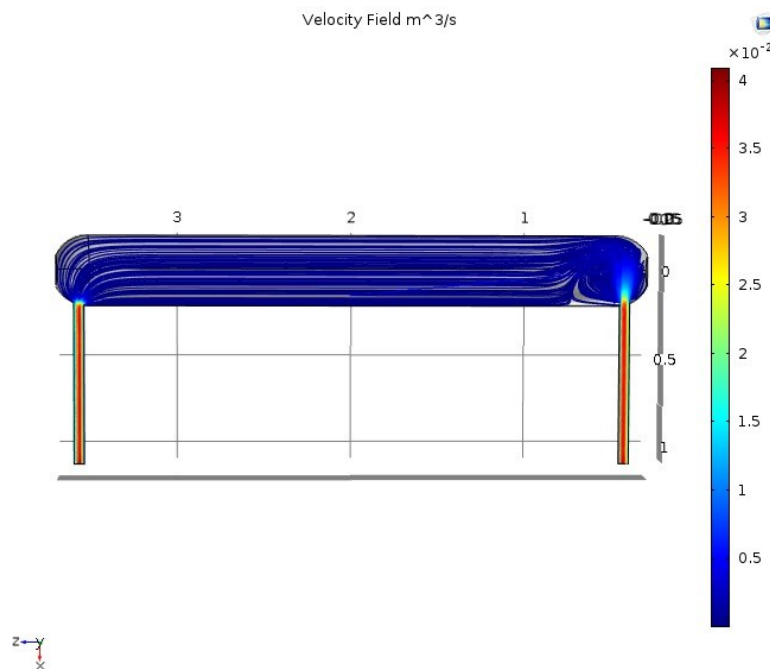
large reactor.

Figure 11: Smaller Diameter Model Streamlines Example

Results and Analysis of Tracer Test

The results of the tracer tests for the two types of caps are shown in Figure 12. The figure indicates that the solution contained approximately 5% tartrazine in water at the 400 minute mark. However, when the reactor was drained at that time, the remaining solutions did not contain 5% tartrazine, but instead about 18% for both types of caps. The difference between the constant concentration reading and the final drained concentration suggests that the solution is not mixing well in the reactor. The tracer test and the COMSOL® modeling both suggest incomplete mixing.
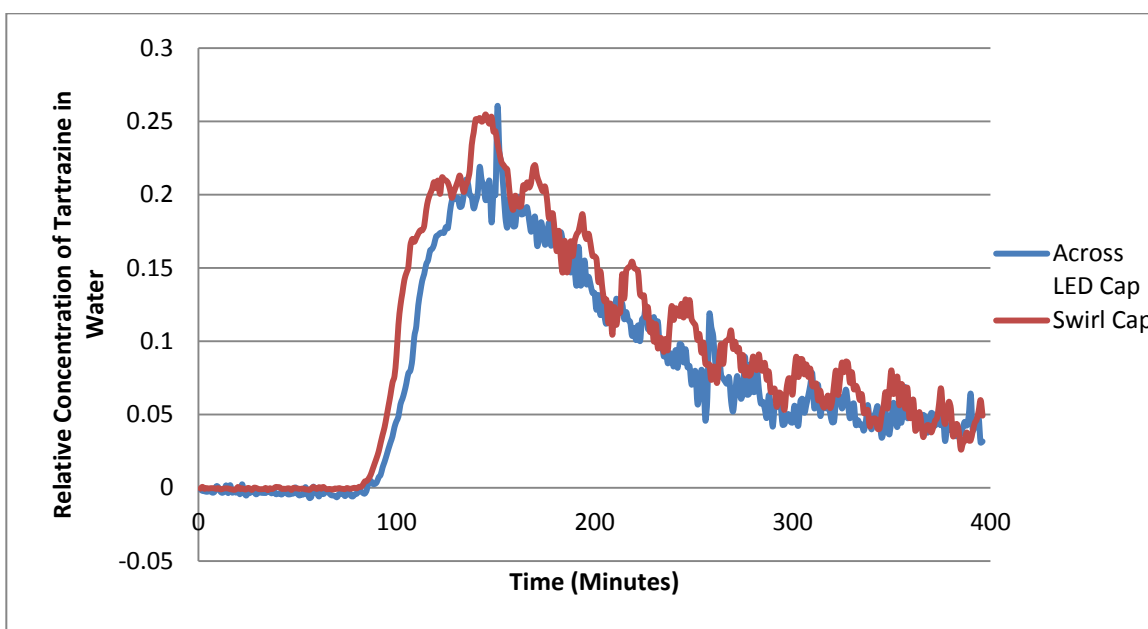

Figure 12: Tracer Test Results

Analysis of Low and High Power AOP Experiments

To determine whether the type of material or type of cap significantly affected the tartrazine degradation within the reactor, multiple analyses of variance (ANOVA) of the rate constant for each reactor and cap configuration were conducted in JMP® analytical software.

38

The results of the whole model ANOVA are shown in Table 4, and subsequent effect tests from the ANOVA are shown in Table 5.

Table 4: Whole Model ANOVA

Source	DF	Sum of Squares	Mean Square	F Ratio
Model	12	0.00913652	0.000761	155.6417
Error	35	0.00017121	4.892e-6	**Prob > F**
C. Total	47	0.00930773		<.0001*

Table 5: Whole Model Effects Test

Source	Nparm	DF	Sum of Squares	F Ratio	Prob > F
Swirl	1	1	0.00001892	3.8678	0.0572
Reactor Type	3	3	0.00002505	1.7069	0.1834
High Power (1) Low Power (0)	1	1	0.00482912	987.1759	<.0001*
Reactor Type*High Power (1) Low Power (0)	3	3	0.00000484	0.3296	0.8040
Swirl*Reactor Type	3	3	0.00005048	3.4397	0.0271*
Swirl*High Power (1) Low Power (0)	1	1	0.00005118	10.4626	0.0027*

The whole model showed that the residuals of the k_{st} values were normally distributed, and the Durbin-Watson test had a value of 2.71, indicating that the residuals were independent. From Table 4, the initial whole model Analysis of Variance had a $p<.0001$, which suggested that at least one of the parameters tested was significantly different than another. The whole model effect tests revealed that there was a significant interaction between the rate constants of high power and low power UV LEDs. Although expected, those interactions indicated that the high and low power tests could be analyzed individually. The whole model also revealed that the interaction between swirl*Reactor type was significant, and so was Swirl*High power versus low Power. Those last two interactions were explored in further analysis of the high and low power UV LEDs. The low power analyses are shown in Table 6 and Table 7.

Table 6: Low Power UV LED ANOVA

Source	DF	Sum of Squares	Mean Square	F Ratio
Model	7	.00002326	3.3231e-6	7.699
Error	16	0.00000691	4.315e-6	**Prob > F**
C. Total	23	0.00003017		<.0004

Table 7: Low Power UV LED Effects Test

Source	Nparm	DF	Sum of Squares	F Ratio	Prob > F
Swirl	1	1	0.00000694	16.0748	0.0010*
Reactor Type	3	3	0.00001078	8.3240	0.0015*
Swirl*Reactor Type	3	3	0.00000171	1.3186	0.3030

A one-way ANOVA for the low power UV LED trials, shown in Table 6, indicated that the interaction between k_{st} and cap type, "swirl" or "across LED", was statistically significant at α= 0.05. Another one-way ANOVA for the interaction between k_{st} and reactor type showed that it was also significant at α= 0.05. Further analysis compared cap type, reactor material, and k_{st} values.

The "swirl" cap experiments had larger least-square means values than the "across LED" caps. A two-way ANOVA of the rate constant response between reactor type and type of cap indicated that there is a significant difference between k_{st} values of reactors that used "swirl caps", and reactors that used "across LED" Caps. Figure 11 illustrates the least-square (LS) Means of the k_{st} values versus reactor type and cap type.
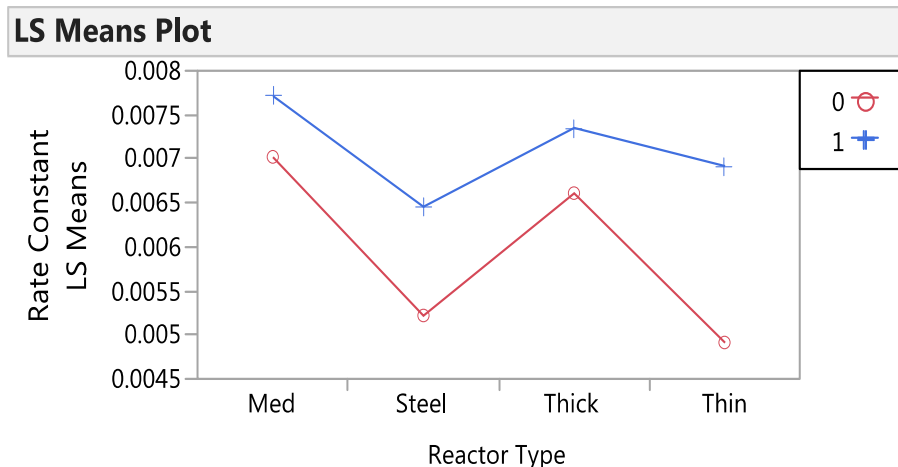
LS Means Plot

Figure 13: LS Means Plot of K_{st} Values for the Interaction Between Reactor Type and Cap Type Low Power

The blue positive series shows the "swirl" caps, and the red circle series shows the "across LED" comparisons. Tukey analysis revealed that the medium thickness Teflon reactor was significantly different than the steel and thin Teflon reactors, but not significantly different than the thick Teflon. The thick reactor performed at an intermediate level between the medium Teflon and the steel. This analysis also showed that the medium thickness reactor using "swirl" caps had the highest mean rate constant, and that the "swirl" caps had consistently higher rate constants than the "across" caps.

Table 8: High Power UV LED ANOVA

Source	DF	Sum of Squares	Mean Square	F Ratio
Model	7	0.00014347	0.000020	2.8161
Error	16	0.00011645	7.278e-6	**Prob > F**
C. Total	23	0.00025992		0.0409*

Table 9: High Power UV LED Effects Test

Source	Nparm	DF	Sum of Squares	F Ratio	Prob > F
Swirl	1	1	0.00003373	4.6337	0.0470*
Reactor Type	3	3	0.00003257	1.4916	0.2547
Swirl*Reactor Type	3	3	0.00009663	4.4256	0.0190*

The high power tests did not yield nearly as many significant differences between factors as the low. Like the low power, a one-way ANOVA indicated that the interaction between k_{st} and cap type, "swirl" or "across LED", was statistically significant at $\alpha = 0.05$. The ANOVA is shown in Table 8. However, the LS Means plot showed that the "across LED" cap provided higher rate constants, which is the opposite interaction exhibited in the low power experiments. The LS Means plot is shown in Figure 14. Unlike the low power experiments, no other significant differences were observed, which is seen in Table 9. The ANOVA for the interaction between k_{st} and reactor type showed no significant differences. The Tukey analysis showed all reactor types were on the same level as well. The complete JMP® analysis can be found in Appendix D.
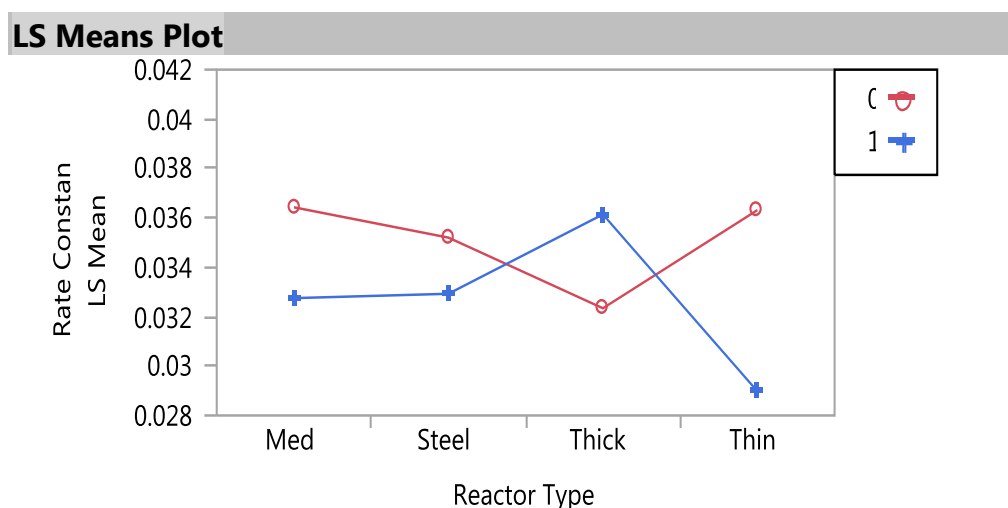

Figure 14: LS Means Plot of Kst Values for the Interaction Between Reactor Type and Cap Type High Power

There is a possible explanation as to why the high power UV LEDs did not yield significant material differences as compared to the low power LEDs. As the COMSOL® model in Figure 10 displayed, the water flows in a vortex upon entering the reactor. The high power UV LEDs may not be affected by that vortex. UV LEDs produce two peaks in illumination, with one in the visible light "blue" range (Murakami, Taguchi, & Yoshino, 2000). The visible light caused the yellow solution to fluoresce green, which could be seen through the Teflon reactor walls. Observation of the reactor with the lights out, during the high power experiments, showed that the UV LEDs were illuminating the solution across the entire reactor. This demonstrated that the lights penetrated the initial fluid vortex. The low power UV LEDs did not display the same illumination. Only the caps could be seen glowing in the dark under low power conditions.

This research can be compared to previous AFIT research with regards to the computed degradation rate constants. Revisiting Table 1 shows that Duckworth (2014) and Fyda et al. (2015) had similar rate constants between the large and small reactors with methylene blue. This research can follow Mudimbi's findings for the steel reactor. Mudimbi found a mean rate constant of 0.0013. The steel "across LED" cap reactor had a mean rate constant of .0052. The difference between rate constants in the large and small reactors is much smaller for methylene blue that it is for tartrazine. The small reactor degraded tartrazine nearly five times greater than the large, which supports Fyda et al's (2015) conclusion that the small reactor with 2/7ths as many LEDs was just as effective as the large reactor. In fact, this research suggests that the small reactor is much more efficient than the large reactor, an effect that might be partially explained by the use of end caps made of Teflon machined to remove large angles which could trap energy in the present experiment as opposed to the endcaps made from laboratory-grade silicon stoppers with flat surfaces in the earlier experiments.

Results and Analysis of E. Coli Inactivation Experiments

The first set of E. coli experiments yielded complete removal of E. coli at 1 mL/min and 10 mL/min. The baseline plates had an average colony count of 13 colony forming units (CFUs). The treated plates had zero colonies after 24 hours of incubation. Neither baselines for the 1ppm and 2ppm chlorine solutions yielded any colonies, so as expected, the treated plates had zero colonies form on them after incubation.

The second set of E. Coli experiments also had promising results. Of the three baseline plates, one plate had poor separation of colonies, resulting in very large colonies that skewed the amount of bacteria present. That plate was excluded from the average of the other two plates. Those plates had an average of 28 CFUs. As for inactivation results, there were no colonies on the 5 mL/min, 10 mL/min, 15 mL/min, and 25 mL/min plates. There was one observable colony on one plate for the 20 mL/min, which means the average colony count was 1/3 for those plates, or 1 colony in 30 mL of water. This was surprising that it happened on the 20-mL/min trials, but not for the 25 mL/min run. Applying Equation 4 for the 20-mL/min experiment yields a 2-log removal of E. coli from the water. Based on the results of all other trials, the log removal may be much higher than 2-log. More testing starting at 20 mL/min is recommended.

Summary

The AOP results and analysis indicate that material and water flow cap configuration do significantly affect the efficiency of a low powered UV LED reactor when configured as shown in this experiment.   Water flow caps also affect the AOP of high power UV LED reactors, but the material comprising the straight walls of the reactor itself is not statistically significant. Bacterial inactivation experiments observed a complete removal of E. coli from water samples up to 15 mL/min and a 2 Log removal at 20 mL/min.

V. Conclusions and Recommendations

This research exhibited the effectiveness of ultraviolet light emitting diodes in driving the advanced oxidation process for various thicknesses of Teflon vessels and compared it to steel. It also demonstrated the inactivation capability of using UV LEDs in a portable reactor container. The findings from this research may prove useful to the development of a field-use portable water disinfection device.

Conclusions of Research

Low powered UV LED experiments showed significant differences in tartrazine degradation between the medium thickness Teflon reactor compared to the thin and steel reactors. There was a significant difference between the rate constants of both high and low power UV LEDs with respect to the type of cap used. The "swirl" cap produced more significant degradation in the low power UV LED tests, but had the opposite effect in the high power tests. Based upon these findings, the medium thickness, "swirl" Teflon reactor is the most efficient in low power UV LED AOP applications. The most efficient high power reactor for AOP applications is not as clear to determine. There was no significant difference between rate constants of different materials. Finally, the E. coli inactivation experiments yielded complete removal of E. coli up to 15 mL/min, thus demonstrating disinfection capability for Teflon UV LED reactors.

Investigative Questions Answered

This thesis sought to answer multiple research questions. Research question 1 asked if a Teflon continuous flow reactor has a more effective advance oxidation process (AOP) than a steel reactor of the same dimensions when exposed to UV LEDs. The results indicate that Teflon can increase reactor efficiency, but it depends on the thickness. The medium thickness

reactors of both UV LED power levels outperformed the steel reactor of either cap type. The thick and thin reactors had no statistically significant difference in AOP as compared to steel for either high or low power LEDs.

The second research question asked if material wall thickness affects the efficiency of Teflon reactors. Wall thickness does affect the efficiency. The medium wall thickness had a greater rate of AOP than the thin reactor that was statistically significant in the low power tests. It also had a higher mean k_{st} than the thick reactor, although it was not statistically significantly greater. The medium thickness reactor was not statistically significant in the high power tests, but still had a higher mean k_{st} than both the thick and thin reactors.

Research question three asked if the entry angle for water in the Teflon reactor affected mixing in a reactor. Due to software licensing and time constraints, only the "across LED" configuration was mathematically modeled using COMSOL®. The tracer test indicated that the "swirl" cap configuration had a higher tartrazine concentration at each peak of the fluctuations by approximately 1-2%. However, that test is inconclusive because only one trial per cap configuration was performed. Future research should model the "swirl" cap configuration to see if there is a different streamline path. If so, that provides more evidence that the water entry angle for this reactor affects the mixing.

The fourth research question investigated whether the entry angle for water affects the efficiency of the portable reactor. This question was answered through the AOP tests. In both the high and the low power tests, the cap type had a significant interaction with the rate constant. Unfortunately, the significant cap type is not consistent between the two UV LED power levels. The "swirl" type cap yielded higher rate constants in the low power tests, while the high power tests experienced the opposite results. The high power LEDs' ability to penetrate the vortex

46

discovered from the COMSOL® modeling may contribute to the difference in results. As stated from the research question three discussion, the "swirl" caps were not modeled, so that vortex may not exist in the caps.

The final research question asked if a continuous flow, portable, Teflon reactor can disinfect water to EPA drinking water standards. The EPA does not have a set log reduction standard, but instead has a maximum contaminant level (MCL). The level dictates that any detectable E. coli concentration is in violation of the Revised Total Coliform Rule (US EPA, 2013). Unfortunately, there was one colony that formed after treatment during the 20mL/min test. That bacterium may have had the ideal flow path of minimum UV exposure through the reactor. The 25 mL/min test did not yield any bacterial growth, so those two flow rate conditions will need to be replicated in future AFIT research to see if the same results will be produced. If E. coli is present in those future tests, then it can be concluded that this reactor can treat up to 15 mL/min of water to EPA standards.

There is a set of standards for military operations using microbiological water purifiers known as NSF Protocol P248, which were discovered during the course of this thesis research. This protocol calls for a small water purifier to demonstrate a log 6 removal of E. coli to be approved by the NSF for field use (NSF, 2012). The medium thickness reactor achieved log 6 removal up to 15mL/min. NSF procedures were not followed during this thesis, but now that this reactor has germicidal capabilities, future tests should adhere to NSF protocol P248 so that new designs can be approved for field use.

Significance of Research

Teflon wall thickness provided insight into how it affects the advanced oxidation process. As Teflon gets thicker, its weight also increases. This is a concern for making a portable device,

because the user prefers the most powerful and lightest device. Now a relationship between rate constant and Teflon thickness has been established, and it is shown in Figure 14.
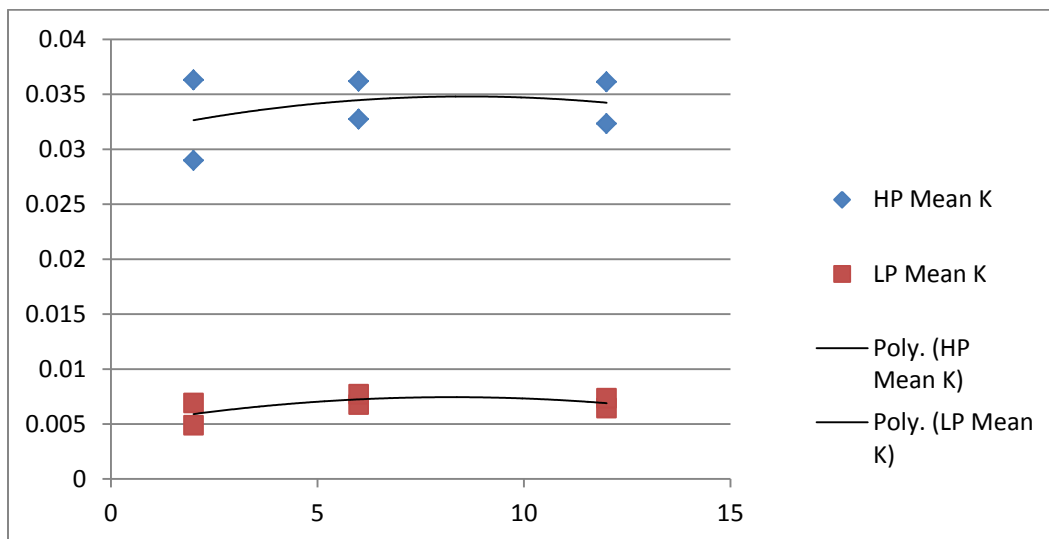

Figure 15: Rate Constant as a Function of Thickness

From Figure 15, an optimal thickness can be predicted using a polynomial trend line. It appears that a thickness of 8-9mm may yield higher rate constants. Portable devices may exhibit the best inactivation efficiency at that thickness.

Finally, the inactivation of E. coli demonstrates proof of concept for a portable UV LED water purification device. The high power UV LEDs executed greater disinfection than expected, and can now provide a path to a smaller, more powerful device.

Recommendations for Future Research

This research focused on comparing steel and Teflon reactors using UV LEDs that were positioned opposite to each other in the end caps. The LED placement may not have been the optimal location for UV reflectance off of the reactor material. New research should be

conducted using LEDs that are facing the reactor walls at different angles. Also, the reactor diameter in this research was constant. The ultimate goal is to provide a portable disinfection device, so a smaller diameter reactor should be researched. Furthermore, the trend line in Figure 15 suggests that 8-9mm may contain the optimal thickness for Teflon AOP efficiency; that thickness should be incorporated into new experiments.

Next, only one microorganism was studied in this thesis. E. coli is a bacterium that is easily inactivated. Future UV LED research should test the viral inactivation capability of either this reactor or one of the future designs recommended in the previous paragraph. Finally, all flow rates were relatively slow compared to how fast a human can drink water. Future tests should measure and attempt disinfection experiments at that flow rate.

Summary

Low power UV LED experimentation yielded AOP results that demonstrate more efficiency than previous AFIT research. Low power UV LED tests also revealed that the medium thickness reactor has a statistically significant higher rate constant than the steel and thin cylinder reactors. All high power UV LED tests had rate constants ten times higher than the low UV LEDs, but exhibited no significant difference between materials or thicknesses. High power UV LEDs can inactivate E. coli in water. A UV LED portable water disinfection unit is a possible drinking water purification alternative.

Appendix A- AOP UV LED Experimental Setup Procedures

Mix hydrogen peroxide (.005 mol) and Tartrazine (5 mol/L) solution:

1) Fill 1L volumetric flask with 500mL of reverse osmosis deionized water and drop in a stir bar

2) Using a weighing tray, measure 0.02672g of Tartrazine , and mix into 1L volumetric flask. Rinse remaining Tartrazine in tray with deionized water into the flask

3) Weigh 2.87953g of hydrogen peroxide (30% in water) in weighing tray, and mix into volumetric flask. Rinse remaining peroxide in tray with deionized water

4) Fill remainder of flask with reverse osmosis deionized water and use stir plate to stir solution for 10 minutes

5) Retrieve sample and prepare 0%, 25%, 50%, 75%, and 100% dilutions of sample for calibration

UV LED and Heat Sink Assembly:

Although not required, the sturdiest and most convenient method to transfer UV LEDs between caps is to solder the wires to the UV LED and slide the wires through the copper heat sinks.

1) Slip copper slug over UV LED

2) Solder positive wire to LED lead that has the bump on the LED case

3) Solder negative wire to middle LED lead

4) Use heat shrink to cover exposed wire and solder

5) Slide wires through heat sink and solder connections to ends of the wires

Assemble Reactor:

1) Choose desired material and cap for experiment

2) Put o-ring on UV LED and attach LED/heat sink assembly to caps by screwing the two hex-head screws

3) Insert o-rings into caps

4) Place top and bottom caps on reactor body tube

5) Attach reactor to test tube clamp stand

Set up Cary-60 UV-Vis Spectrophotometer:

1) Log on to desktop- Username:Cary60; no password

2) Open "Cary 60" program

3) Open "Scan" File

4) Click "setup"

5) X-mode= Start at 435nm Stop at 425nm

6) Cycle Mode= Count=180, Time=1.00 Minute

7) Scan controls=Fastest

8) Insert DI water into Cuvette, and insert Cuvette into Spectrophotometer

9) Click "Zero"

Collect Calibration Values

1) Use 1mL syringe to load flow cuvette through with 0% solution

2) Open panel, load cuvette into Cary-60 UV-Vis, and close panel

3) Click "Rapid Result" and record absorbance on desktop notepad

4) Repeat steps 1, 2, and 3 with 25%,50%,75%, and 100% solutions

Run Experiment

1) Setup tubing through peristaltic pump

2) Insert one end of tubing into Tartrazine and peroxide solution and the other end to bottom

cap of reactor (DO NOT ATTACH TUBING TO TOP CAP YET- It may cause an air bubble in the next step, which may pop apart the reactor)

3) Rotate reactor's clamp so that it is holding the reactor horizontally- This is done to release air out of the top hose barb while filling with solution

4) Start pump and increase flow rate to desired speed- Be careful not to load too fast, as this may cause excess pressure in reactor, and pop it apart

5) Once solution starts to flow out of top hose barb, stop pump, rotate and tighten down clamp so that reactor is vertical again, start pump, and adjust pump to experimental speed

6) Attach tubing to top cap and run to UV-Vis Cuvette

7) Watch the cuvette fill and make sure there are no air bubbles

8) Attach final tubing from cuvette to collection container

9) Close UV-Vis lid as close to tubing as possible, and then place a piece of paper over the remaining opening of lid

10) Start UV-Vis program

11) During 2:00 Minute countdown use a graduated cylinder and stopwatch to calibrate pump to desired experimental flow rate

12) Let the UV-Vis take two readings, and then turn on the UV LEDs

Appendix B- Graphical Presentation of Relative Concentration of Tartrazine as a Function of Time
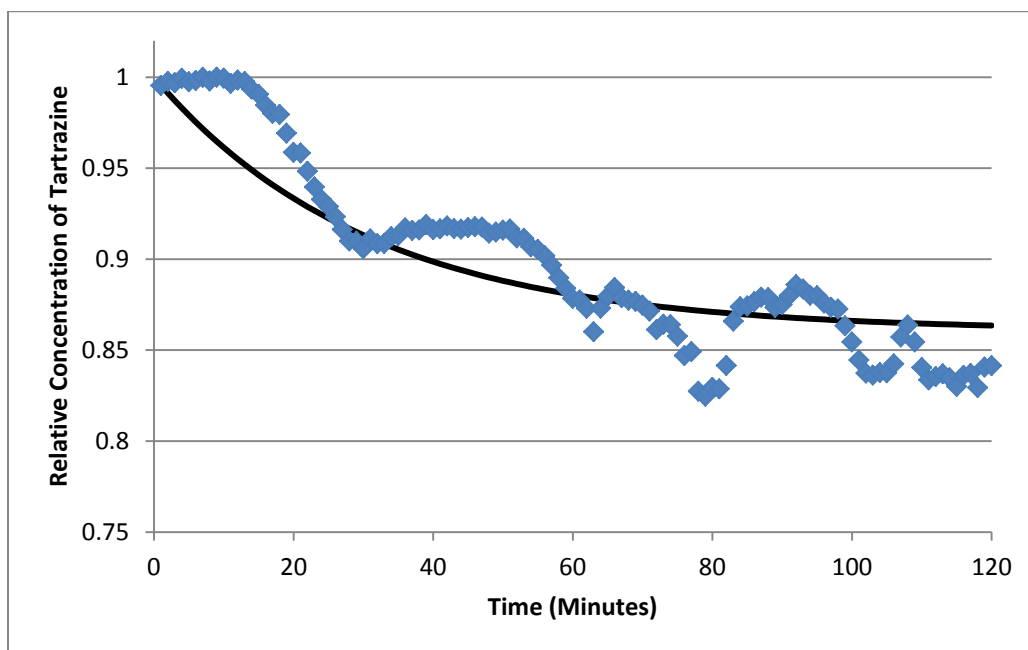
Figure 16: Thin Teflon, Across LED Caps Trial 2, Low Power
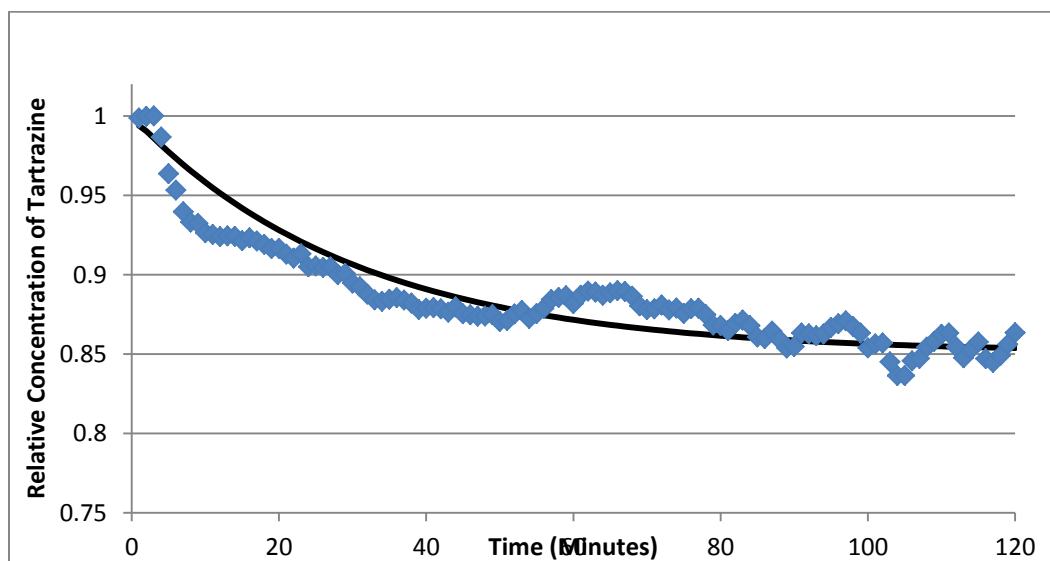
Figure 17: Thin Teflon, Across LED Caps Trial 2, Low Power
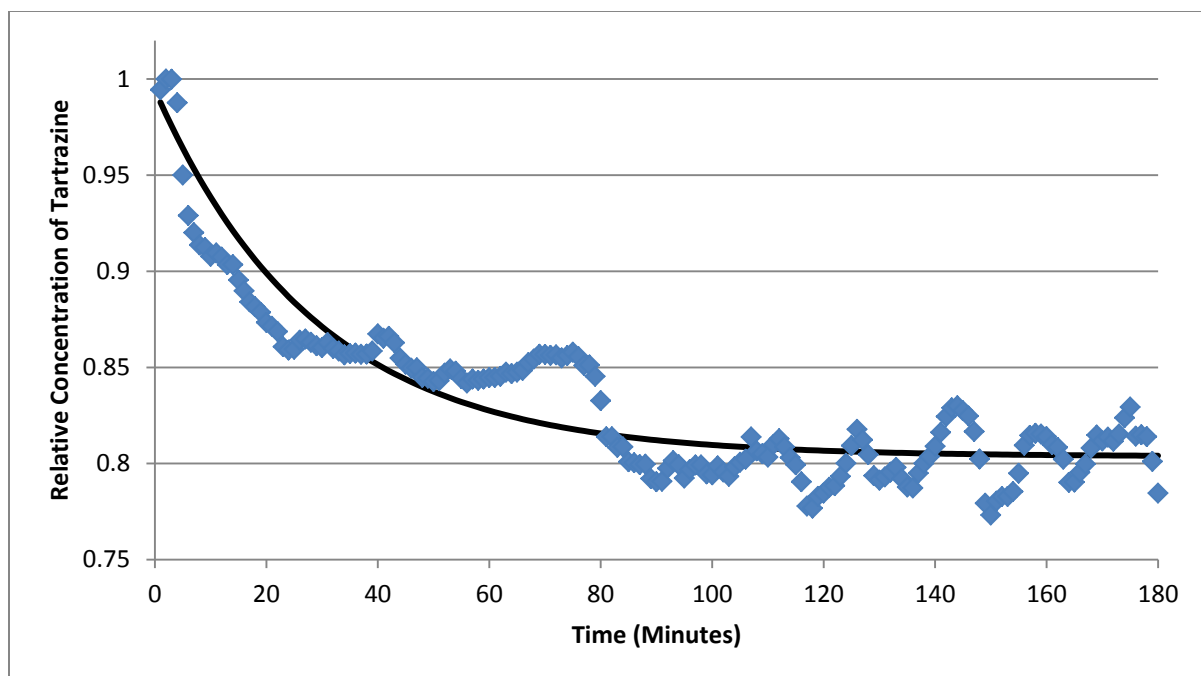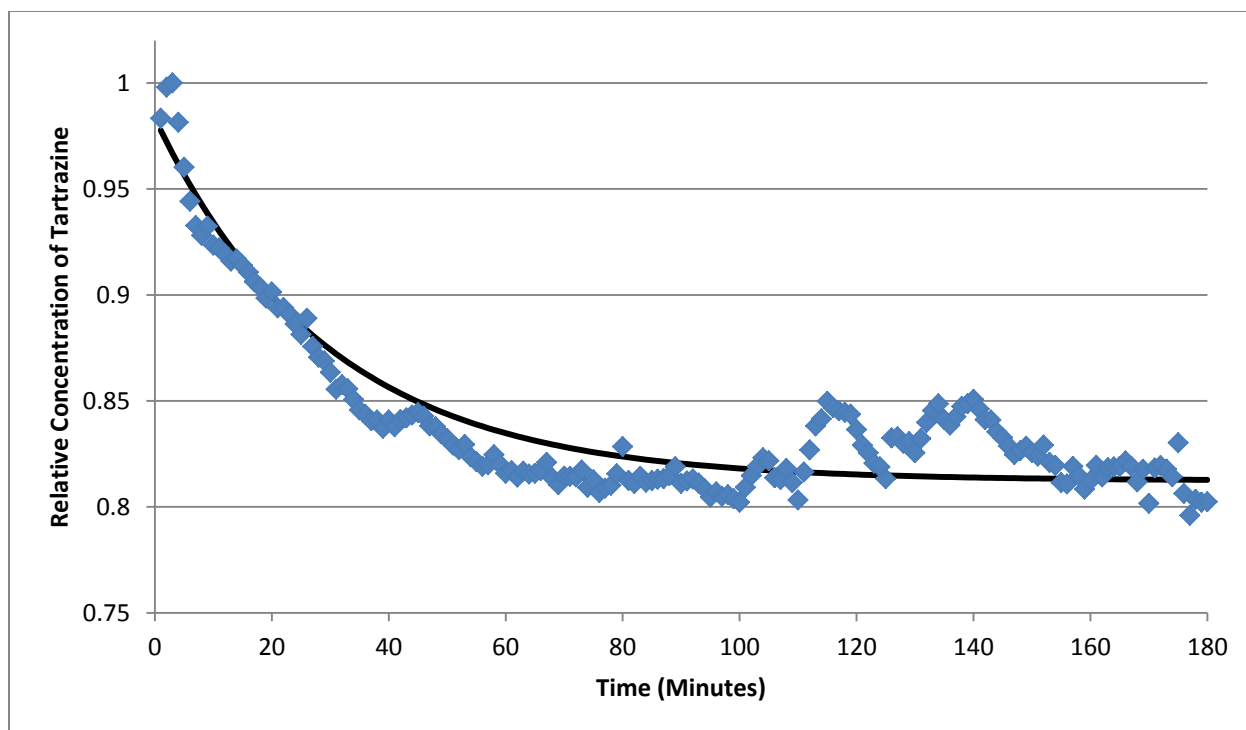
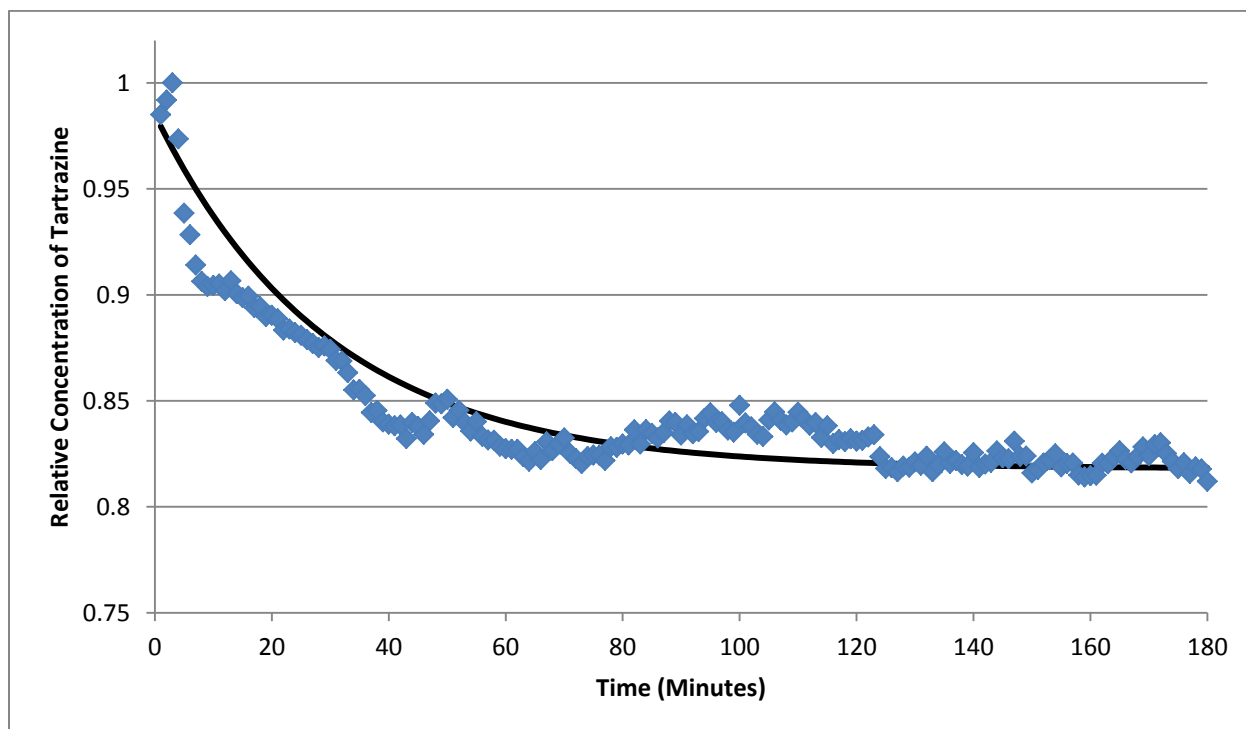Figure 18: Thin Teflon, Across LED Caps Trial 3, Low Power
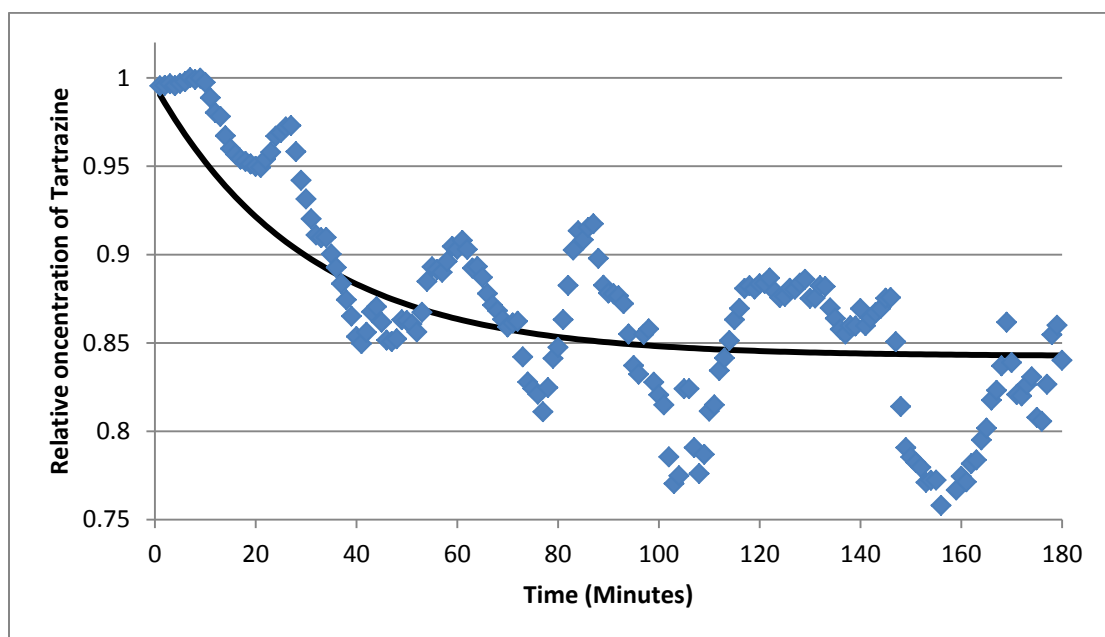
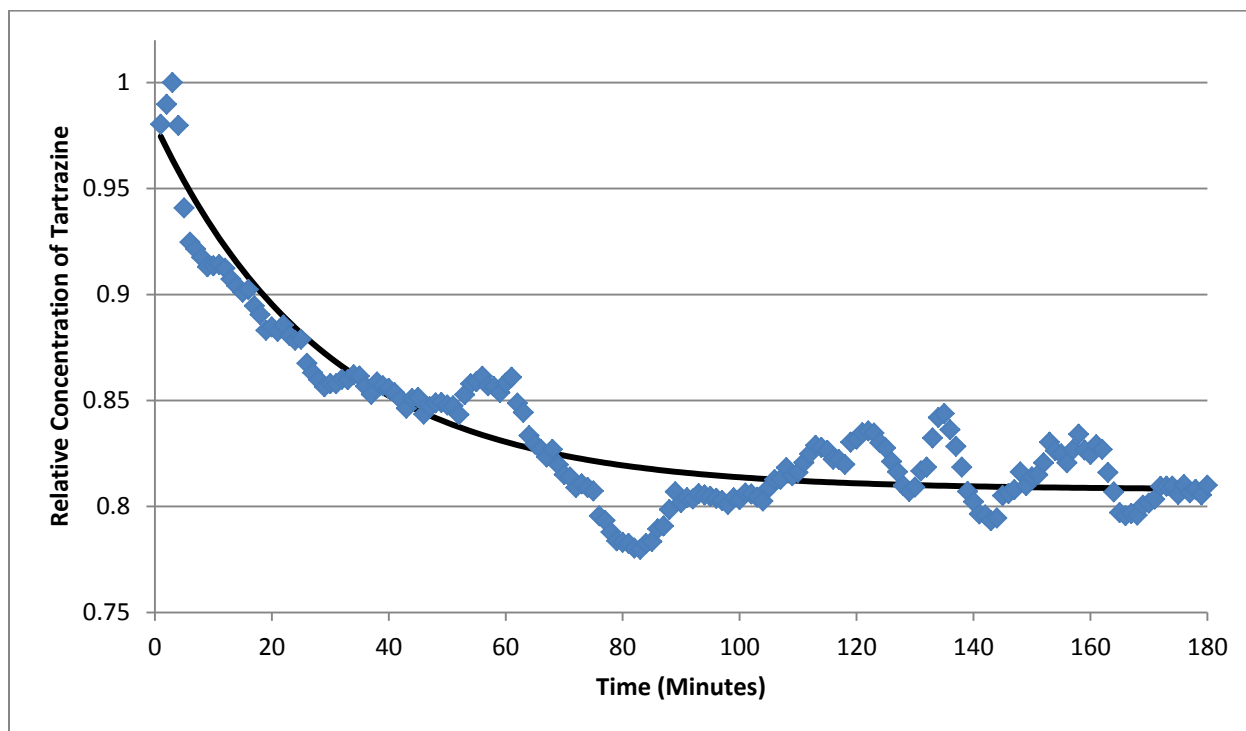Figure 19: Thin Teflon, Swirl Caps Trial 1, Low Power
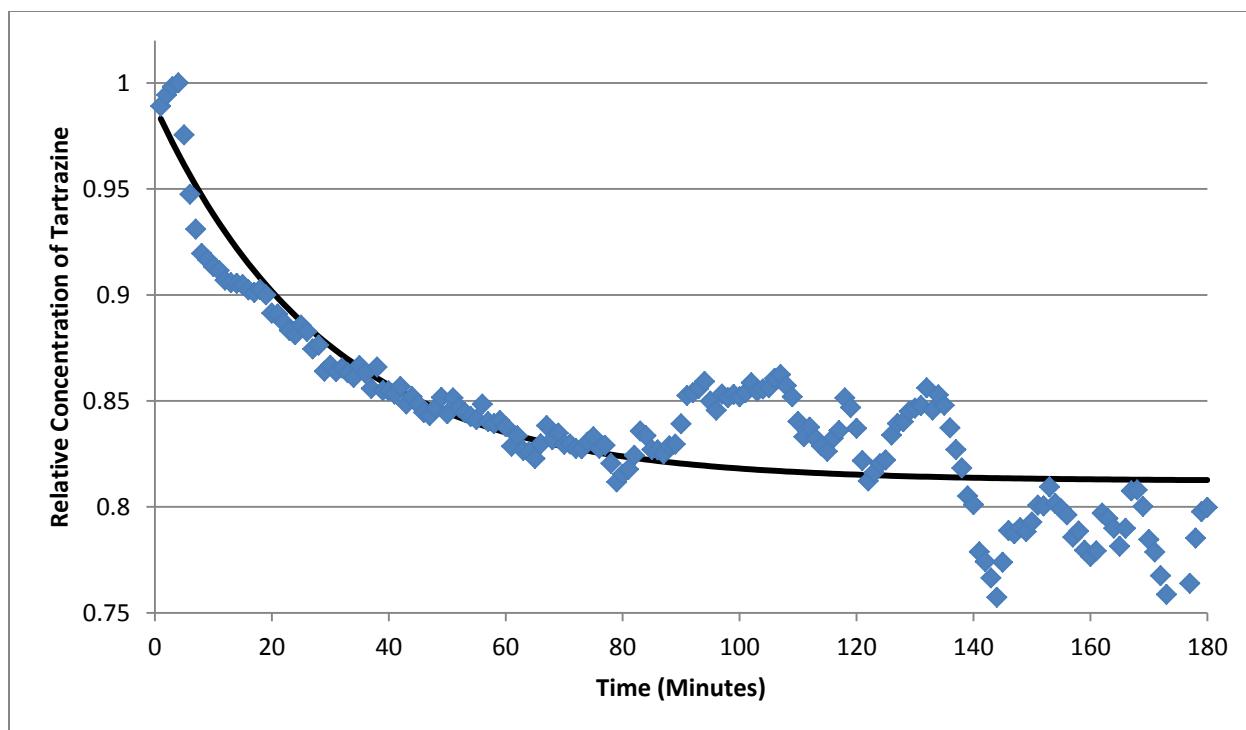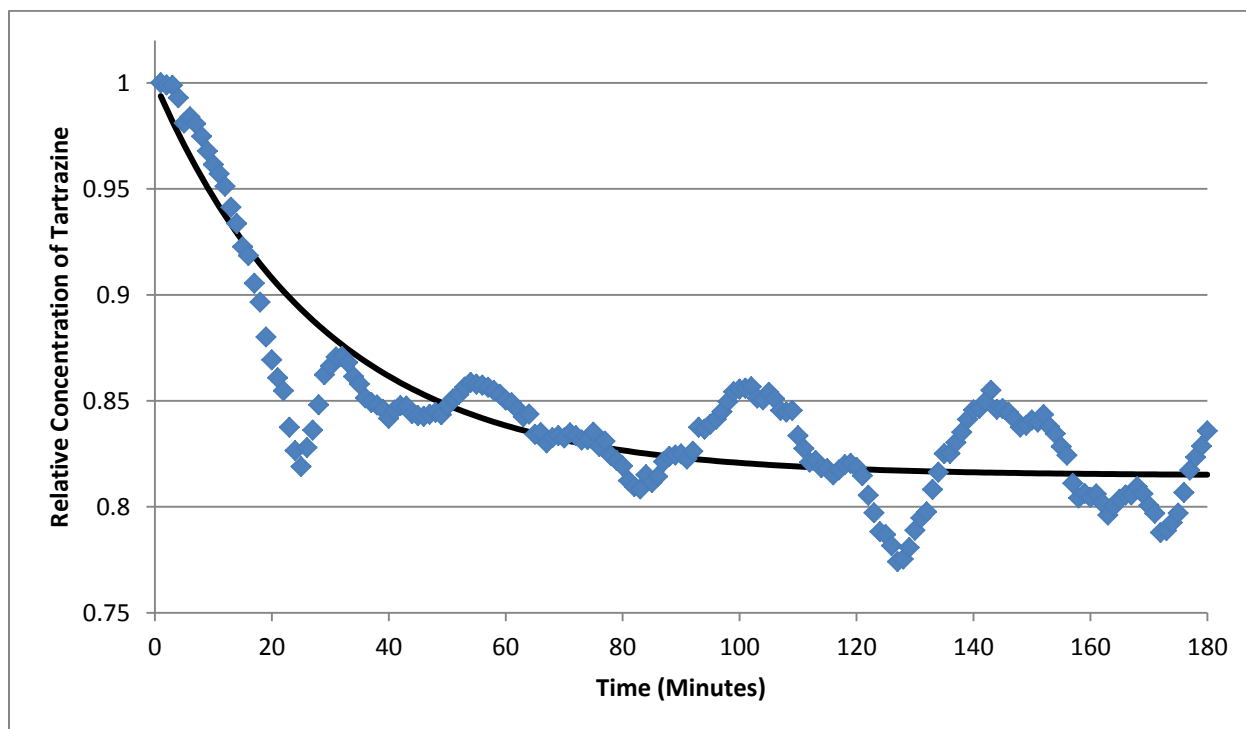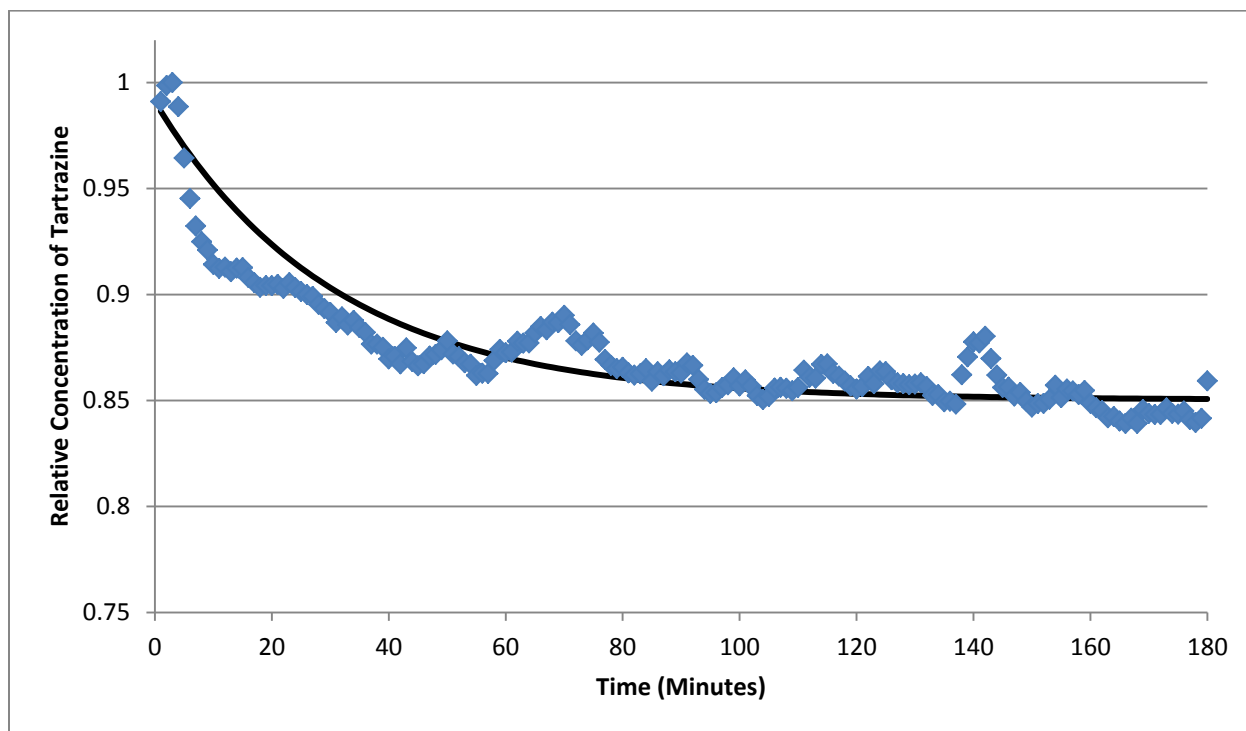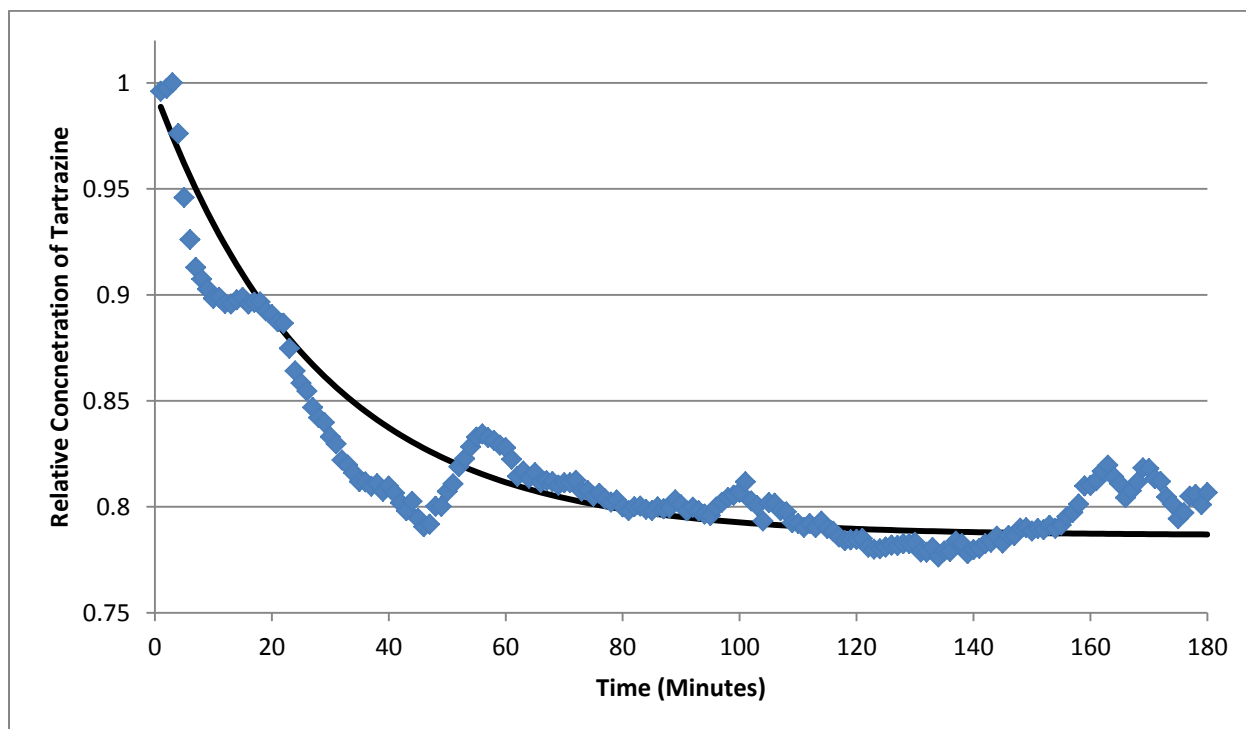
Figure 20: Thin Teflon, Swirl Caps, Trial 2, Low Power
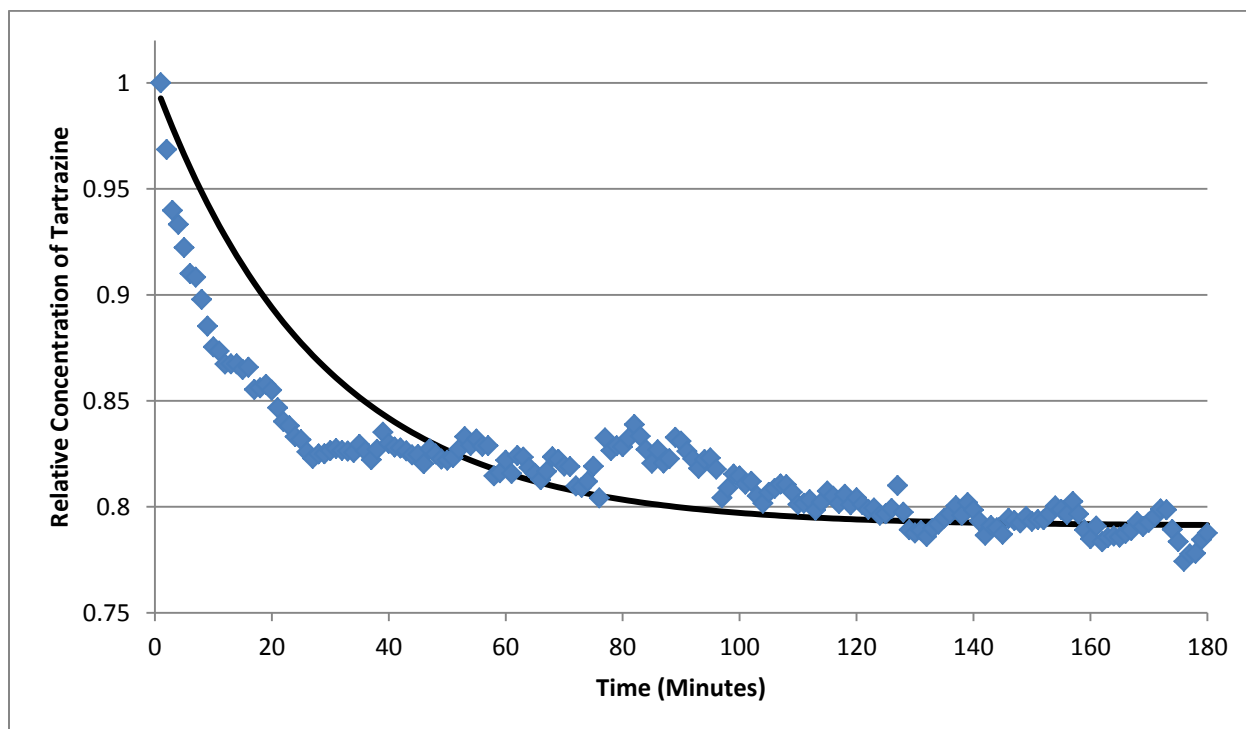
Figure 21: Thin Teflon, Swirl Caps, Trial 3, Low Power
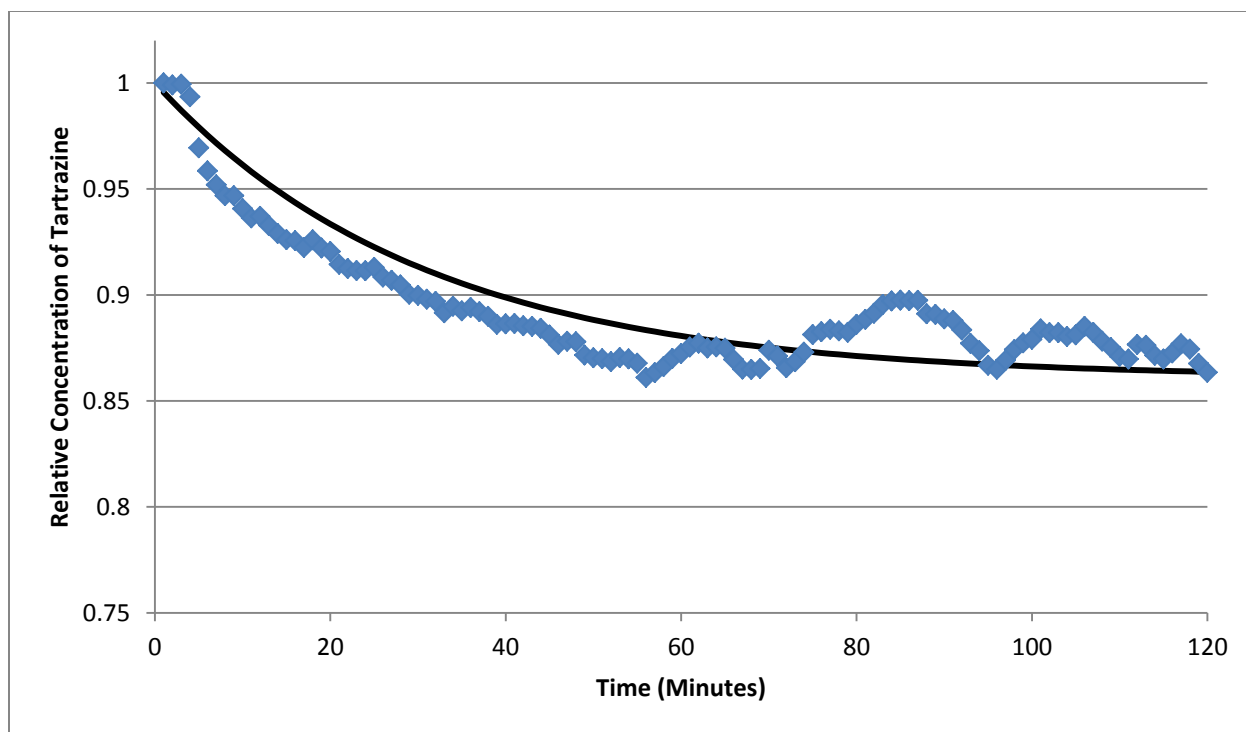
Figure 22: Steel, Across LED Caps, Trial 3, Low Power
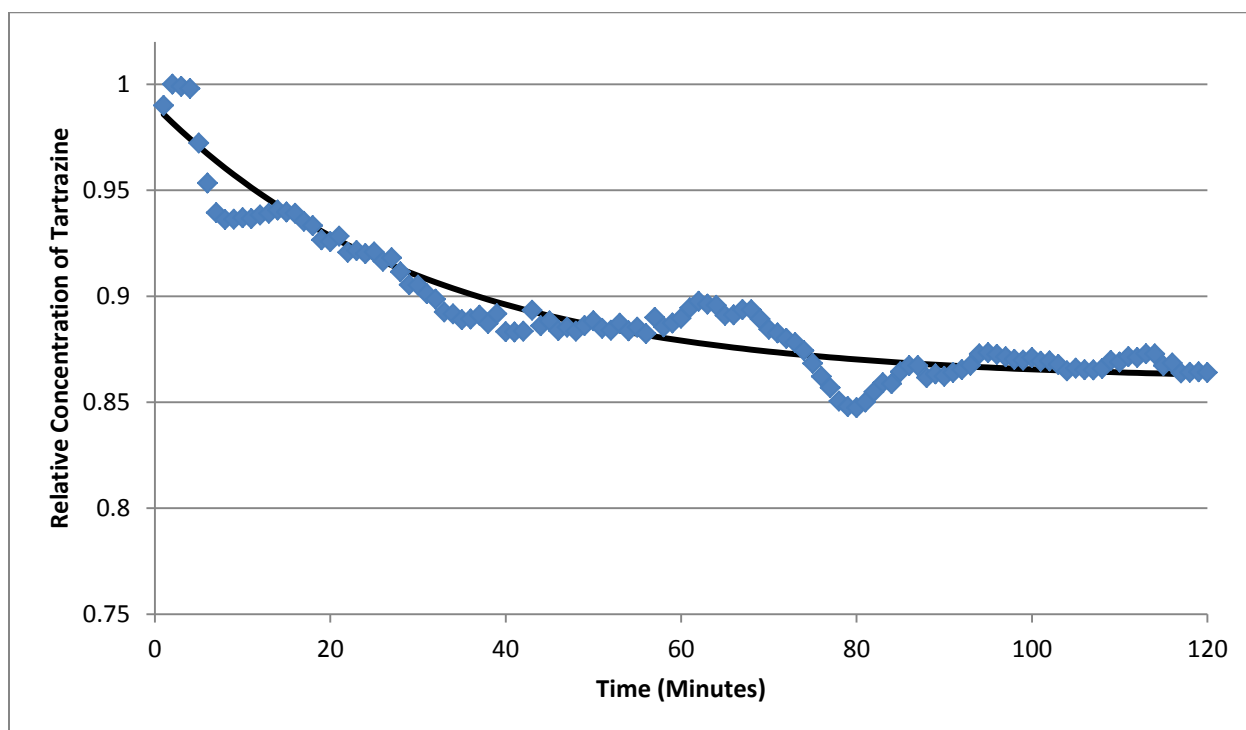
Figure 23: Steel, Across LED Caps, Trial 2, Low Power

Figure 24: Steel, Across LED Caps, Trial 3, Low Power

Figure 25: Steel, Swirl Caps, Trial 1, Low Power

57

Figure 26: Steel, Swirl Caps, Trial 2, Low Power

Figure 27: Steel, Swirl Caps, Trial 3, Low Power

58

Figure 28: Med Teflon, Across LED Caps, Trial 1, Low Power
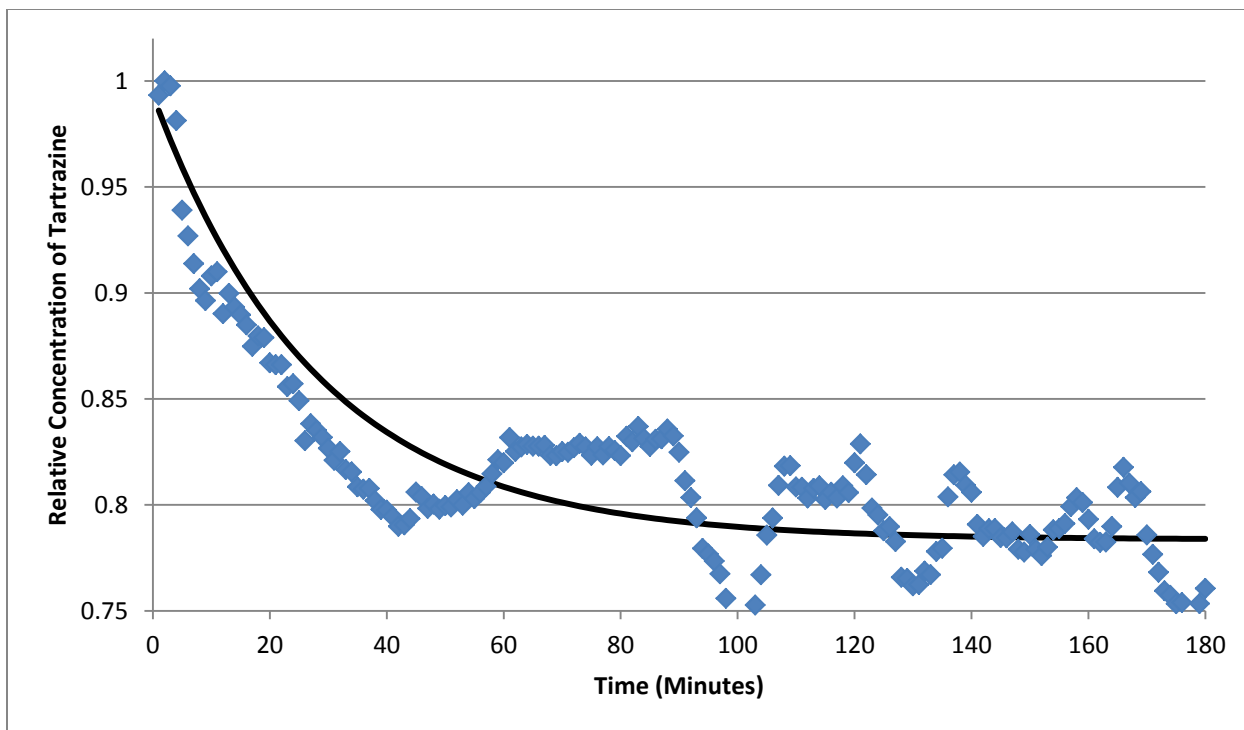

Figure 29: Med Teflon, Across LED Caps, Trial 2, Low Power

59

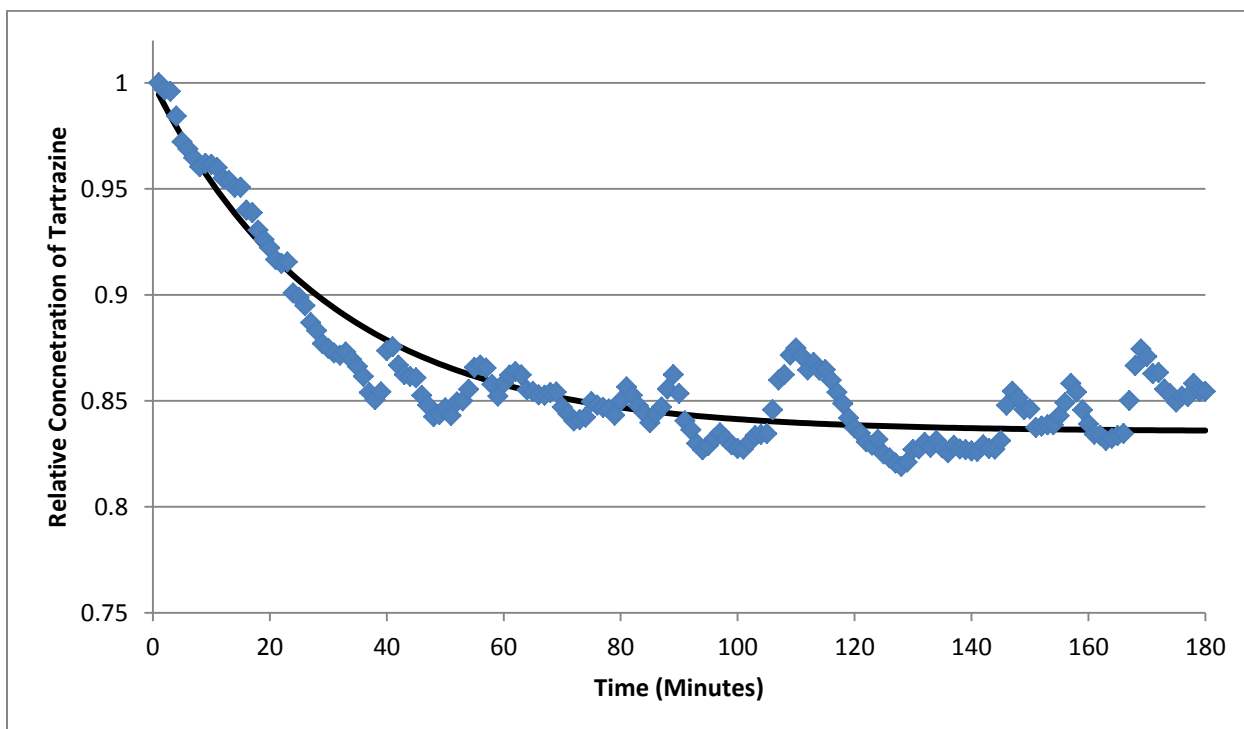Figure 30: Med Teflon, Across LED Caps, Trial 3, Low Power

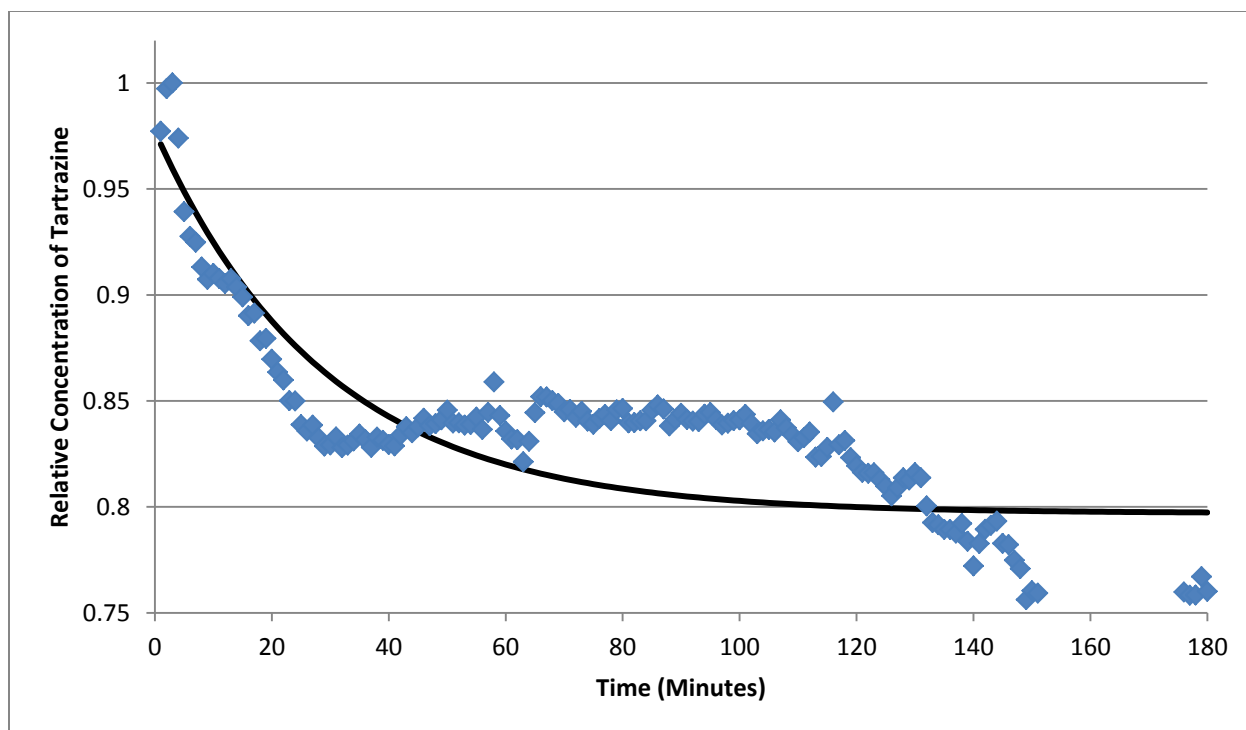Figure 31: Thick Teflon, Across LED Caps, Trial 1, Low Power

60

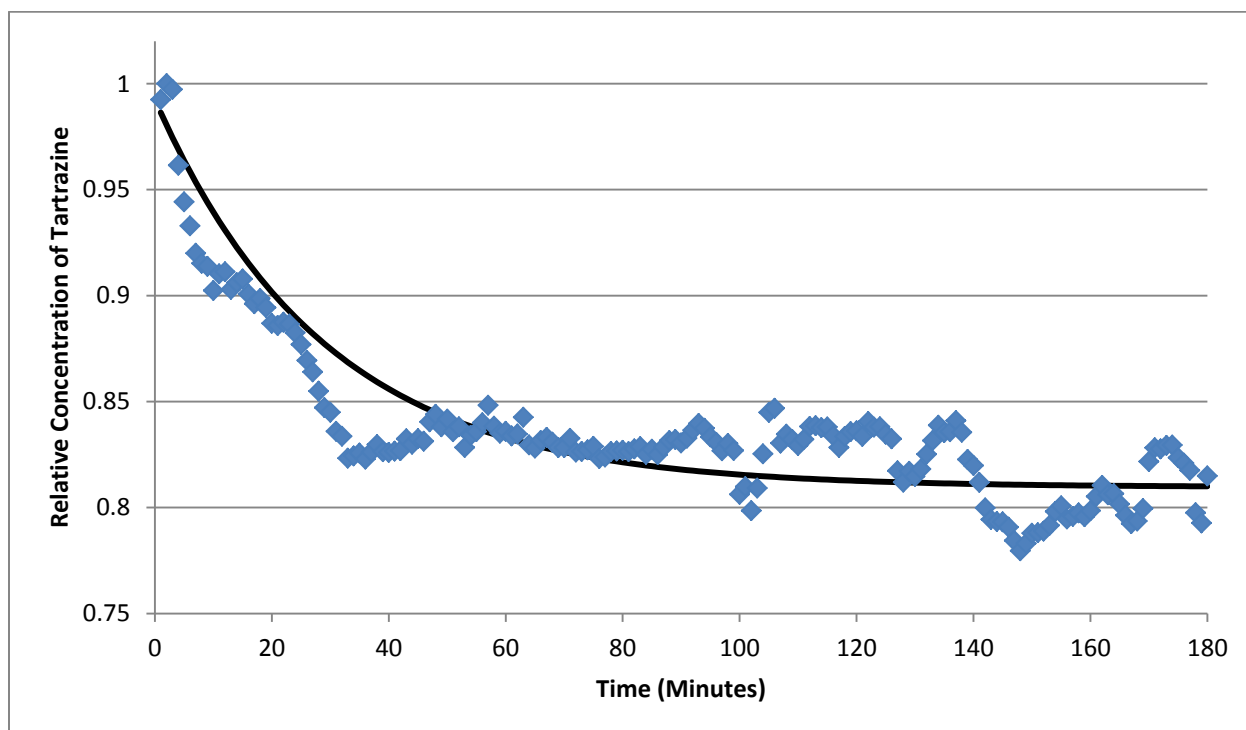Figure 32: Thick Teflon, Across Caps, Trial 2, Low Power

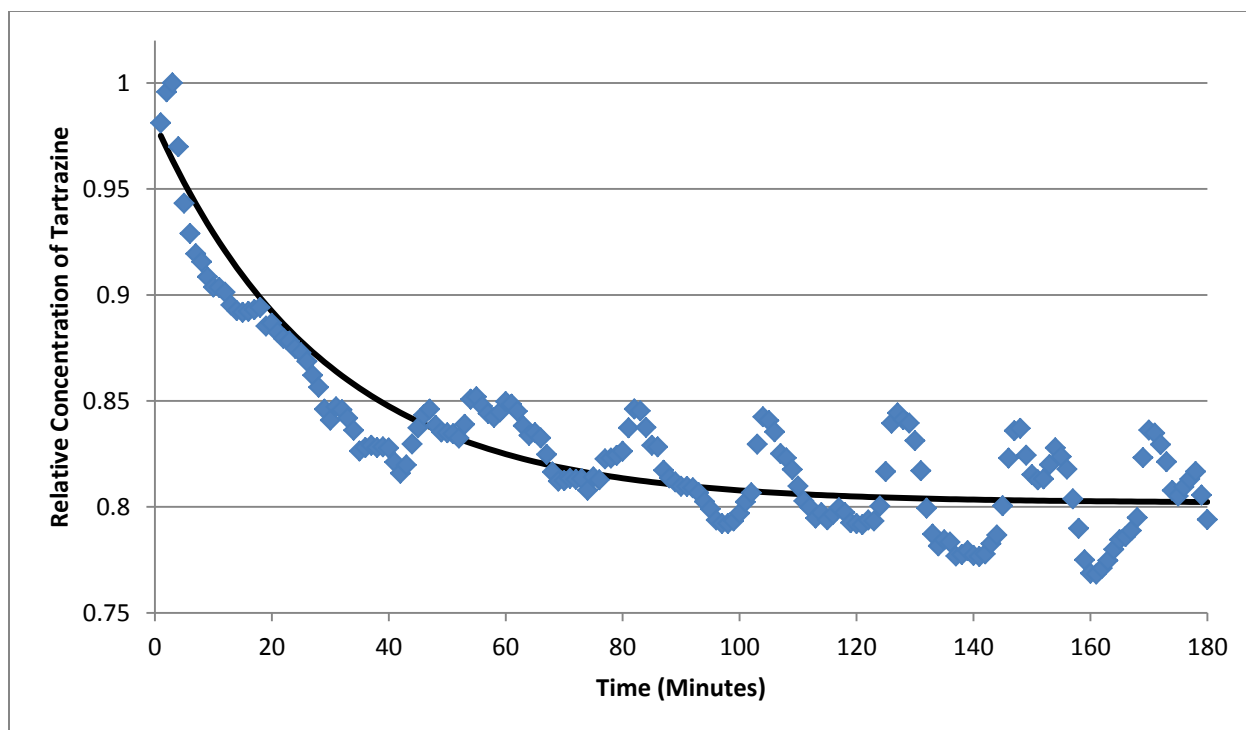Figure 33: Thick Teflon, Across LED Caps, Trial 3, Low Power

61

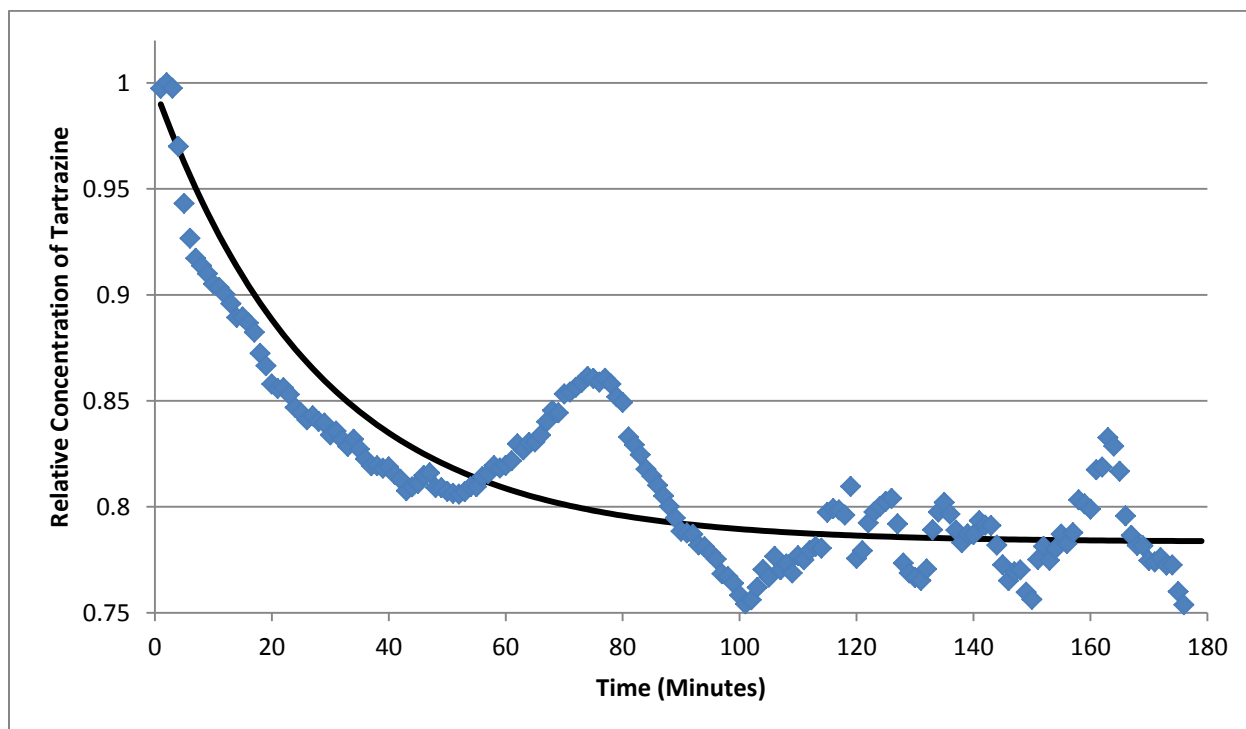Figure 34: Thick Teflon, Swirl Caps, Trial 1, Low Power

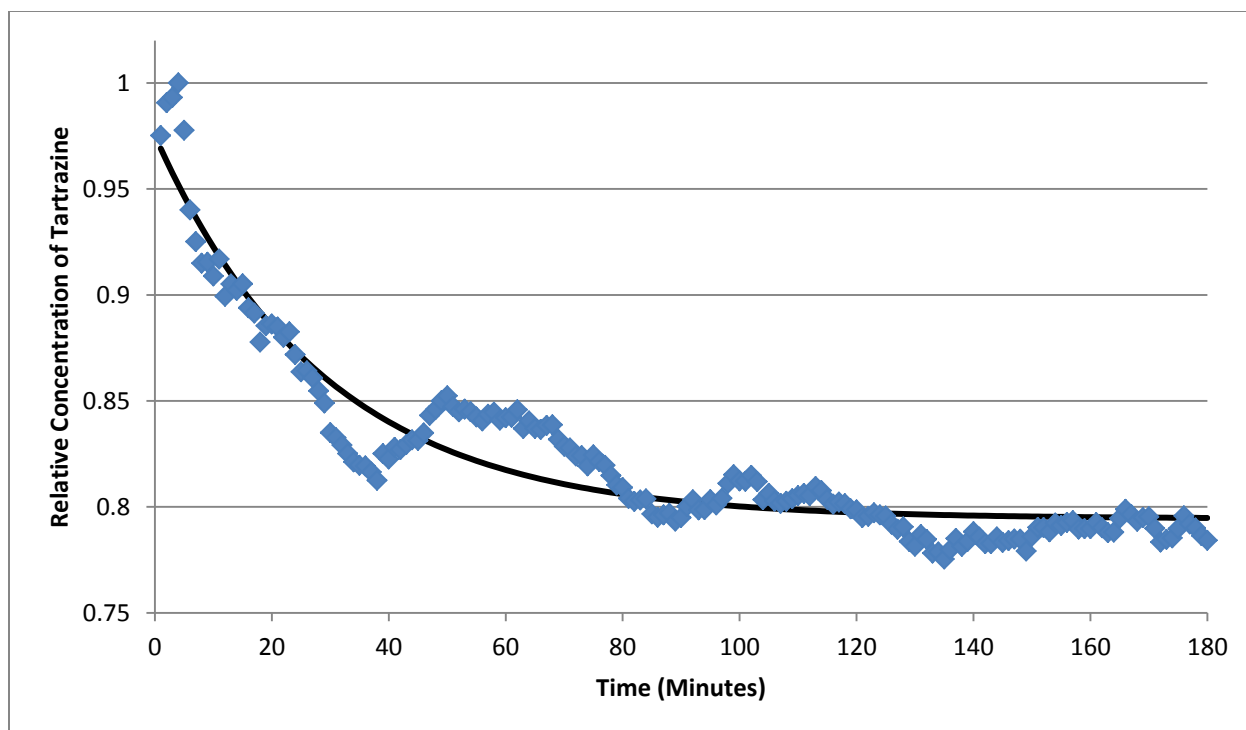Figure 35: Thick Teflon, Swirl Caps, Trial 2, Low Power

Figure 36: Thick Teflon, Swirl Caps, Trial 3, Low Power
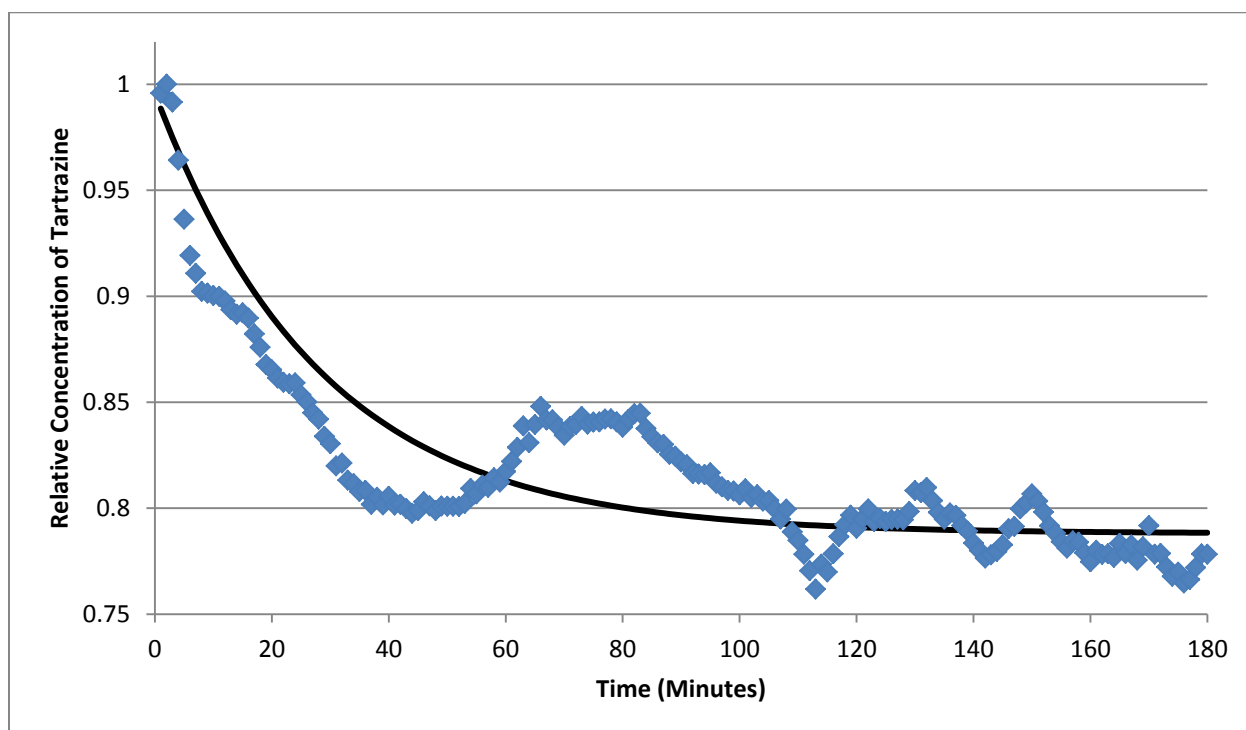

Figure 37: Med Teflon, Swirl Caps, Trial 1, Low Power

63
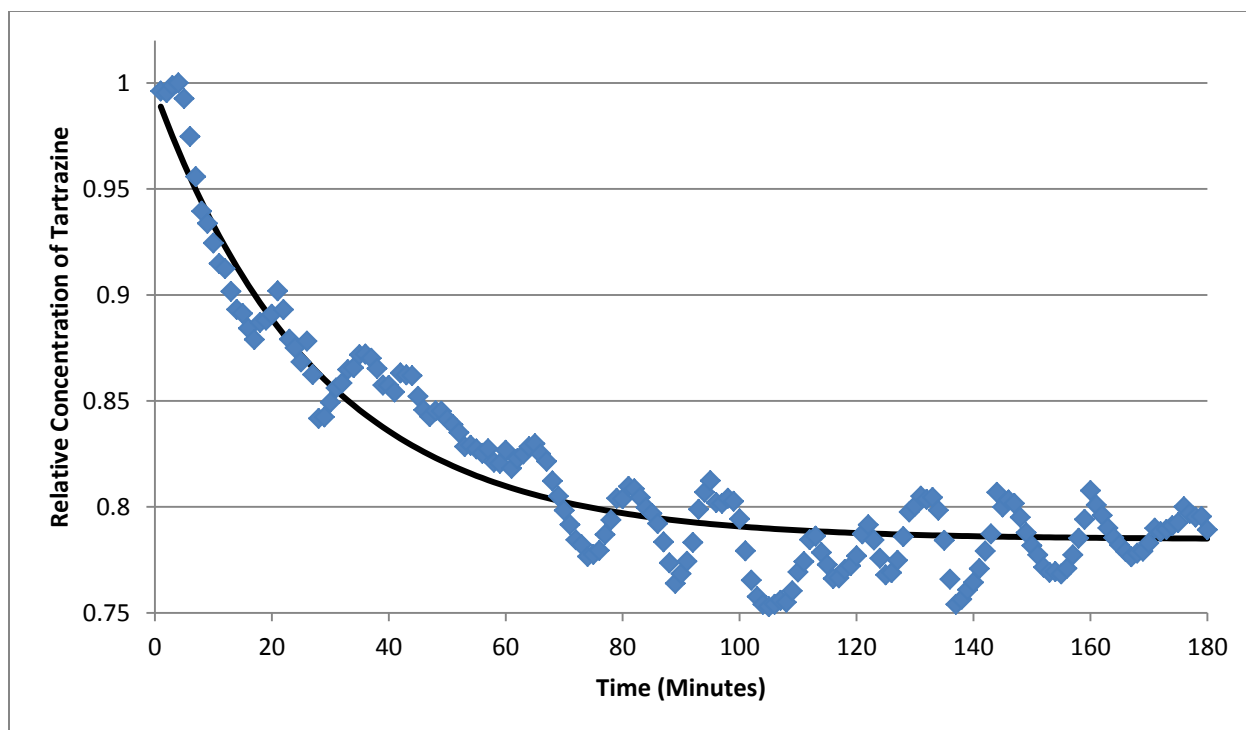
Figure 38: Med Teflon, Swirl Caps, Trial 2, Low Power

Figure 39: Med Teflon, Swirl Caps, Trial 3, Low Power

Figure 40: Steel, Swirl Caps, Trial 1, High Power
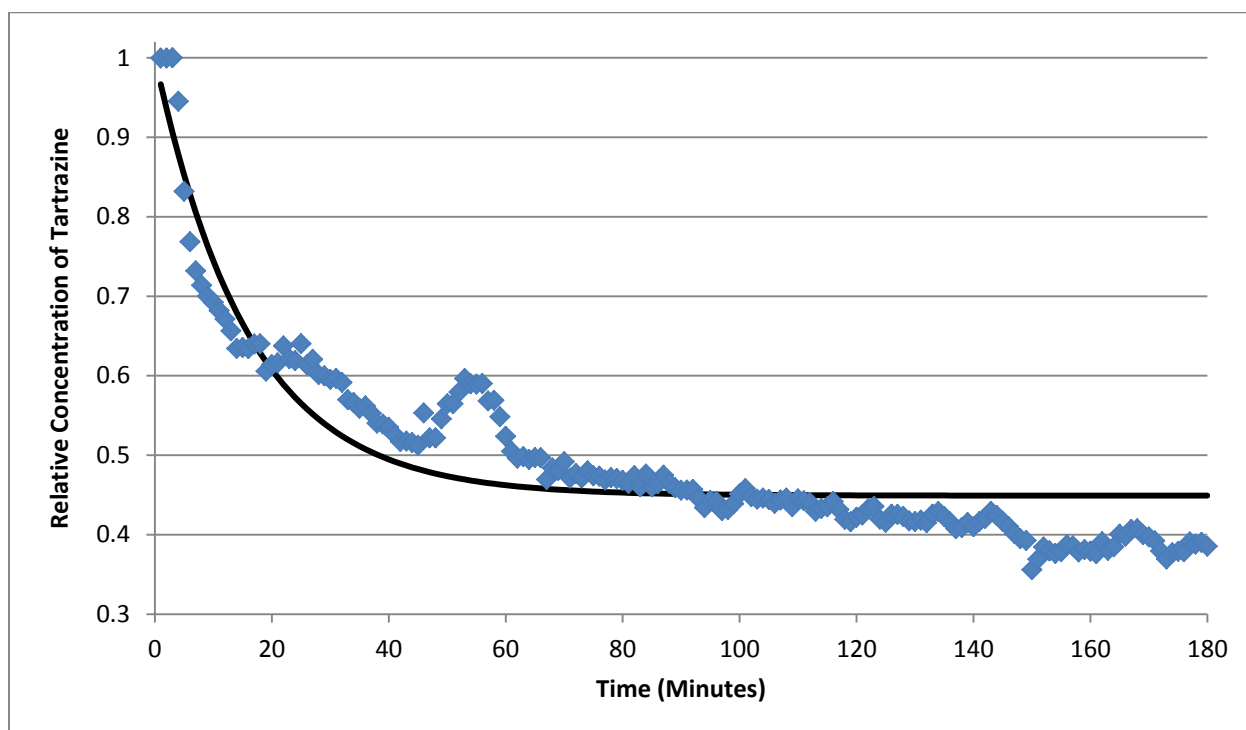
Figure 41: Steel, Swirl Caps, Trial 2, High Power
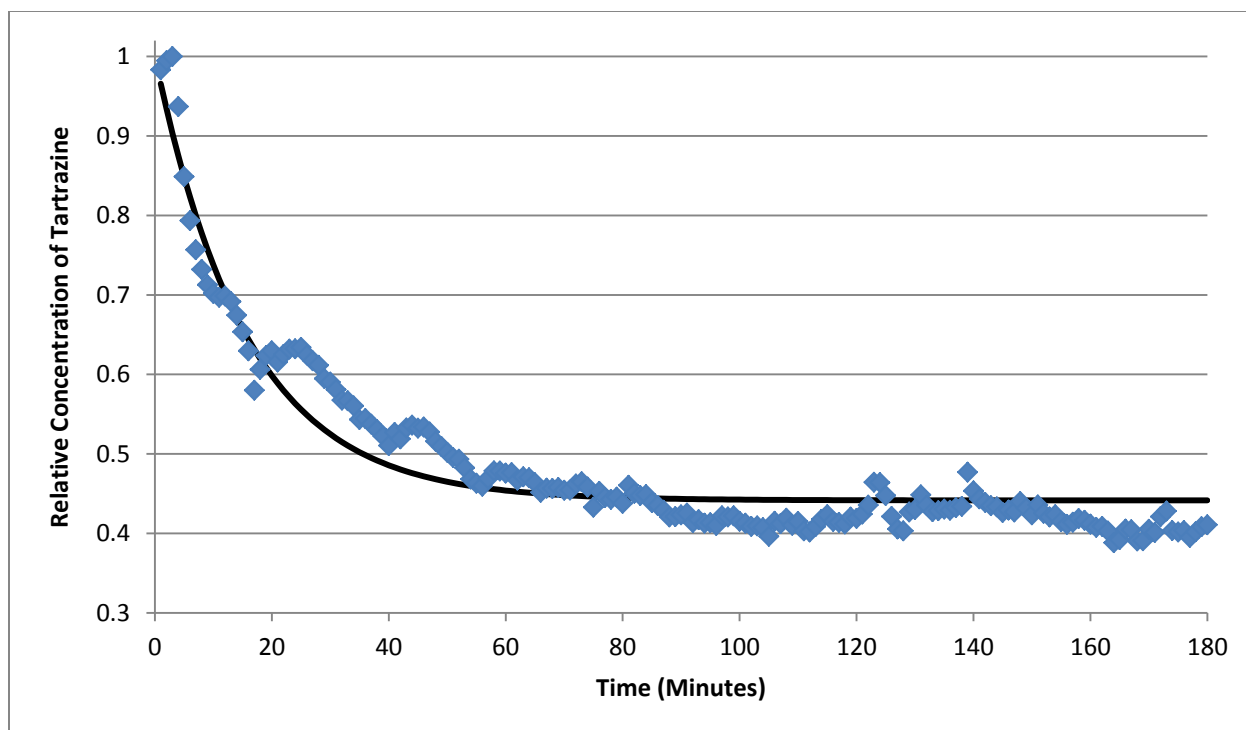
Figure 42: Steel, Swirl Caps, Trial 3, High Power
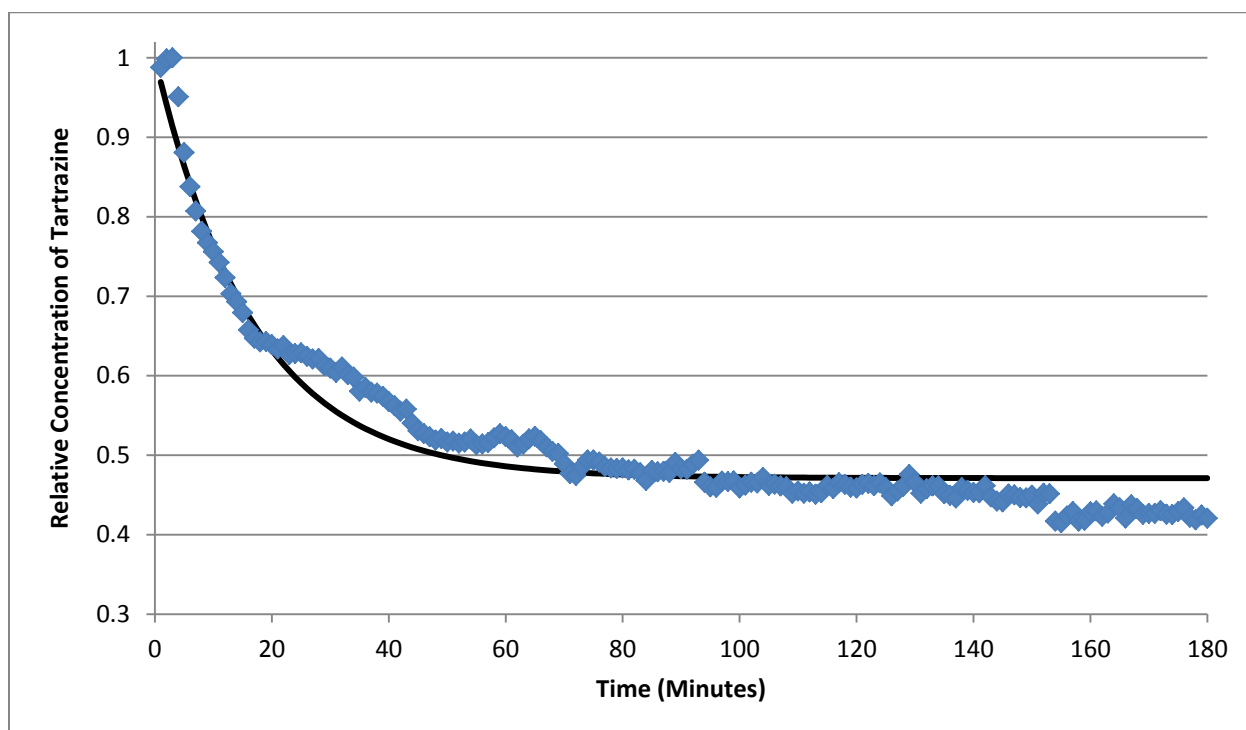
Figure 43: Steel, Across LED Caps, Trial 1, High Power

Figure 44: Steel, Across LED Caps, Trial 2, High Power
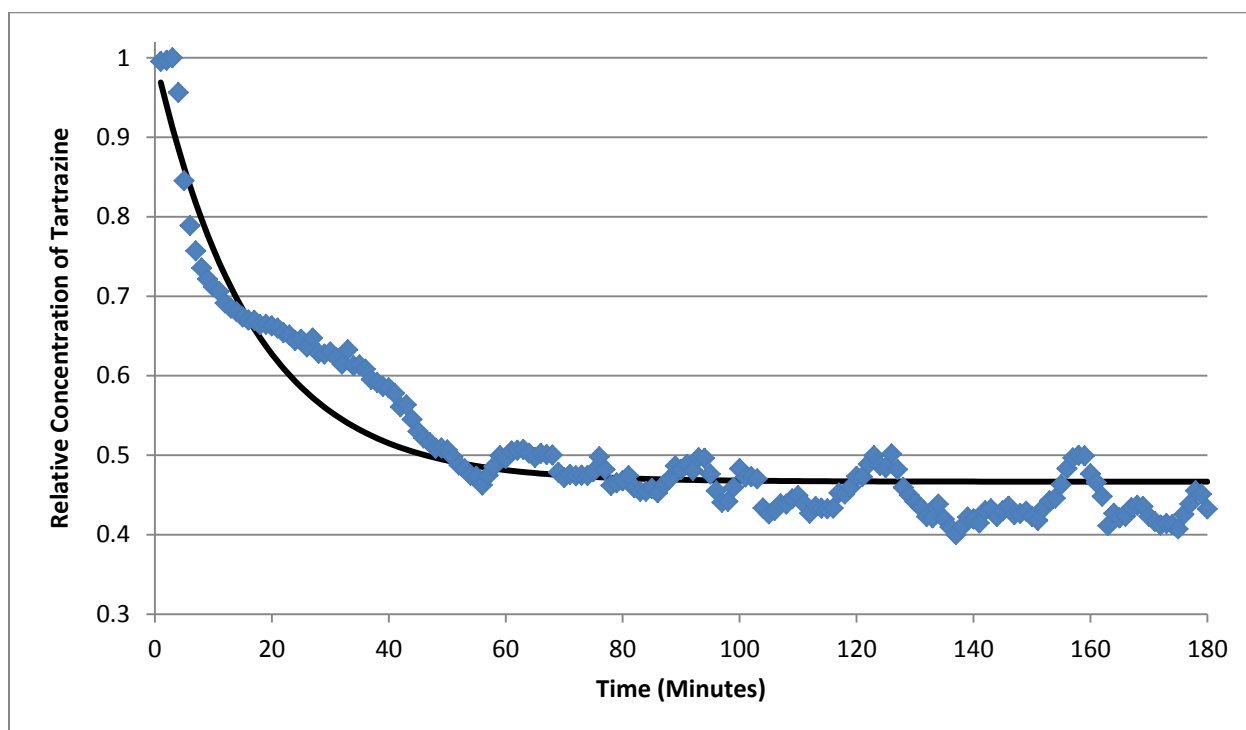
Figure 45: Steel, Across LED Caps, Trial 3, High Power

Figure 46: Thin Teflon, Swirl Caps, Trial 1, High Power

Figure 47: Thin Teflon, Swirl Caps, Trial 2, High Power

Figure 48: Thin Teflon, Swirl Caps, Trial 3, High Power

Figure 49: Thin Teflon, Across LED Caps, Trial 1, High Power

69

Figure 50: Thin Teflon, Across LED Caps, Trial 2, High Power
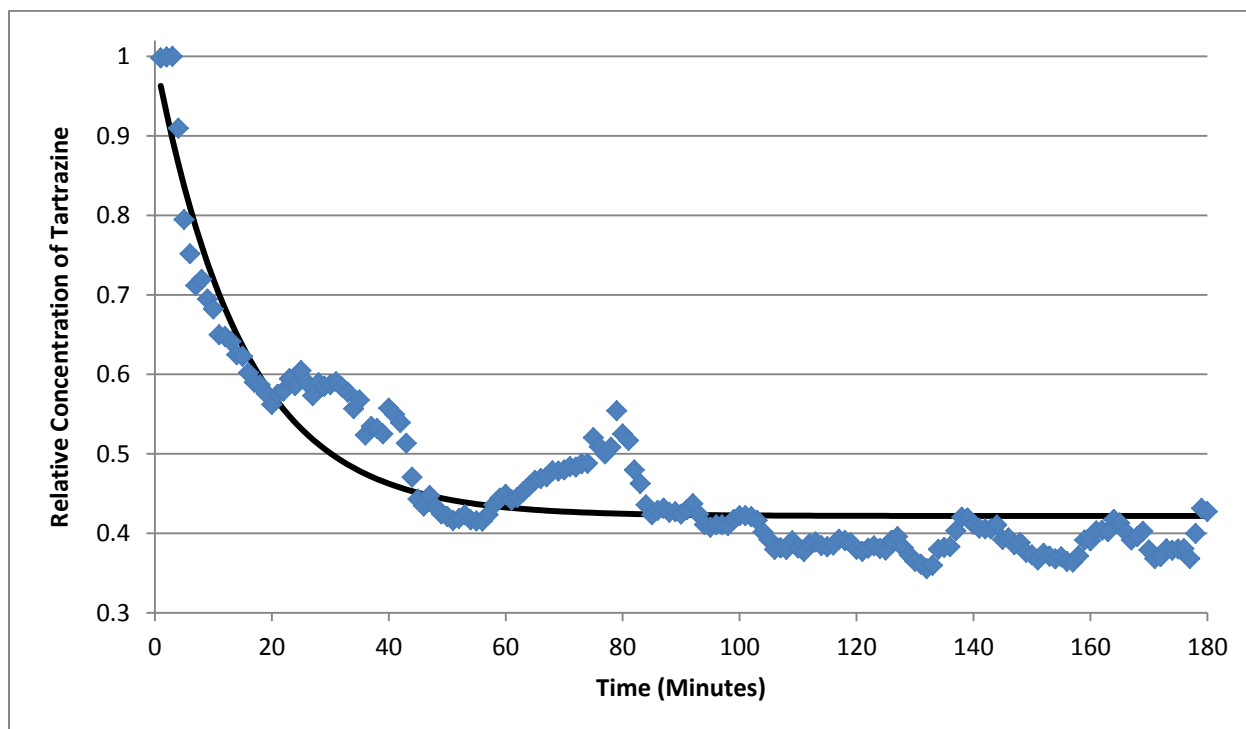
Figure 51: Teflon, Across LED Caps, Trial 3, High Power
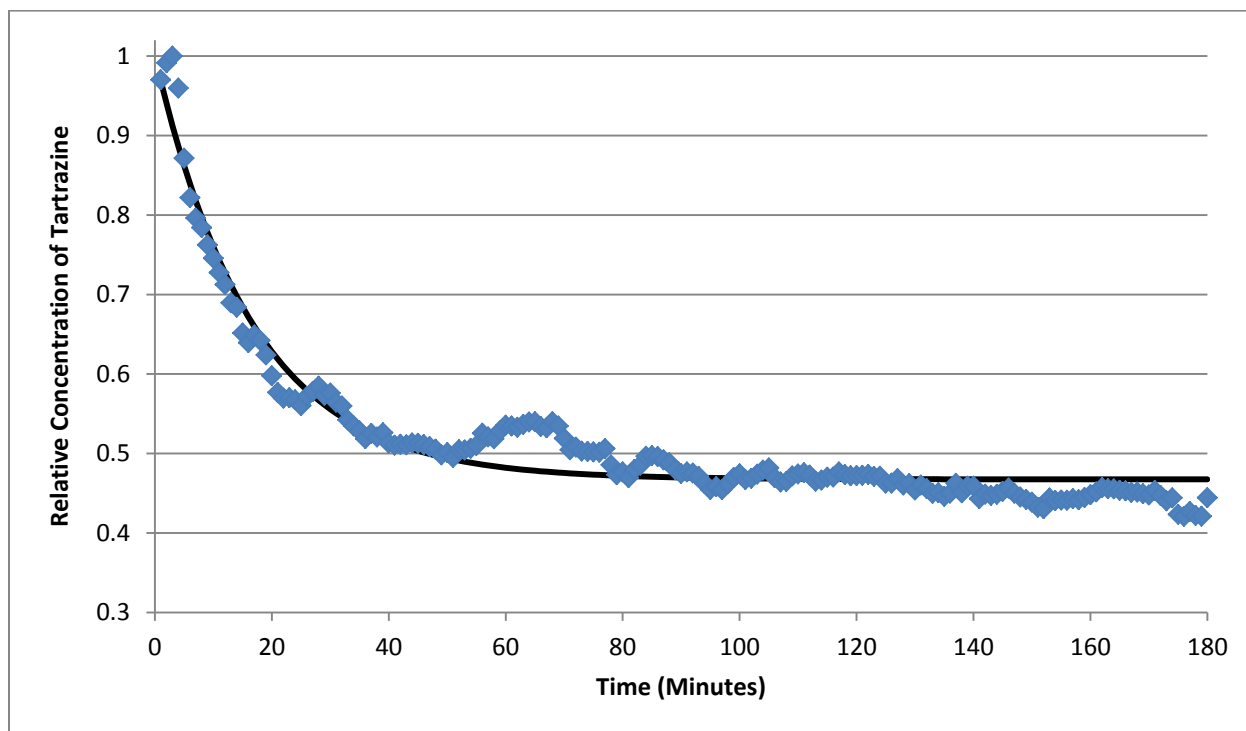
Figure 52: Med Teflon, Swirl Caps, Trial 1, High Power
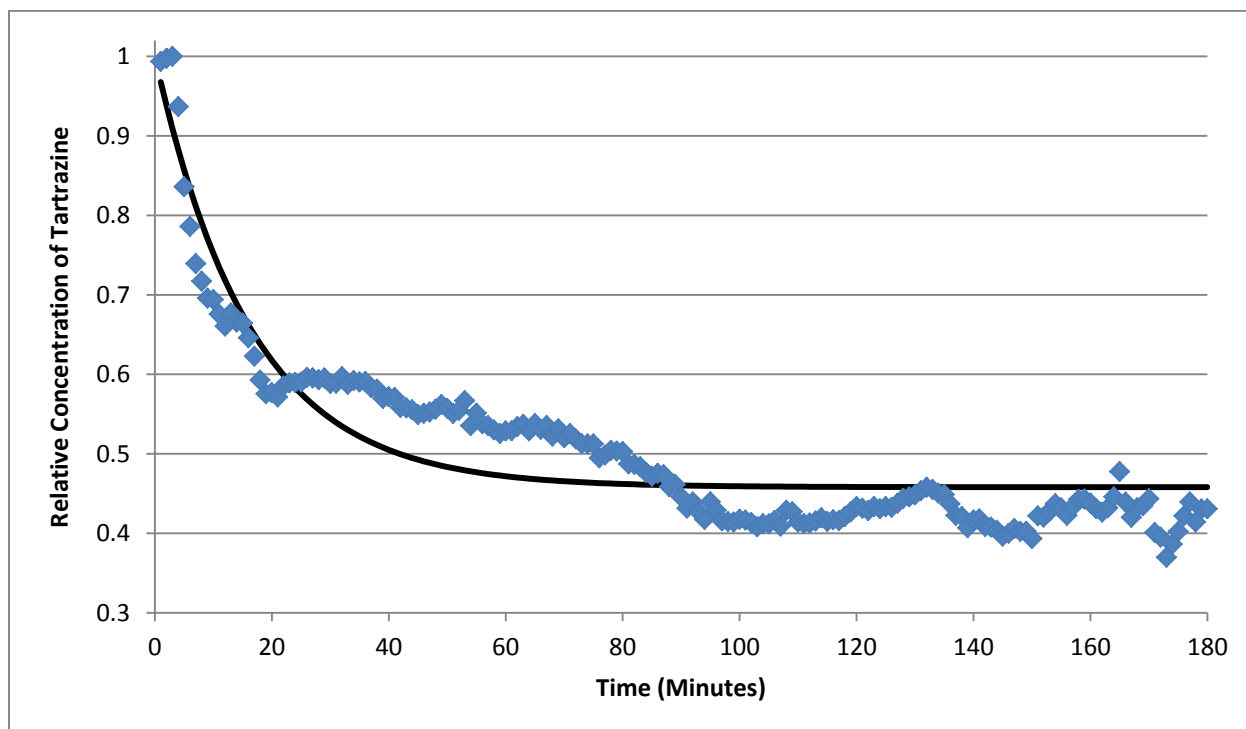
Figure 53: Med Teflon, Swirl Caps, Trial 2, High Power
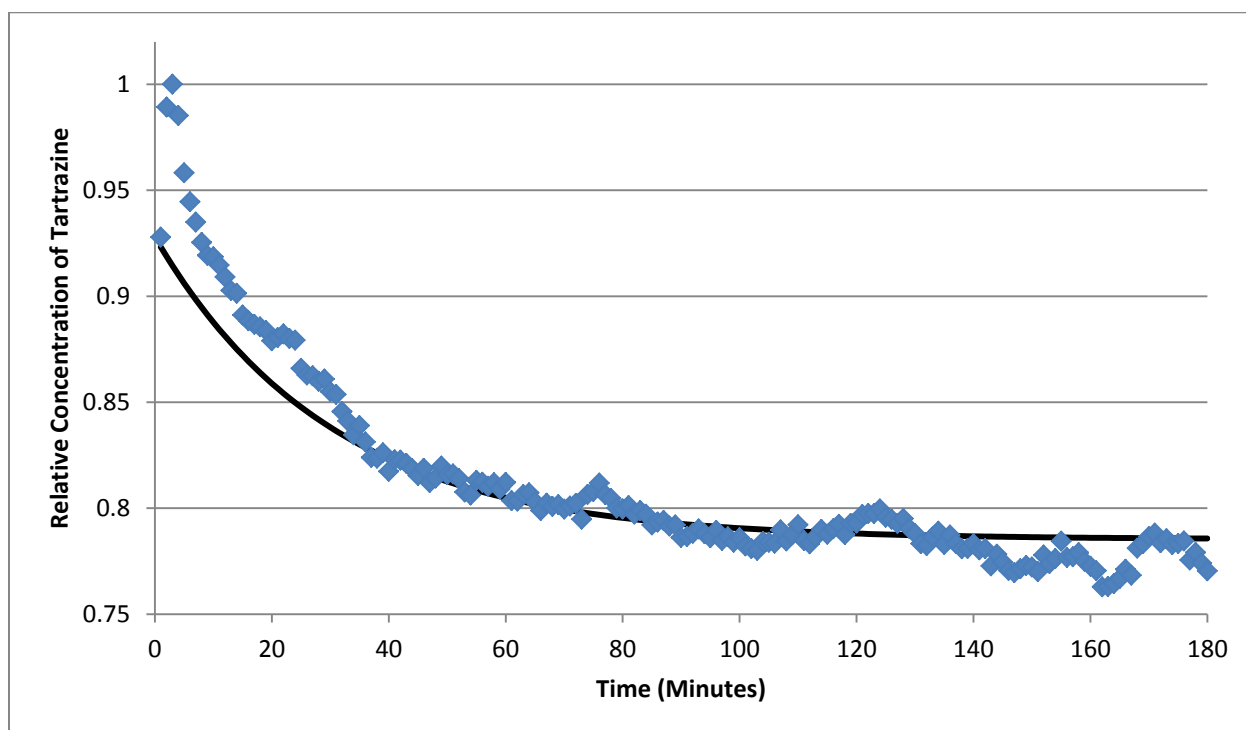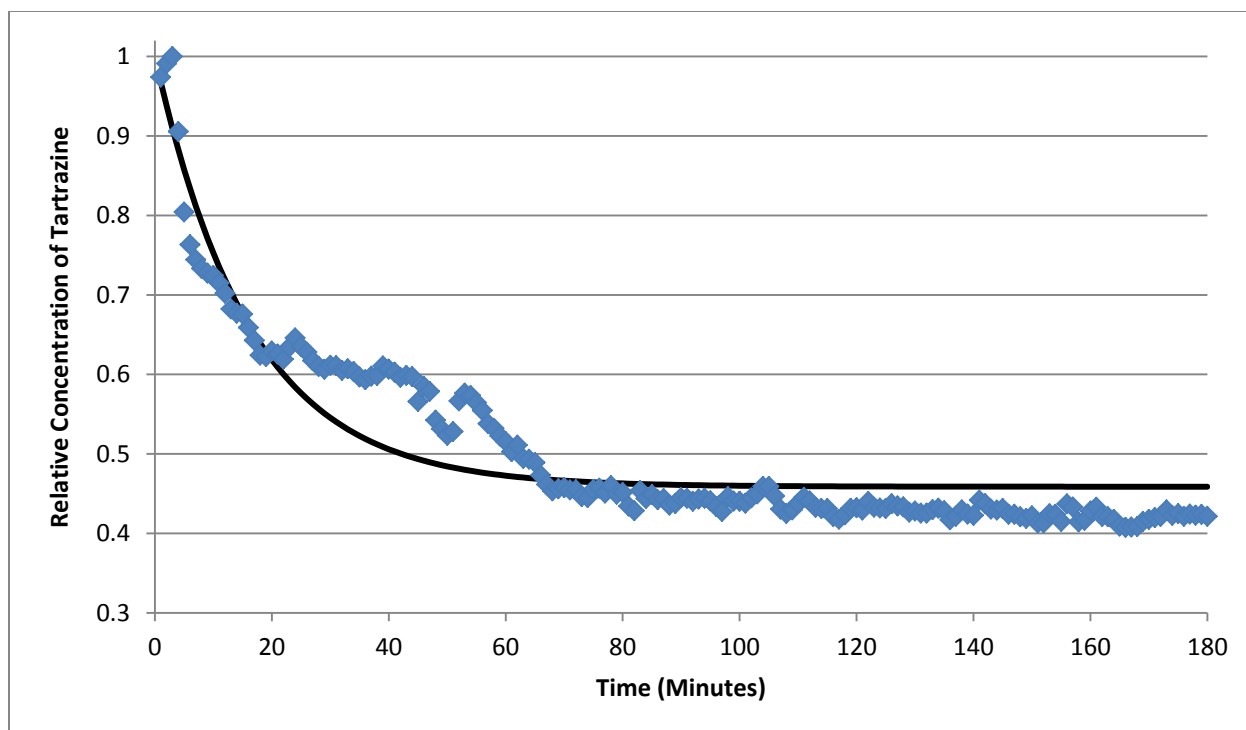
71
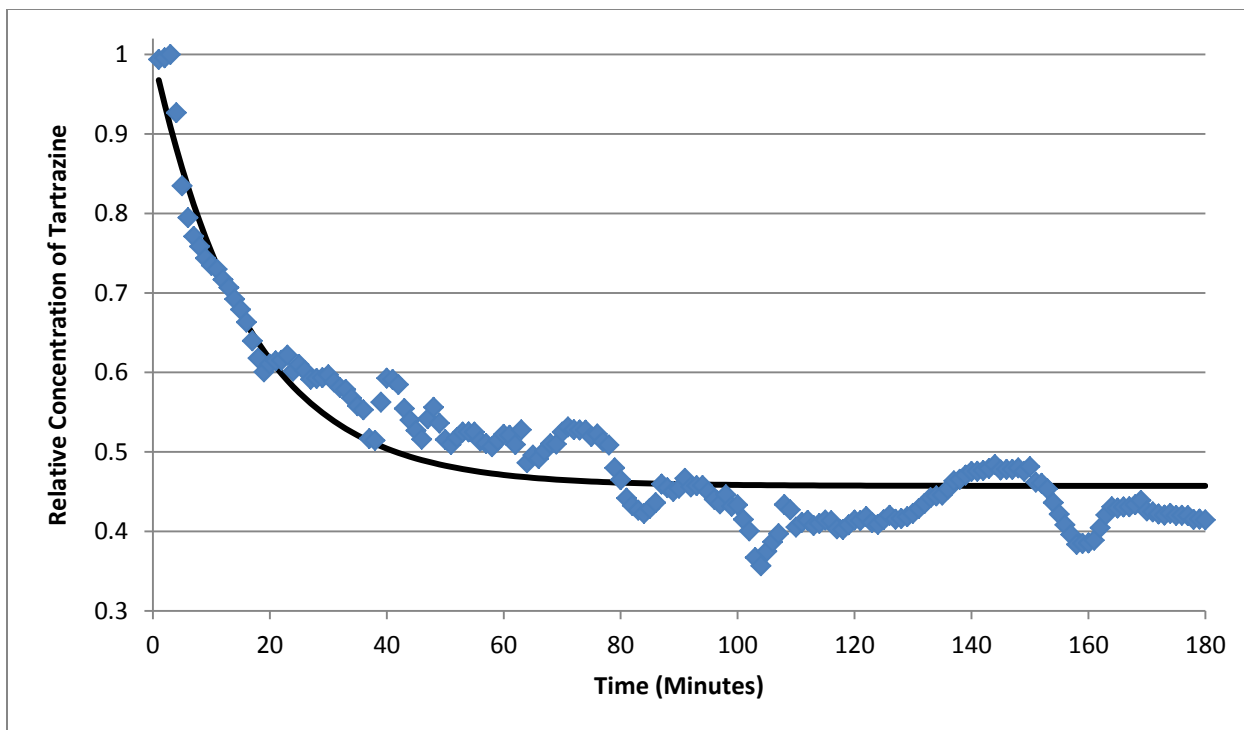
Figure 54: Med Teflon, Swirl Caps, Trial 3, High Power
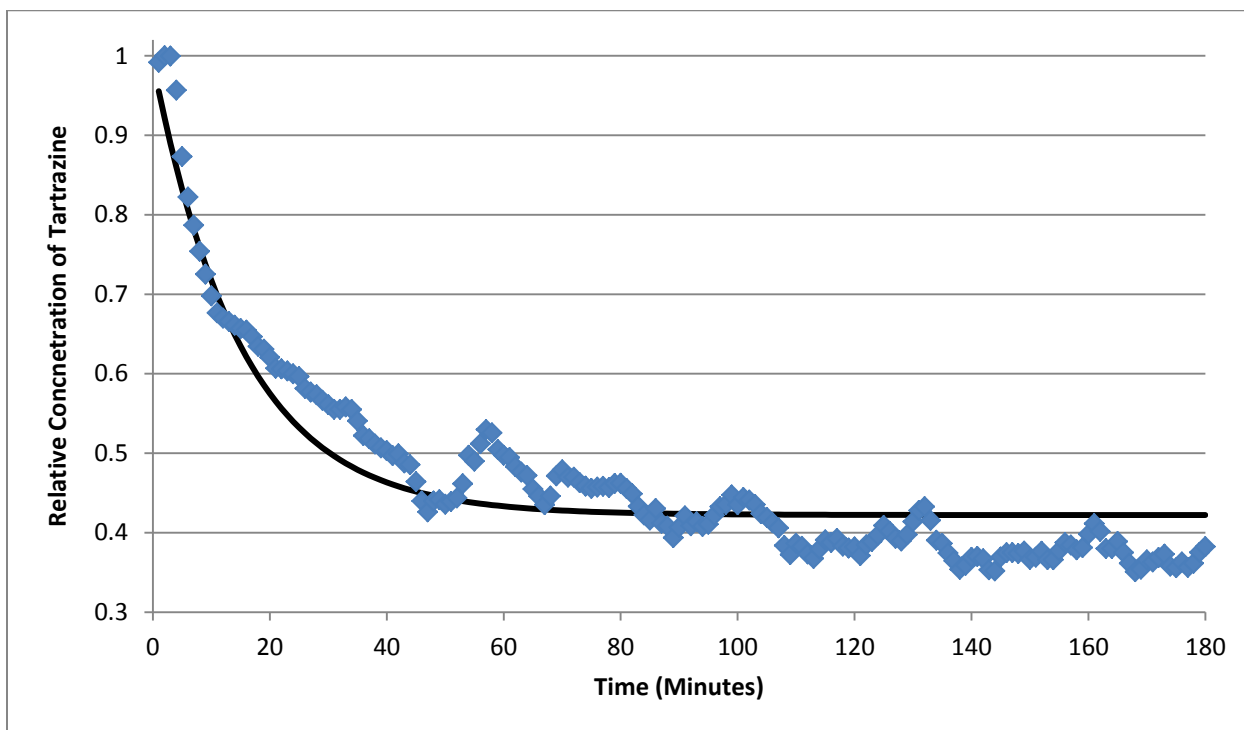
Figure 55: Med Teflon, Across LED Caps, Trial 1, High Power
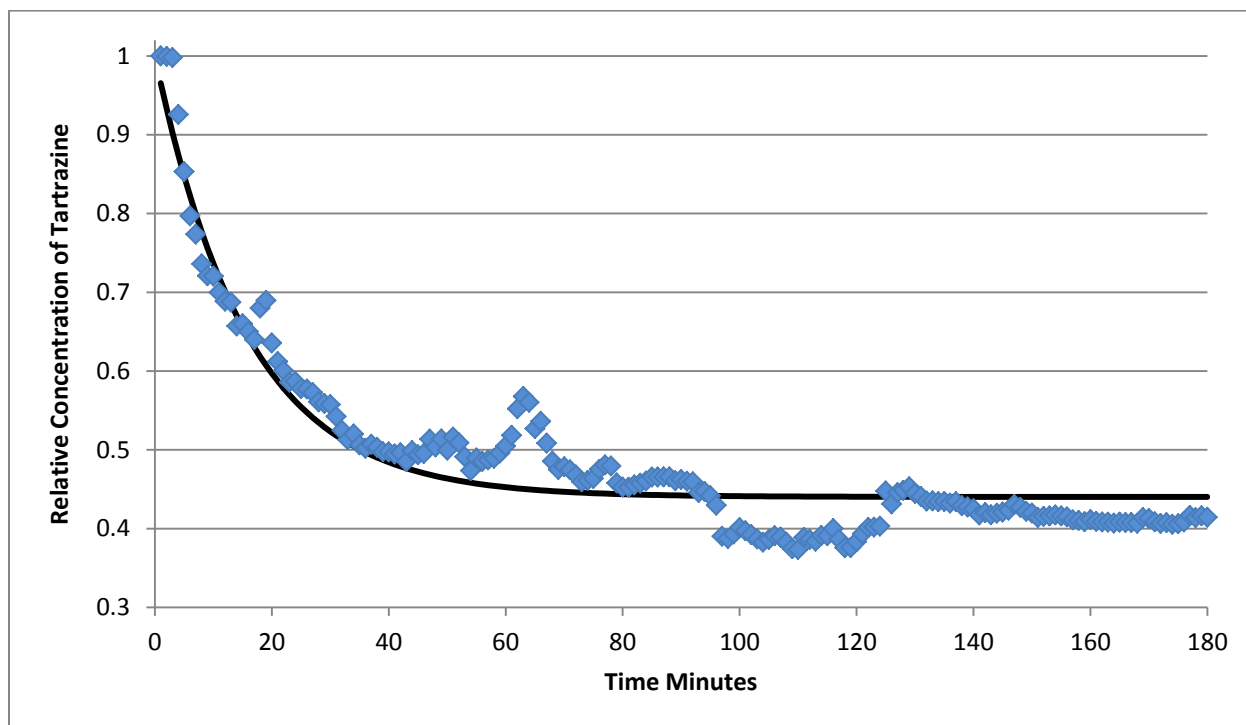
Figure 56: Med Teflon, Across LED Caps, Trial 2, High Power
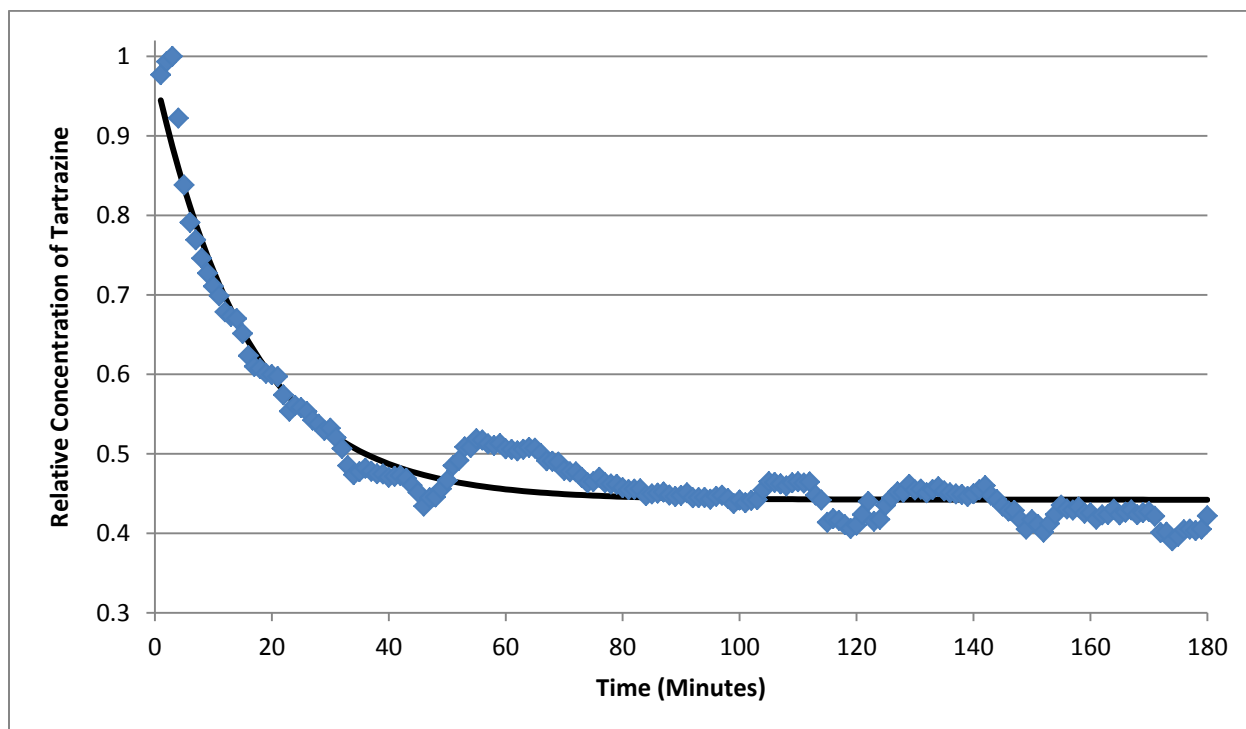
Figure 57: Med Teflon, Across LED Caps, Trial 3, High Power
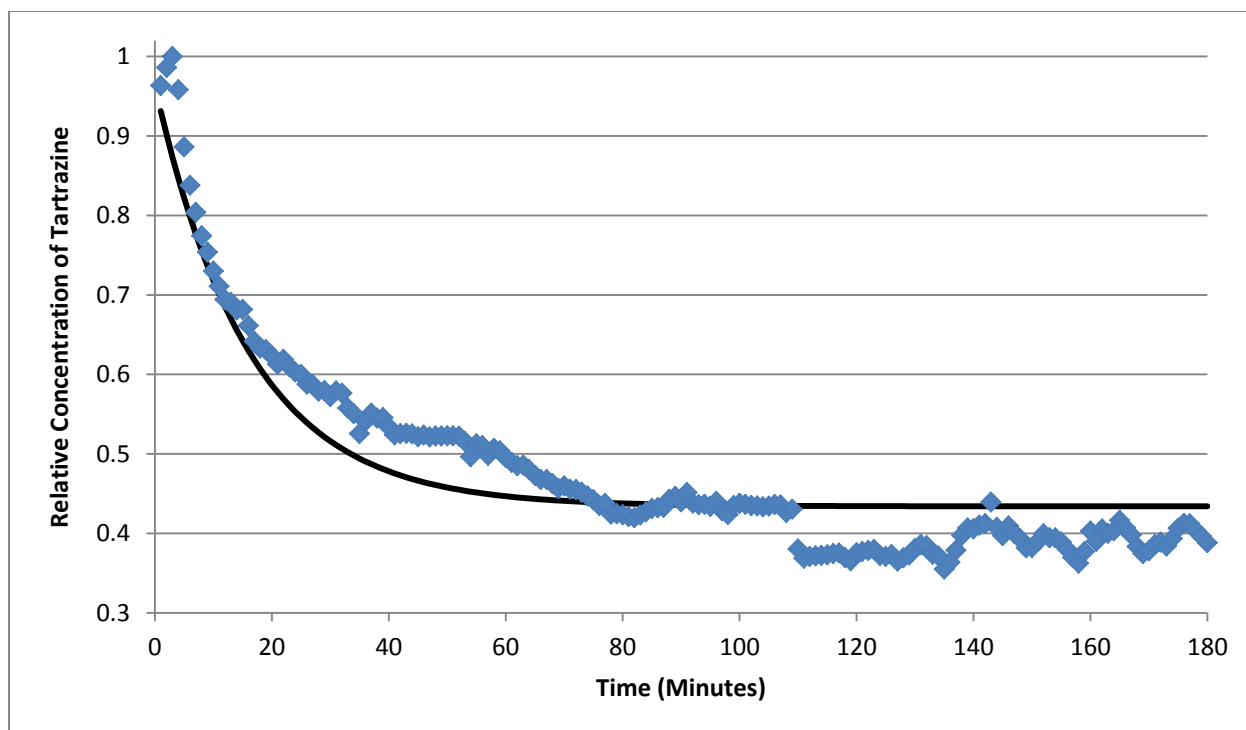
Figure 58: Thick Teflon, Swirl Caps, Trial 1 High Power
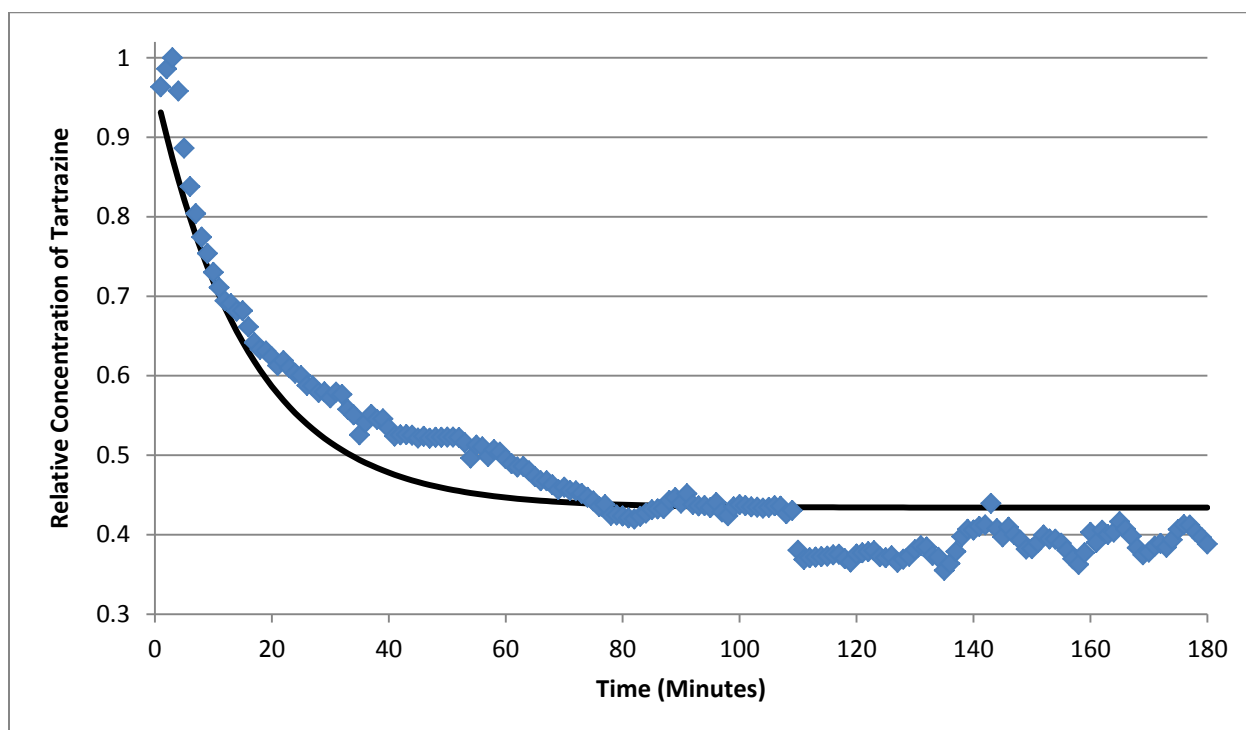
Figure 59: Thick Teflon, Swirl Caps, Trial 2, High Power
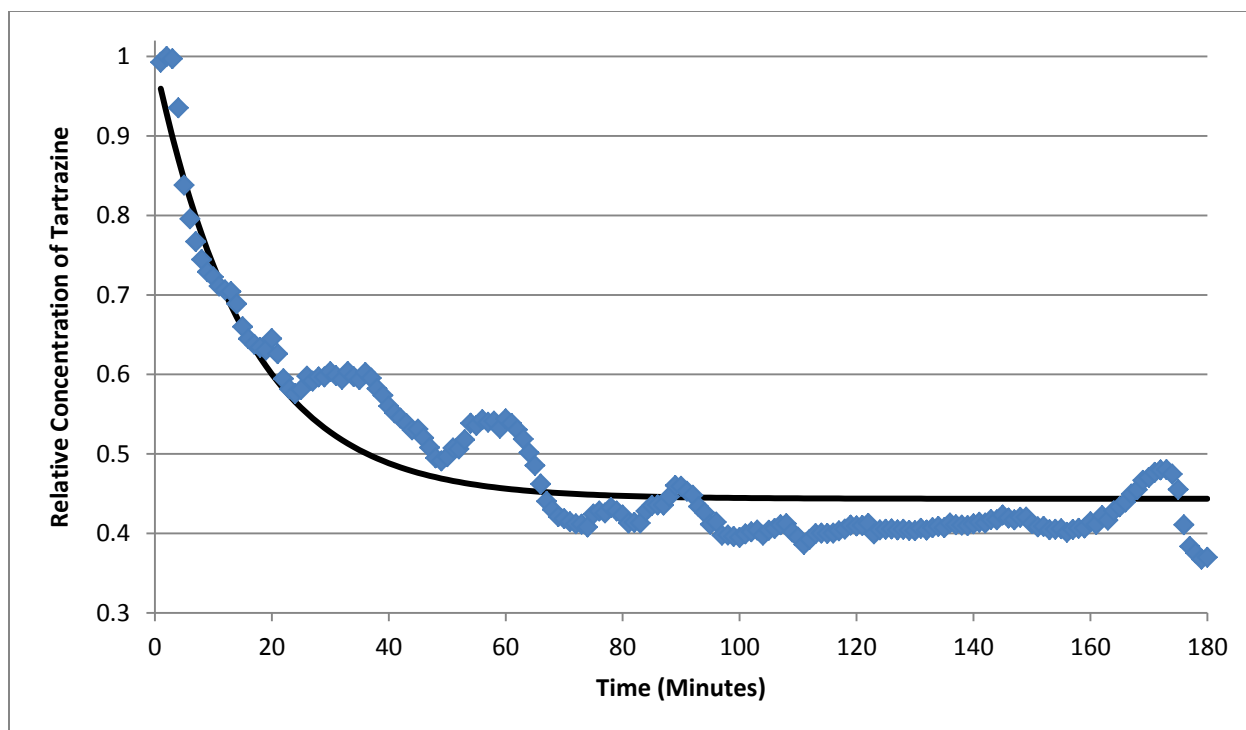
Figure 60: Thick Teflon, Swirl Caps, Trial 3, High Power

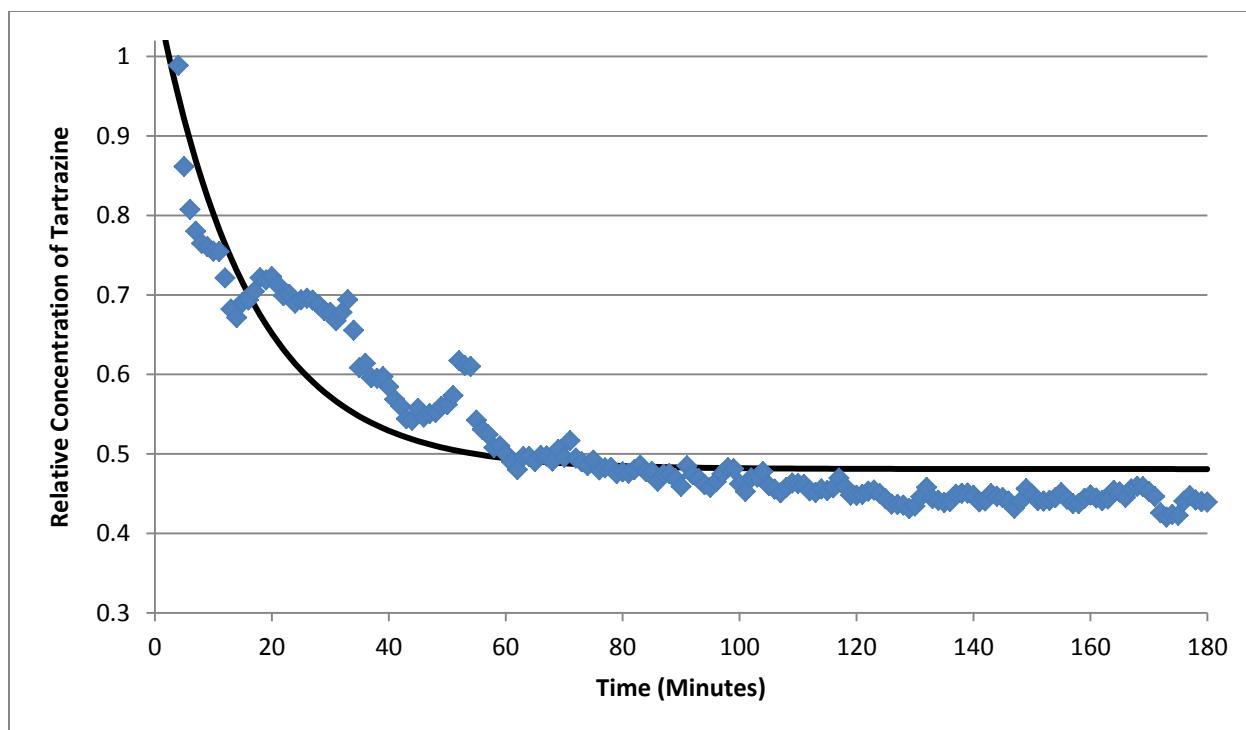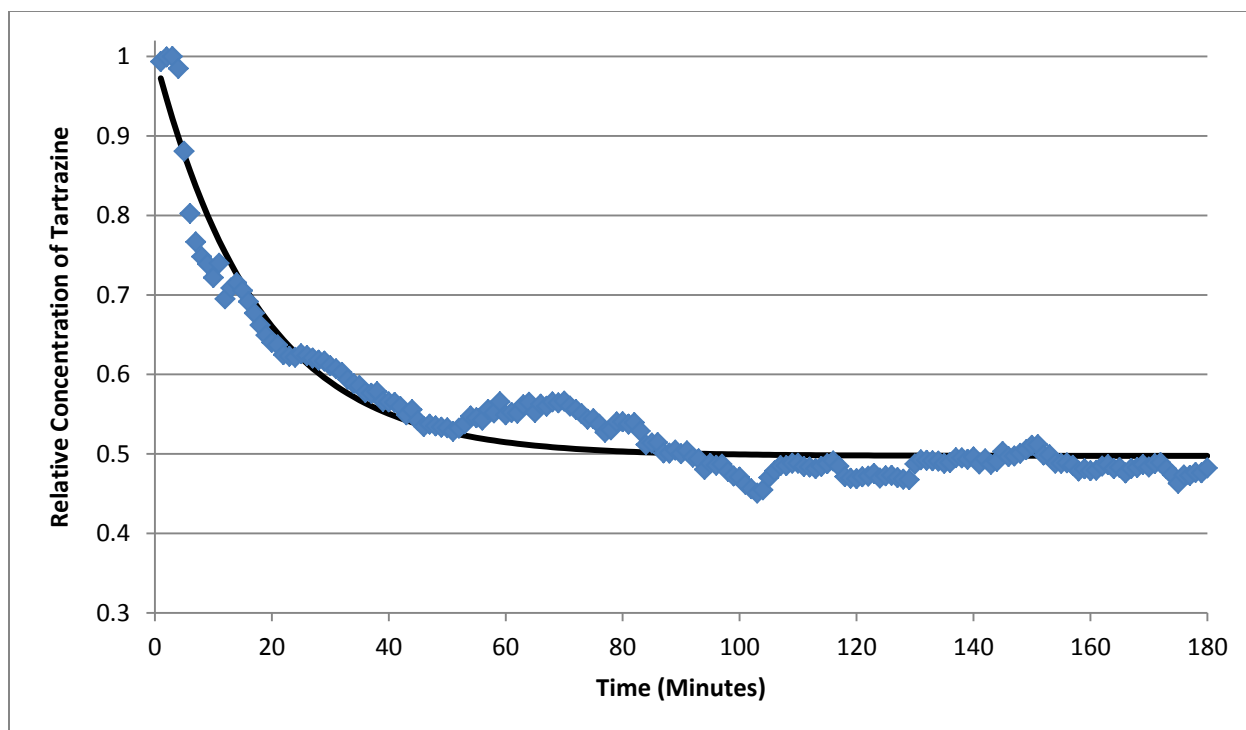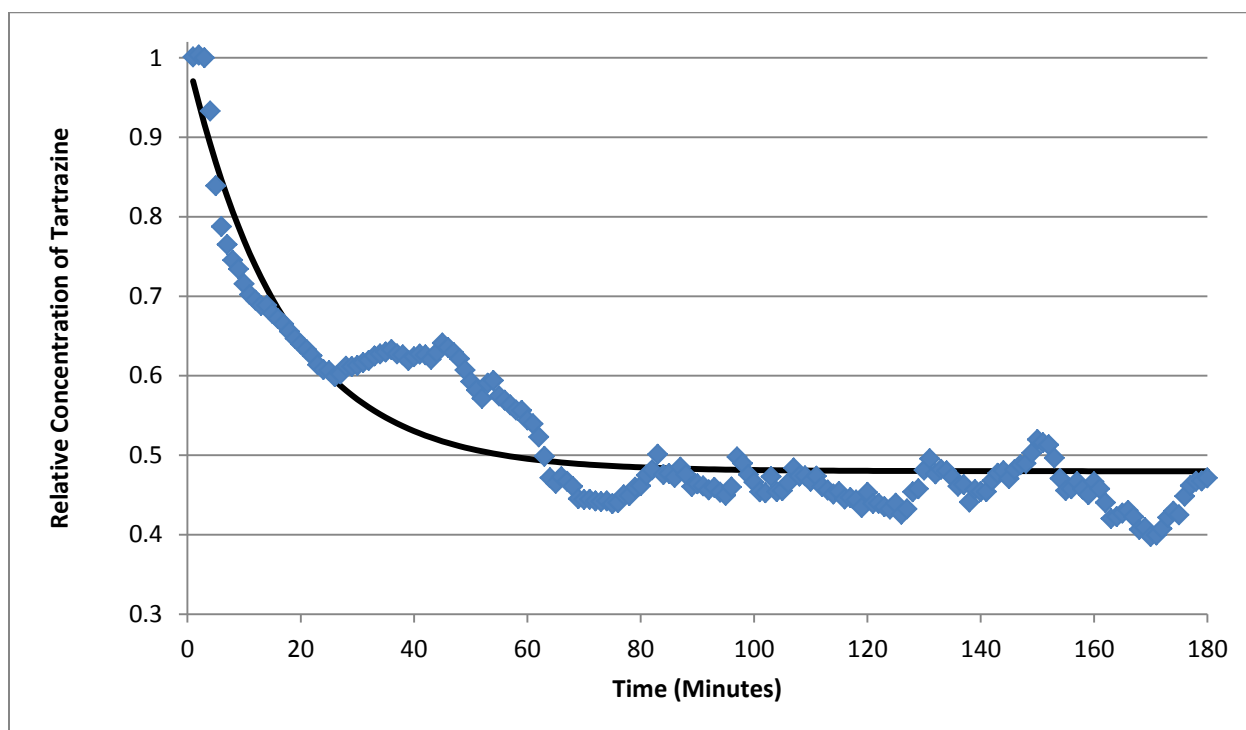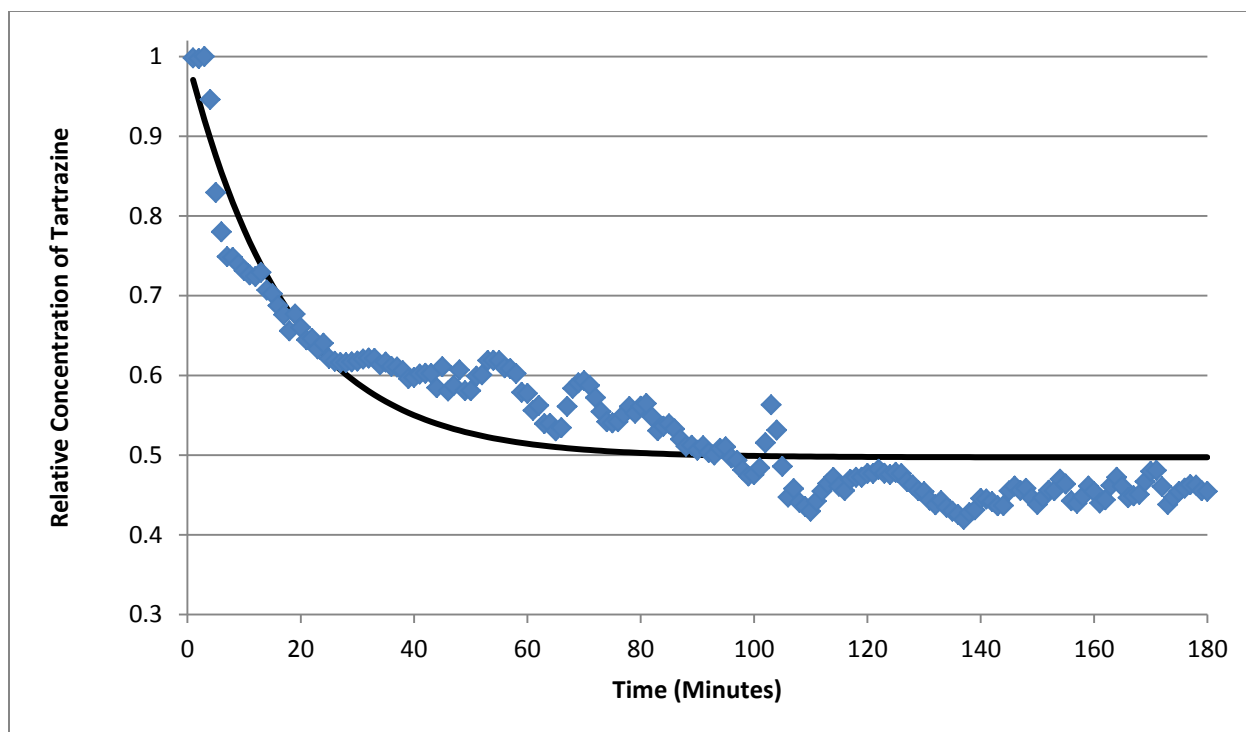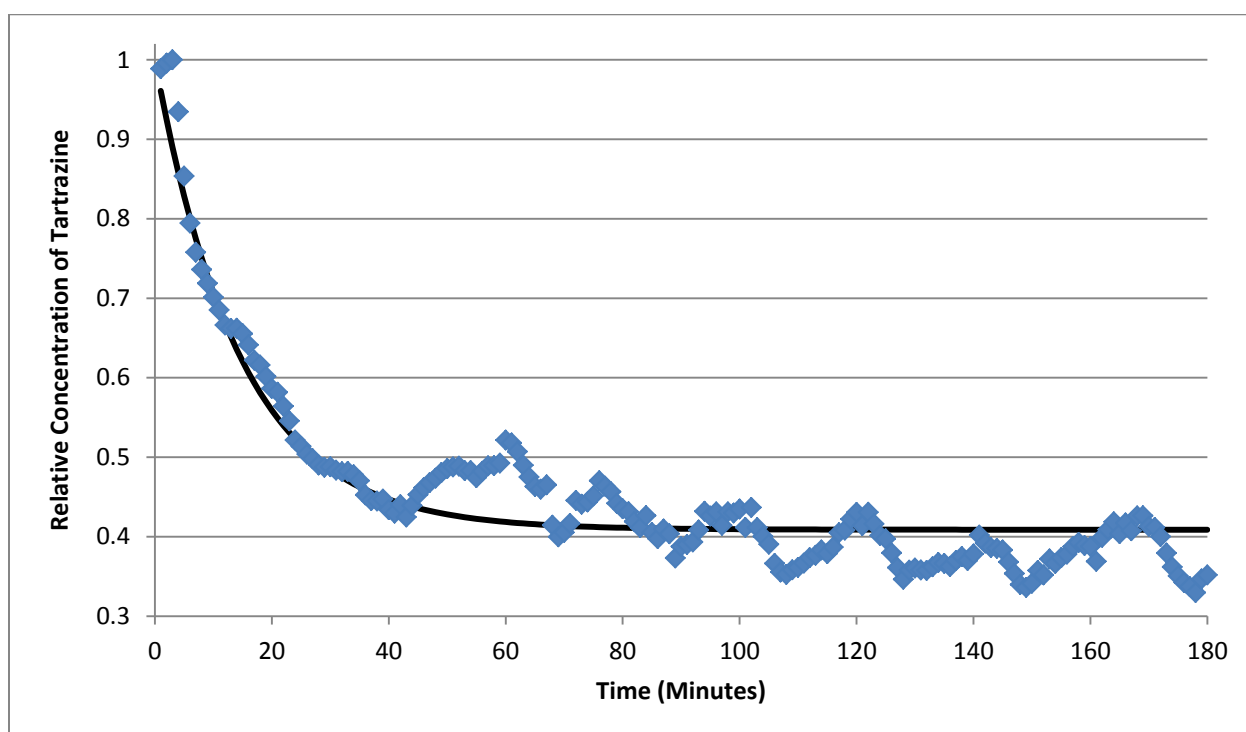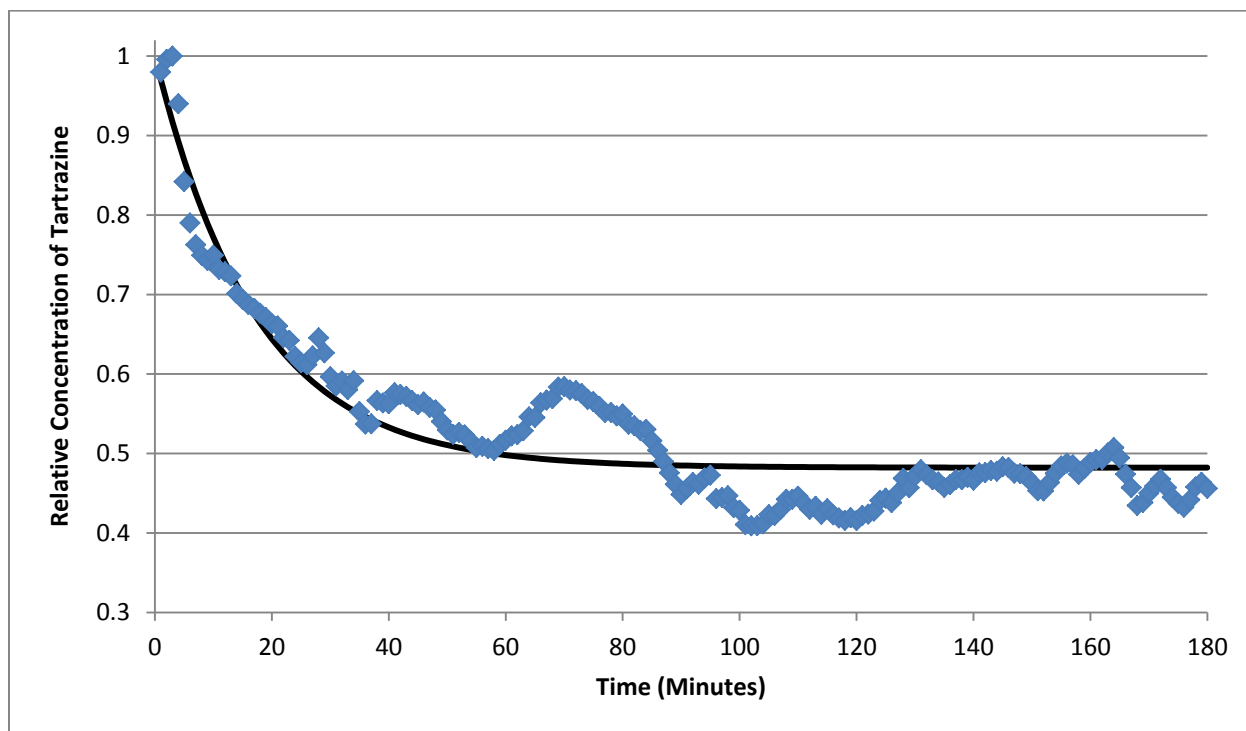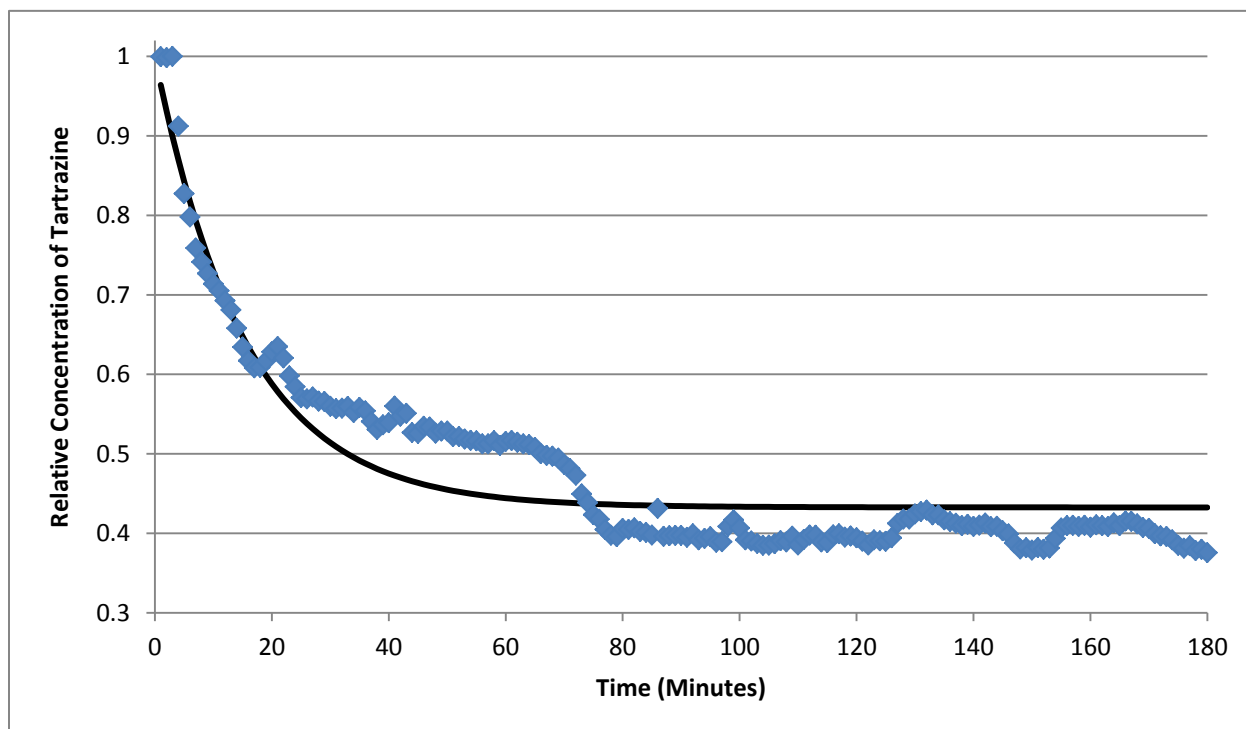Figure 61: Thick Teflon, Across LED Caps, Trial 1, High Power

75
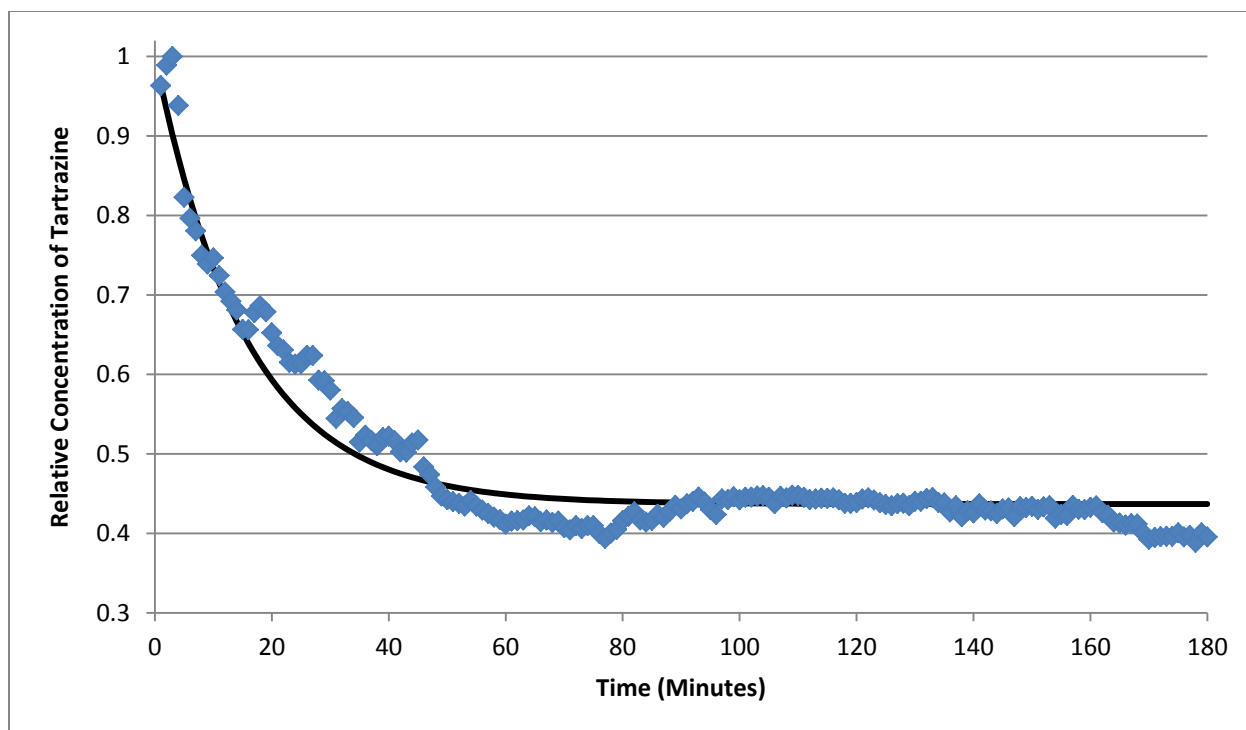
Figure 62: Thick Teflon, Across LED Caps, Trial 2, High Power
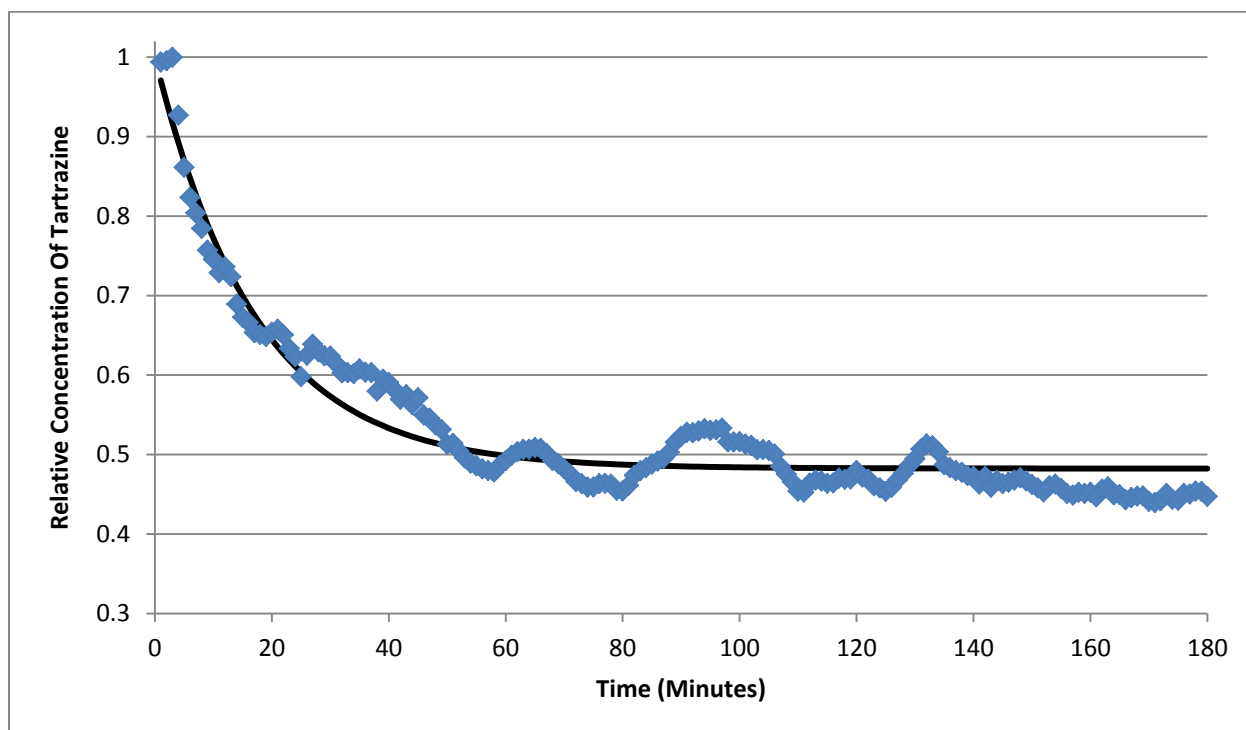
Figure 63: Thick Teflon, Across LED Caps, Trial 3, High Power

76

Appendix C- Calculated Low and High Power Rate Constants (K_{st})

Table 10: High and Low Power Rate Constants for each Reactor Configuration

Trial	LP R^2	LP Rate Constant	HP R^2	HP Rate Constant
Steel A1	0.7676	0.004523	0.9173	0.03819
Steel A2	0.8852	0.004606	0.8904	0.03199
Steel A3	0.8405	0.006526	0.8528	0.03542
Steel S1	0.7964	0.006283	0.8263	0.03433
Steel S2	0.8236	0.006722	0.885	0.03303
Steel S3	0.776	0.006364	0.9308	0.03142
Thin A1	0.8097	0.00453	0.9008	0.04049
Thin A2	0.8315	0.004906	0.8652	0.03007
Thin A3	0.6172	0.005245	0.8509	0.03838
Thin S1	0.8145	0.006857	0.827	0.03035
Thin S2	0.7227	0.006508	0.9254	0.02827
Thin S3	0.5388	0.007394	0.8121	0.02832
Med A1	0.7473	0.00496	0.8817	0.03775
Med A2	0.8442	0.007609	0.94	0.03537
Med A3	0.706	0.007754	0.8996	0.03546
Med S1	0.7032	0.007543	0.9435	0.03189
Med S2	0.9042	0.007693	0.8303	0.03313
Med S3	0.9599	0.007911	0.8739	0.03323
Thick A1	0.8742	0.005508	0.9368	0.03608
Thick A2	0.5839	0.007209	0.9281	0.03003
Thick A3	0.7467	0.006609	0.7661	0.03091
Thick S1	0.7687	0.006981	0.8801	0.03656
Thick S2	0.734	0.007747	0.867	0.03514
Thick S3	0.8876	0.007331	0.8685	0.03672

Appendix D- COMSOL® Generated Streamlines
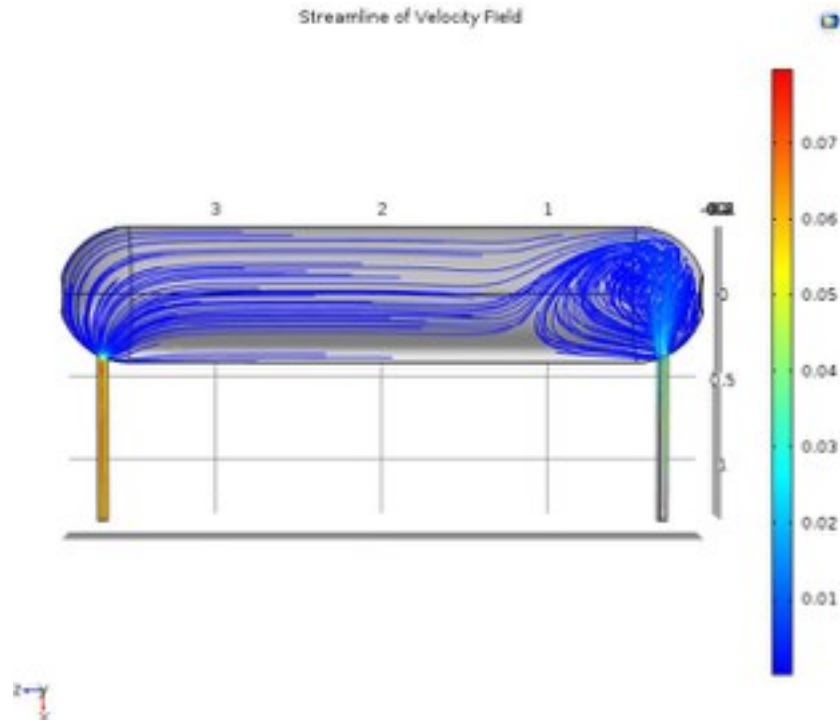
Figure 64: 1 mL/Min Streamline Model Experimental Reactor
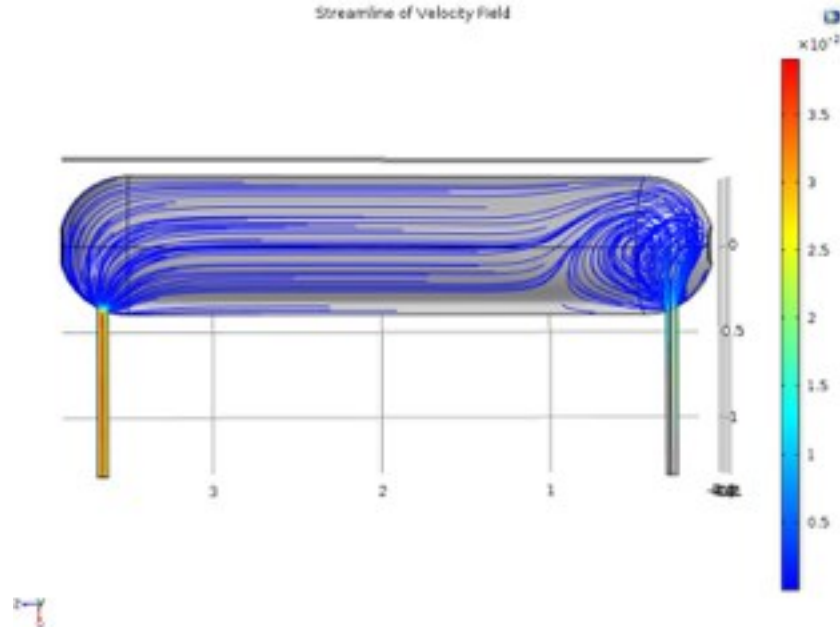
Figure 65: 2 mL/Min Streamline Model Experimental Reactor
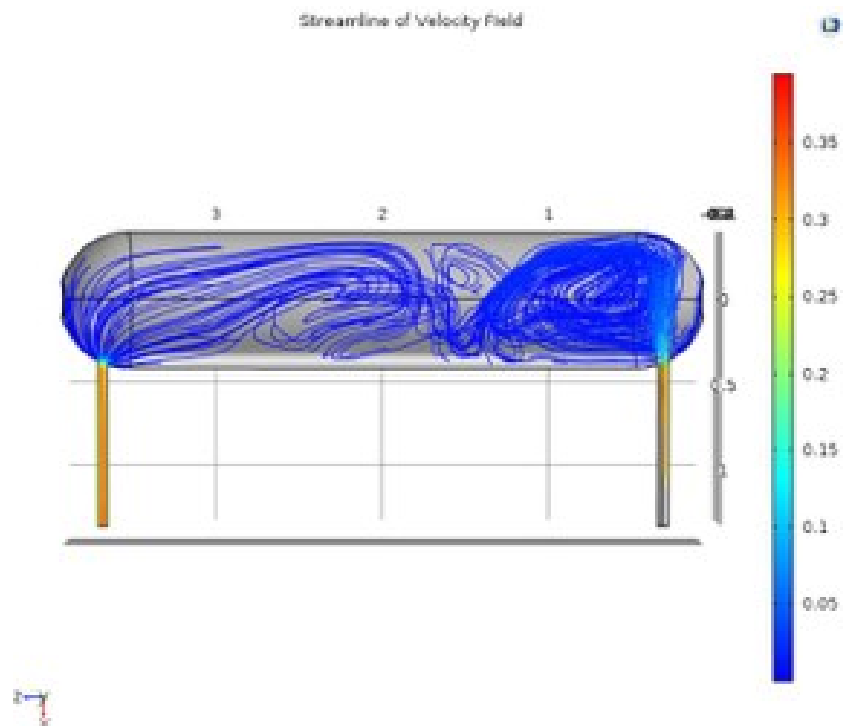
Figure 66: 10 mL/Min Streamline Model Experimental Reactor
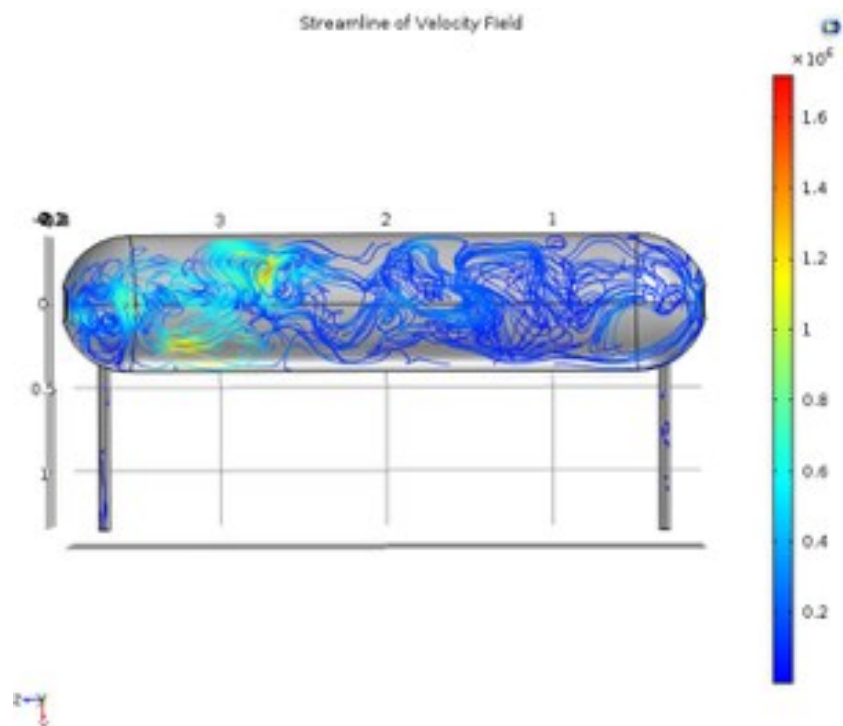
Figure 67: 100 mL/Min Streamline Model Experimental Reactor

Streamline of Velocity Field
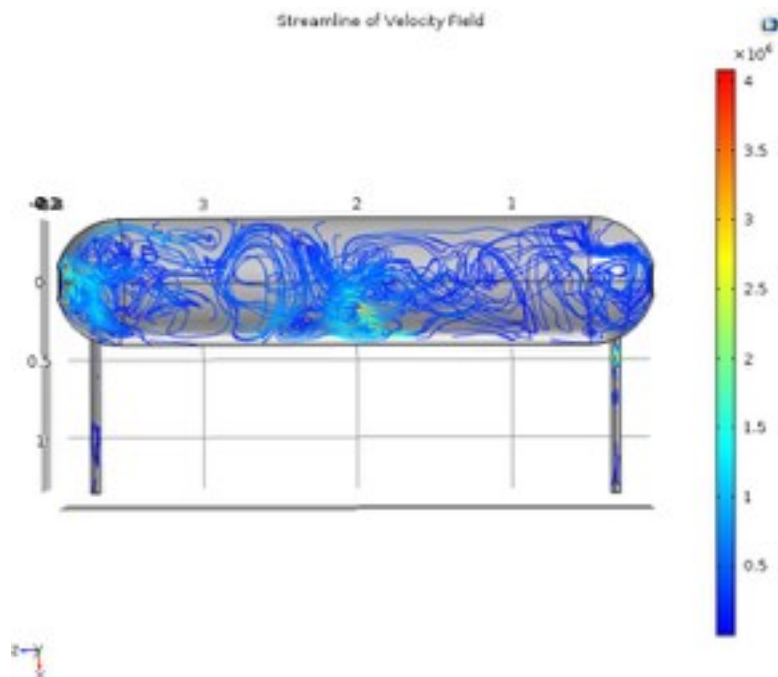
Figure 68: 1 L/Min Streamline Model Experimental Reactor

Velocity Field m^3/s
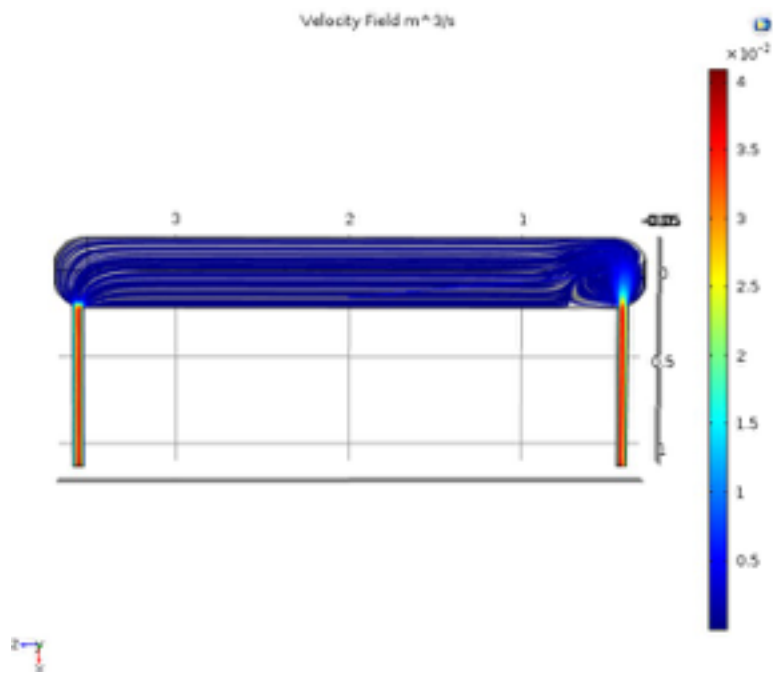
Figure 69: 1 mL/Min Streamline Model Design Reactor

Velocity Field m^3/s
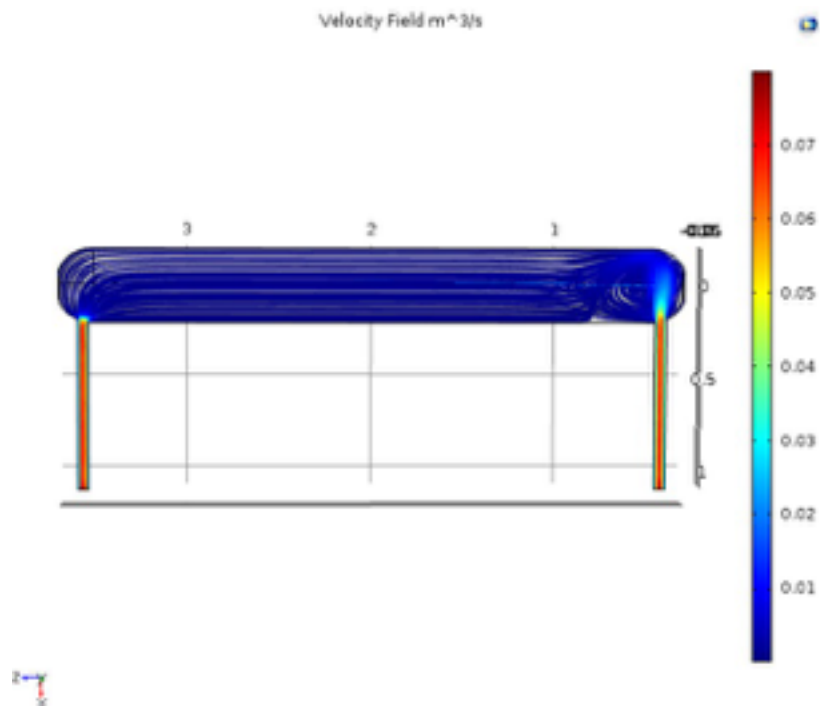
Figure 70: 2 mL/Min Streamline Model Design Reactor

Velocity Field m^3/s
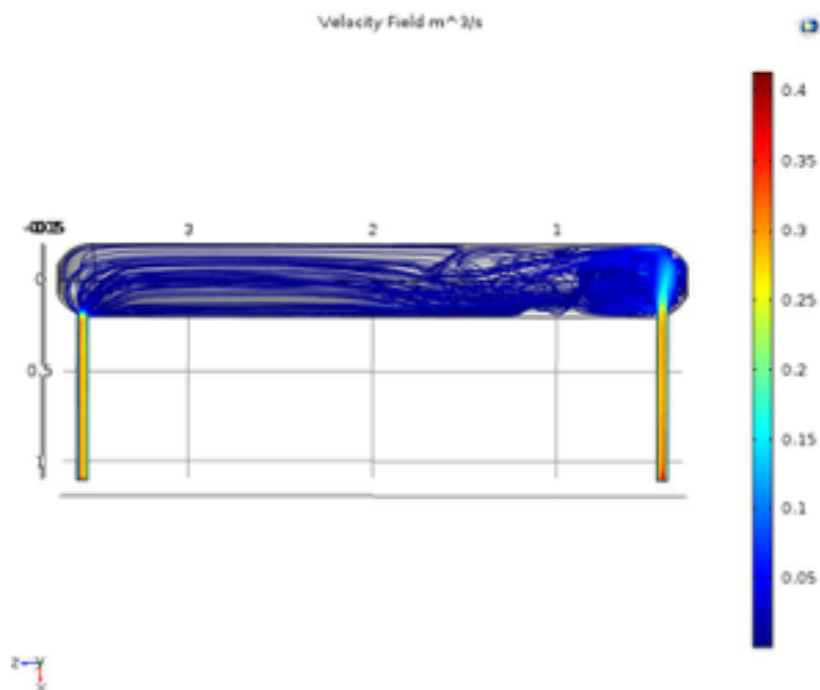
Figure 71: 10 mL/Min Streamline Model Design Reactor
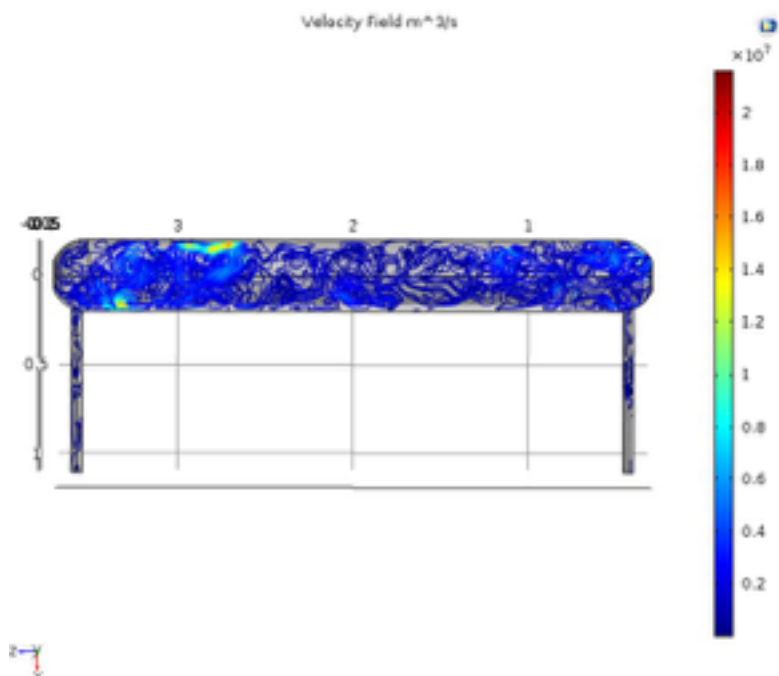
Figure 72: 100 mL/Min Streamline Model Design Reactor
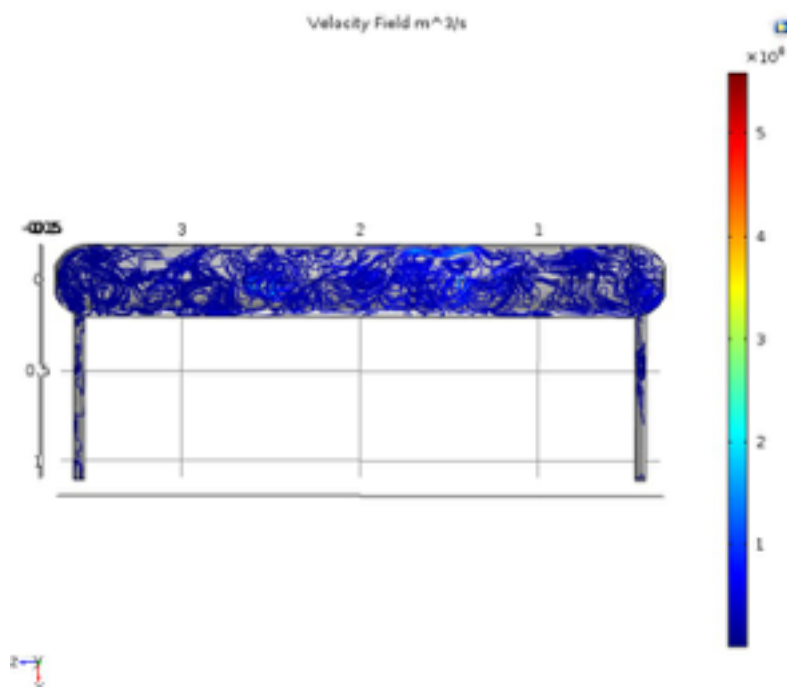
Figure 73: 1 L/Min Streamline Model Design Reactor

Whole Model

Response Rate Constant
Whole Model
Actual by Predicted Plot

RSq=0.98 RMSE=0.0022
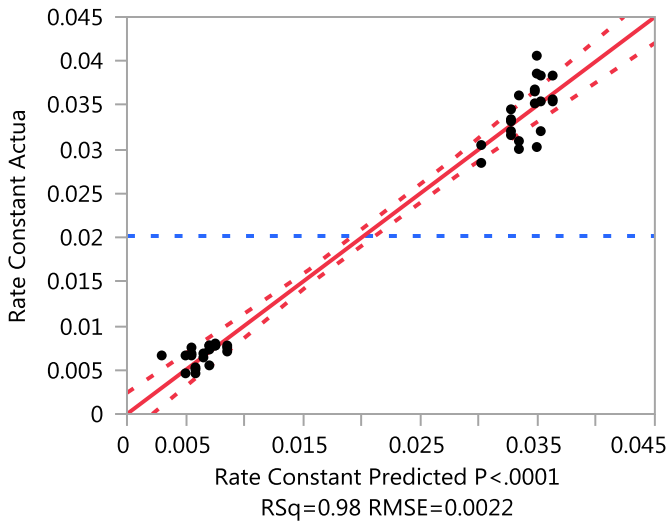
Summary of Fit

RSquare	0.981605
RSquare Adj	0.975298
Root Mean Square Error	0.002212
Mean of Response	0.020178
Observations (or Sum Wgts)	48

Analysis of Variance

Source	DF	Sum of Squares	Mean Square	F Ratio
Model	12	0.00913652	0.000761	155.6417
Error	35	0.00017121	4.892e-6	**Prob > F**
C. Total	47	0.00930773		<.0001*

Lack Of Fit

Source	DF	Sum of Squares	Mean Square	F Ratio
Lack Of Fit	3	0.00004786	0.000016	4.1383
Pure Error	32	0.00012336	3.855e-6	**Prob > F**
Total Error	35	0.00017121		0.0138*
				Max RSq

Parameter Estimates

Term	Estimate	Std Error	t Ratio	Prob>|t|
Intercept	0.0052443	0.000702	7.47	<.0001*

Term	Estimate	Std Error	t Ratio	Prob>|t|
Swirl[1-0]	0.0018669	0.000949	1.97	0.0572
Reactor Type[Med]	0.0018027	0.000924	1.95	0.0591
Reactor Type[Steel]	-0.000208	0.000983	-0.21	0.8340
Reactor Type[Thick]	-0.002282	0.001285	-1.78	0.0845
High Power (1) Low Power (0)[1-0]	0.0298257	0.000949	31.42	<.0001*
Reactor Type[Med]*High Power (1) Low Power (0)[1-0]	-0.000482	0.001093	-0.44	0.6620
Reactor Type[Steel]*High Power (1) Low Power (0)[1-0]	0.0005191	0.001116	0.47	0.6446
Reactor Type[Thick]*High Power (1) Low Power (0)[1-0]	0.0007678	0.001245	0.62	0.5414
Swirl[1-0]*Reactor Type[Med]	-0.001234	0.001093	-1.13	0.2666
Swirl[1-0]*Reactor Type[Steel]	-0.000266	0.001116	-0.24	0.8131
Swirl[1-0]*Reactor Type[Thick]	0.0037396	0.001245	3.00	0.0049*
Swirl[1-0]*High Power (1) Low Power (0)[1-0]	-0.004238	0.00131	-3.23	0.0027*

Effect Tests

Source	Nparm	DF	Sum of Squares	F Ratio	Prob > F
Swirl	1	1	0.00001892	3.8678	0.0572
Reactor Type	3	3	0.00002505	1.7069	0.1834
High Power (1) Low Power (0)	1	1	0.00482912	987.1759	<.0001*
Reactor Type*High Power (1) Low Power (0)	3	3	0.00000484	0.3296	0.8040
Swirl*Reactor Type	3	3	0.00005048	3.4397	0.0271*
Swirl*High Power (1) Low Power (0)	1	1	0.00005118	10.4626	0.0027*

Residual by Predicted Plot
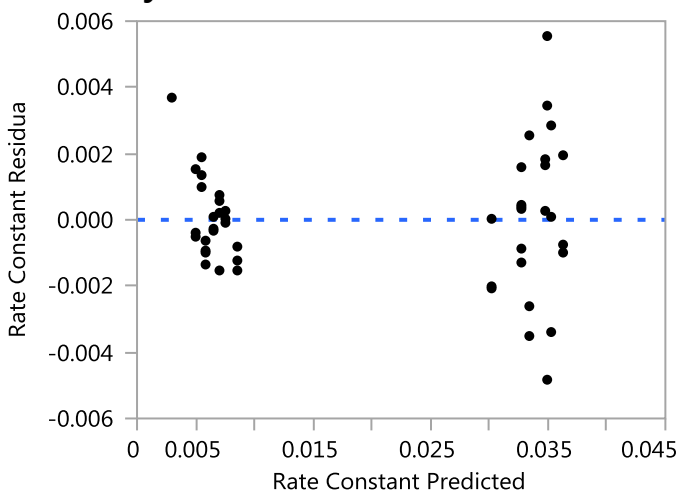
Swirl
Leverage Plot

Rate Constant Leverage Residual (y-axis)
Swirl Leverage, P=0.0572 (x-axis)
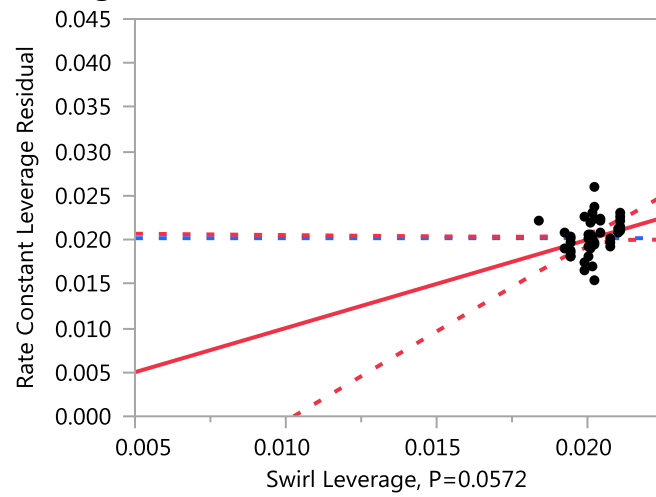
Least Squares Means Table

Level	Least Sq Mean	Std Error	Mean
0	0.00524426	0.00070248	0.020451
1	0.00711117	0.00063848	0.019905

LS Means Plot
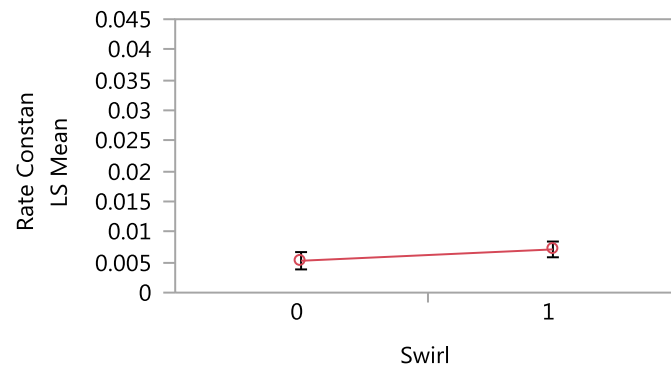
Rate Constant LS Mean (y-axis)
Swirl (x-axis)

Reactor Type
Leverage Plot

Reactor Type Leverage, P=0.1834
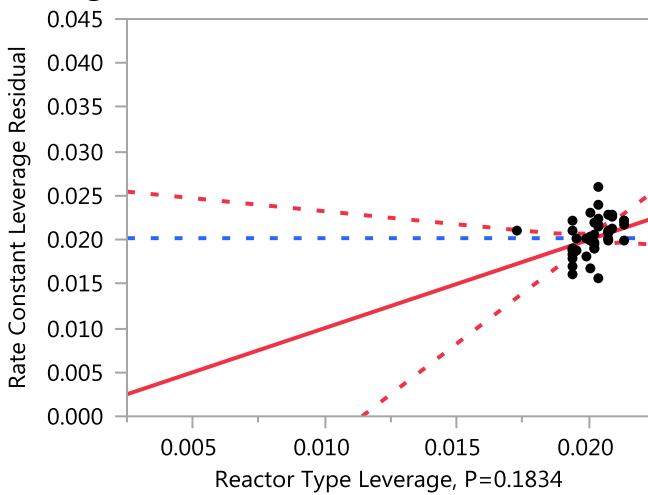
Least Squares Means Table

Level	Least Sq Mean	Std Error	Mean
Med	0.00704692	0.00102324	0.019904
Steel	0.00503673	0.00115336	0.019950
Thick	0.00296213	0.00169559	0.023411
Thin	0.00593125	0.00102324	0.018175

LS Means Plot
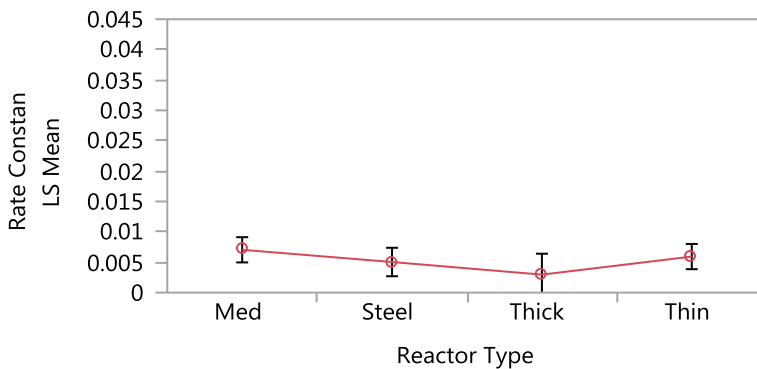
LSMeans Differences Tukey HSD

α=
0.050   Q=
2.6969
LSMean[i] By LSMean[j]

Mean[i]-Mean[j] Std Err Dif Lower CL Dif Upper CL Dif	Med	Steel	Thick	Thin
Med	0	0.00201	0.00408	0.00112
	0	0.00149	0.00189	0.0014
	0	-0.002	-0.001	-0.0027

86

	0	0.00602	0.00919	0.00489
Steel	-0.002	0	0.00207	-0.0009
	0.00149	0	0.00194	0.00149
	-0.006	0	-0.0032	-0.0049
	0.002	0	0.00732	0.00311
Thick	-0.0041	-0.0021	0	-0.003
	0.00189	0.00194	0	0.00189
	-0.0092	-0.0073	0	-0.0081
	0.00102	0.00317	0	0.00213
Thin	-0.0011	0.00089	0.00297	0
	0.0014	0.00149	0.00189	0
	-0.0049	-0.0031	-0.0021	0
	0.00266	0.0049	0.00807	0

Level		Least Sq Mean
Med	A	0.00704692
Thin	A	0.00593125
Steel	A	0.00503673
Thick	A	0.00296213

Levels not connected by same letter are significantly different.

High Power (1) Low Power (0)
Leverage Plot
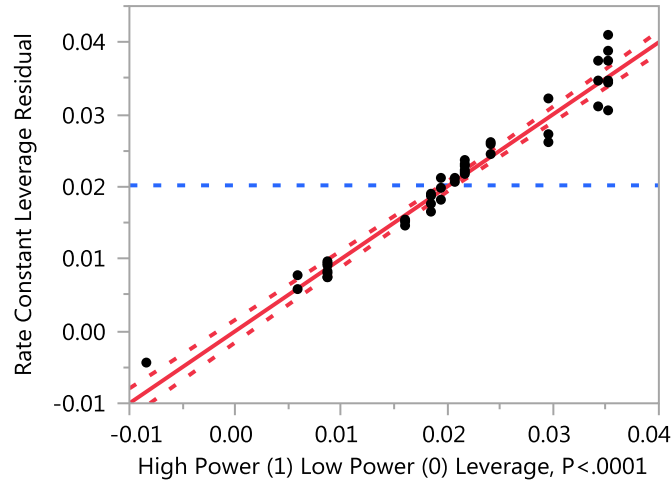
Least Squares Means Table

Level	Least Sq Mean	Std Error	Mean
0	0.00524426	0.00070248	0.006472
1	0.03507000	0.00063848	0.033885

LS Means Plot
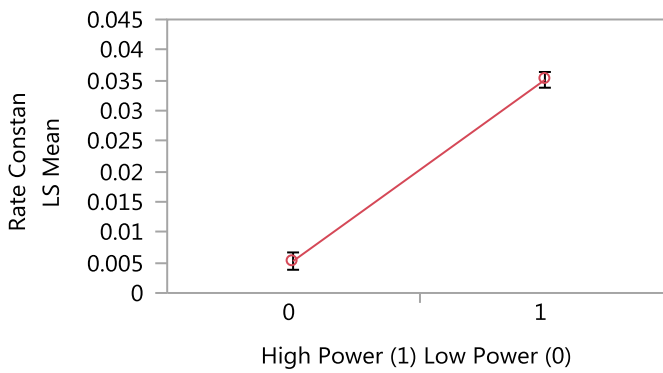
Reactor Type*High Power (1) Low Power (0) Leverage Plot
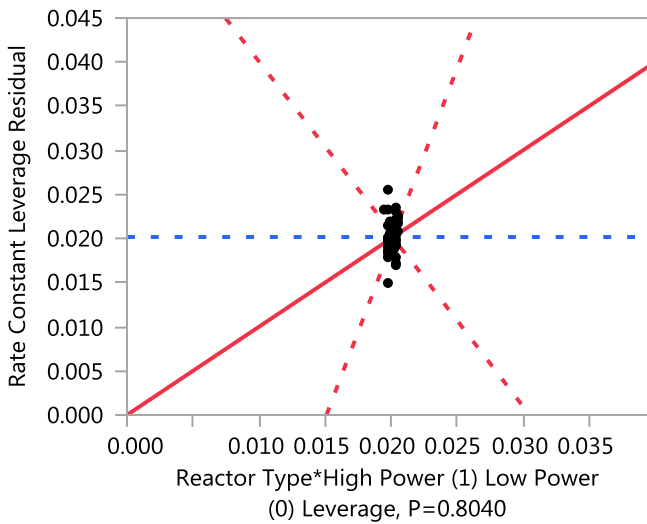
Least Squares Means Table

Level	Least Sq Mean	Std Error
Med,0	0.00704692	0.00102324
Med,1	0.03639078	0.00114797
Steel,0	0.00503673	0.00115336
Steel,1	0.03538160	0.00115336
Thick,0	0.00296213	0.00169559
Thick,1	0.03355562	0.00118597
Thin,0	0.00593125	0.00102324
Thin,1	0.03495200	0.00114797

LS Means Plot
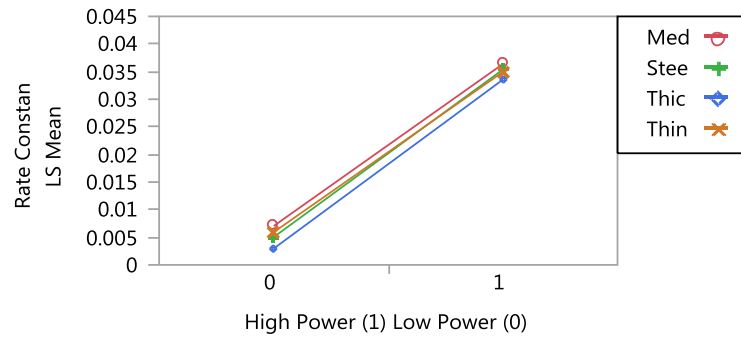
LSMeans Differences Tukey HSD

α=0.050   Q=3.22089

LSMean[i] By LSMean[j]

Mean[i]-Mean[j] Std Err Dif Lower CL Dif Upper CL Dif	Med,0	Med,1	Steel,0	Steel,1	Thick,0	Thick,1	Thin,0	Thin,1
Med,0	0	-0.0293	0.00201	-0.0283	0.00408	-0.0265	0.00112	-0.0279
	0	0.00138	0.00149	0.0016	0.00189	0.0016	0.0014	0.0016
	0	-0.0338	-0.0028	-0.0335	-0.002	-0.0317	-0.0034	-0.033
	0	-0.0249	0.00679	-0.0232	0.01018	-0.0213	0.00562	-0.0228
Med,1	0.02934	0	0.03135	0.00101	0.03343	0.00284	0.03046	0.00144
	0.00138	0	0.0017	0.00156	0.00216	0.0016	0.0016	0.00155
	0.02491	0	0.02589	-0.004	0.02648	-0.0023	0.02532	-0.0035
	0.03378	0	0.03682	0.00602	0.04037	0.008	0.0356	0.00642
Steel,0	-0.002	-0.0314	0	-0.0303	0.00207	-0.0285	-0.0009	-0.0299
	0.00149	0.0017	0	0.00144	0.00194	0.0017	0.00149	0.0017
	-0.0068	-0.0368	0	-0.035	-0.0042	-0.034	-0.0057	-0.0354
	0.00277	-0.0259	0	-0.0257	0.00833	-0.0231	0.00389	-0.0245
Steel,1	0.02833	-0.001	0.03034	0	0.03242	0.00183	0.02945	0.00043
	0.0016	0.00156	0.00144	0	0.00215	0.00161	0.0016	0.00156
	0.02319	-0.006	0.02572	0	0.02549	-0.0034	0.02431	-0.0046
	0.03348	0.004	0.03497	0	0.03935	0.00701	0.03459	0.00544
Thick,0	-0.0041	-0.0334	-0.0021	-0.0324	0	-0.0306	-0.003	-0.032
	0.00189	0.00216	0.00194	0.00215	0	0.00171	0.00189	0.00216
	-0.0102	-0.0404	-0.0083	-0.0394	0	-0.0361	-0.0091	-0.0389
	0.00201	-0.0265	0.00418	-0.0255	0	-0.0251	0.00312	-0.025
Thick,1	0.02651	-0.0028	0.02852	-0.0018	0.03059	0	0.02762	-0.0014
	0.0016	0.0016	0.0017	0.00161	0.00171	0	0.0016	0.0016
	0.02135	-0.008	0.02305	-0.007	0.02507	0	0.02246	-0.0066
	0.03167	0.00233	0.03398	0.00336	0.03611	0	0.03279	0.00377
Thin,0	-0.0011	-0.0305	0.00089	-0.0295	0.00297	-0.0276	0	-0.029
	0.0014	0.0016	0.00149	0.0016	0.00189	0.0016	0	0.00138
	-0.0056	-0.0356	-0.0039	-0.0346	-0.0031	-0.0328	0	-0.0335
	0.00339	-0.0253	0.00568	-0.0243	0.00906	-0.0225	0	-0.0246
Thin,1	0.02791	-0.0014	0.02992	-0.0004	0.03199	0.0014	0.02902	0
	0.0016	0.00155	0.0017	0.00156	0.00216	0.0016	0.00138	0
	0.02276	-0.0064	0.02445	-0.0054	0.02504	-0.0038	0.02459	0
	0.03305	0.00354	0.03538	0.00458	0.03894	0.00656	0.03346	0

Level			Least Sq Mean
Med,1	A		0.03639078
Steel,1	A		0.03538160
Thin,1	A		0.03495200
Thick,1	A		0.03355562
Med,0		B	0.00704692
Thin,0		B	0.00593125
Steel,0		B	0.00503673
Thick,0		B	0.00296213

Levels not connected by same letter are significantly different.

Swirl*Reactor Type
Leverage Plot

Swirl*Reactor Type Leverage, P=0.0271
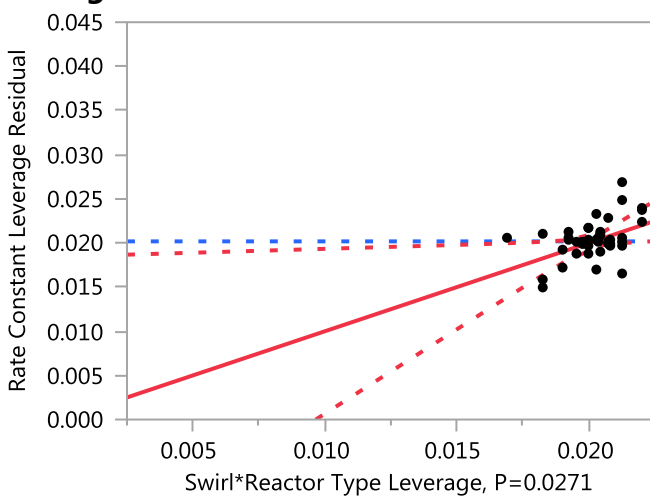
Least Squares Means Table

Level	Least Sq Mean	Std Error
0,Med	0.00704692	0.00102324
0,Steel	0.00503673	0.00115336
0,Thick	0.00296213	0.00169559
0,Thin	0.00593125	0.00102324
1,Med	0.00767978	0.00114797
1,Steel	0.00663794	0.00115336
1,Thick	0.00856862	0.00118597
1,Thin	0.00555833	0.00114797

LS Means Plot

LSMeans Differences Tukey HSD

α=0.050   Q=3.22089

LSMean[i] By LSMean[j]

Mean[i]-Mean[j] Std Err Dif Lower CL Dif Upper CL Dif	0,Med	0,Steel	0,Thick	0,Thin	1,Med	1,Steel	1,Thick	1,Thin
0,Med	0 0 0 0	0.00201 0.00149 -0.0028 0.00679	0.00408 0.00189 -0.002 0.01018	0.00112 0.0014 -0.0034 0.00562	-0.0006 0.00138 -0.0051 0.0038	0.00041 0.0016 -0.0047 0.00555	-0.0015 0.0016 -0.0067 0.00364	0.00149 0.0016 -0.0037 0.00663
0,Steel	-0.002 0.00149 -0.0068 0.00277	0 0 0 0	0.00207 0.00194 -0.0042 0.00833	-0.0009 0.00149 -0.0057 0.00389	-0.0026 0.0017 -0.0081 0.00282	-0.0016 0.00144 -0.0062 0.00302	-0.0035 0.0017 -0.009 0.00193	-0.0005 0.0017 -0.006 0.00494
0,Thick	-0.0041 0.00189 -0.0102 0.00201	-0.0021 0.00194 -0.0083 0.00418	0 0 0 0	-0.003 0.00189 -0.0091 0.00312	-0.0047 0.00216 -0.0117 0.00223	-0.0037 0.00215 -0.0106 0.00326	-0.0056 0.00171 -0.0111 -0.0001	-0.0026 0.00216 -0.0095 0.00435
0,Thin	-0.0011 0.0014 -0.0056 0.00339	0.00089 0.00149 -0.0039 0.00568	0.00297 0.00189 -0.0031 0.00906	0 0 0 0	-0.0017 0.0016 -0.0069 0.00339	-0.0007 0.0016 -0.0058 0.00444	-0.0026 0.0016 -0.0078 0.00252	0.00037 0.00138 -0.0041 0.00481
1,Med	0.00063 0.00138 -0.0038 0.00507	0.00264 0.0017 -0.0028 0.00811	0.00472 0.00216 -0.0022 0.01166	0.00175 0.0016 -0.0034 0.00689	0 0 0 0	0.00104 0.00156 -0.004 0.00605	-0.0009 0.0016 -0.0061 0.00428	0.00212 0.00155 -0.0029 0.0071
1,Steel	-0.0004 0.0016 -0.0056 0.00473	0.0016 0.00144 -0.003 0.00622	0.00368 0.00215 -0.0033 0.01061	0.00071 0.0016 -0.0044 0.00585	-0.001 0.00156 -0.0061 0.00397	0 0 0 0	-0.0019 0.00161 -0.0071 0.00326	0.00108 0.00156 -0.0039 0.00609
1,Thick	0.00152 0.0016 -0.0036 0.00668	0.00353 0.0017 -0.0019 0.009	0.00561 0.00171 8.66e-5 0.01113	0.00264 0.0016 -0.0025 0.0078	0.00089 0.0016 -0.0043 0.00605	0.00193 0.00161 -0.0033 0.00712	0 0 0 0	0.00301 0.0016 -0.0022 0.00818
1,Thin	-0.0015 0.0016 -0.0066 0.00365	0.00052 0.0017 -0.0049 0.00598	0.0026 0.00216 -0.0043 0.00954	-0.0004 0.00138 -0.0048 0.00406	-0.0021 0.00155 -0.0071 0.00286	-0.0011 0.00156 -0.0061 0.00393	-0.003 0.0016 -0.0082 0.00215	0 0 0 0

Level			Least Sq Mean
1,Thick	A		0.00856862
1,Med	A	B	0.00767978
0,Med	A	B	0.00704692
1,Steel	A	B	0.00663794
0,Thin	A	B	0.00593125
1,Thin	A	B	0.00555833
0,Steel	A	B	0.00503673
0,Thick		B	0.00296213

Levels not connected by same letter are significantly different.

Swirl*High Power (1) Low Power (0)

Leverage Plot
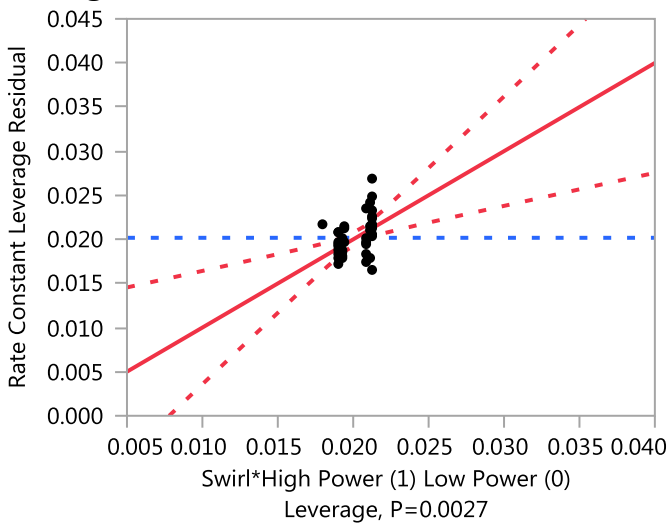
Least Squares Means Table

Level	Least Sq Mean	Std Error
0,0	0.00524426	0.00070248
0,1	0.03507000	0.00063848
1,0	0.00711117	0.00063848
1,1	0.03269917	0.00063848

LS Means Plot
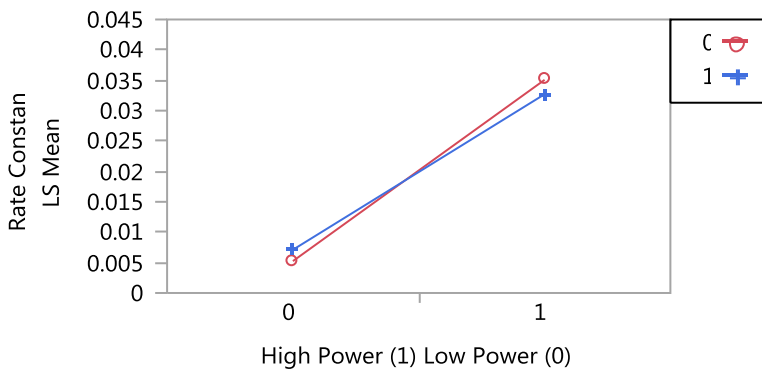
LSMeans Differences Tukey HSD

α=
0.050   Q=
2.6969
LSMean[i] By LSMean[j]

Mean[i]-Mean[j] Std Err Dif Lower CL Dif Upper CL Dif	0,0	0,1	1,0	1,1
0,0	0	-0.0298	-0.0019	-0.0275
	0	0.00095	0.00095	0.00095
	0	-0.0324	-0.0044	-0.03
	0	-0.0273	0.00069	-0.0249
0,1	0.02983	0	0.02796	0.00237
	0.00095	0	0.0009	0.0009
	0.02727	0	0.02552	-0.0001
	0.03239	0	0.03039	0.00481
1,0	0.00187	-0.028	0	-0.0256
	0.00095	0.0009	0	0.0009
	-0.0007	-0.0304	0	-0.028
	0.00443	-0.0255	0	-0.0232
1,1	0.02745	-0.0024	0.02559	0
	0.00095	0.0009	0.0009	0
	0.02489	-0.0048	0.02315	0
	0.03002	6.43e-5	0.02802	0

Level			Least Sq Mean
0,1	A		0.03507000
1,1	A		0.03269917
1,0		B	0.00711117
0,0		B	0.00524426

Levels not connected by same letter are significantly different.

Low Power UV LED Analysis

93

Response Rate Constant

Whole Model

Actual by Predicted Plot
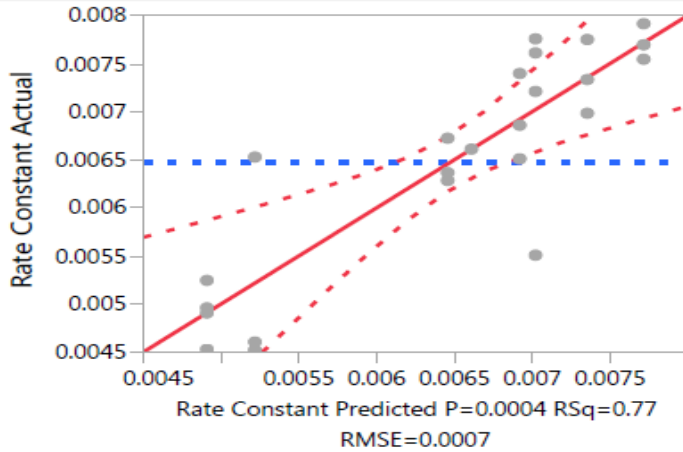
Summary of Fit

RSquare	0.7711
RSquare Adj	0.670956
Root Mean Square Error	0.000657
Mean of Response	0.006472
Observations (or Sum Wgts)	24

Analysis of Variance

Source	DF	Sum of Squares	Mean Square	F Ratio
Model	7	0.00002326	3.3231e-6	7.6999
Error	16	0.00000691	4.3158e-7	Prob > F
C. Total	23	0.00003017		0.0004*

Parameter Estimates

Term	Estimate	Std Error	t Ratio	Prob>|t|
Intercept	0.0059394	0.000222	26.71	<.0001*
Swirl[1-0]	0.0011718	0.000292	4.01	0.0010*
Reactor Type[Med]	0.0010806	0.000322	3.36	0.0040*
Reactor Type[Steel]	-0.000721	0.000348	-2.07	0.0550
Reactor Type[Thick]	0.0006696	0.000515	1.30	0.2120
Swirl[1-0]*Reactor Type[Med]	-0.000476	0.00046	-1.04	0.3157
Swirl[1-0]*Reactor Type[Steel]	6.6229e-5	0.000479	0.14	0.8917
Swirl[1-0]*Reactor Type[Thick]	-0.000428	0.000611	-0.70	0.4938

Effect Tests

Source	Nparm	DF	Sum of Squares	F Ratio	Prob > F
Swirl	1	1	0.00000694	16.0748	0.0010*
Reactor Type	3	3	0.00001078	8.3240	0.0015*
Swirl*Reactor Type	3	3	0.00000171	1.3186	0.3030

Response Rate Constant

Whole Model

Residual by Predicted Plot
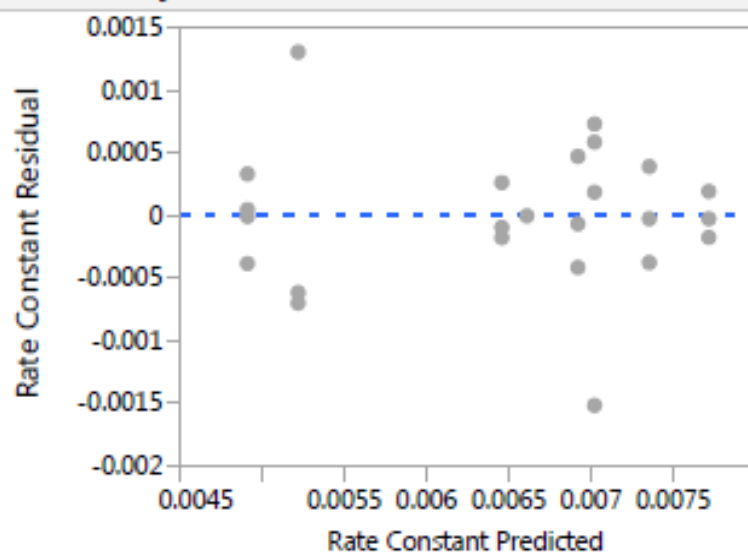
Swirl
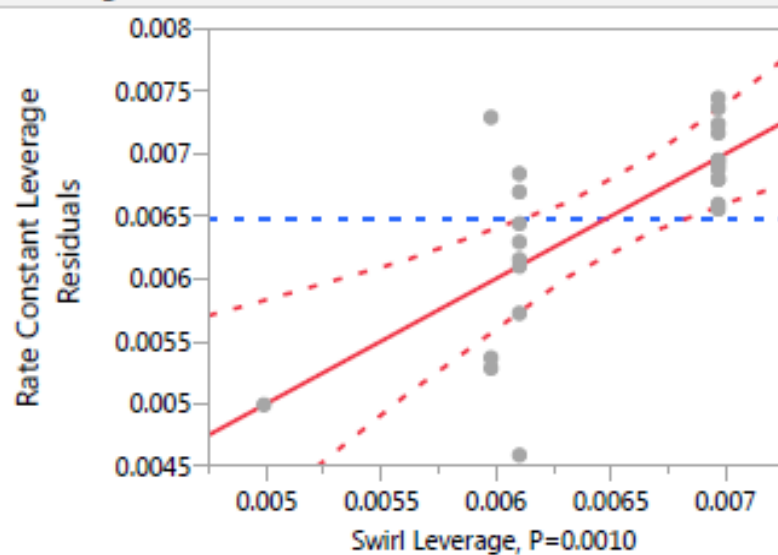
Leverage Plot

Least Squares Means Table

Level	Least Sq Mean	Std Error	Mean
0	0.00593940	0.00022238	0.005832
1	0.00711117	0.00018964	0.007111

Response Rate Constant
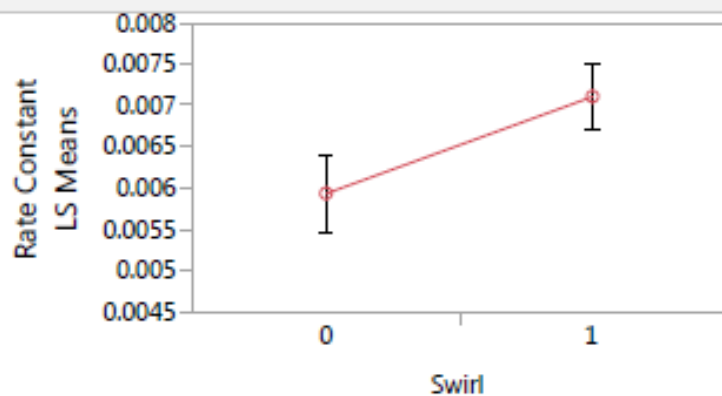
Swirl

LS Means Plot

Swirl

Reactor Type

Leverage Plot
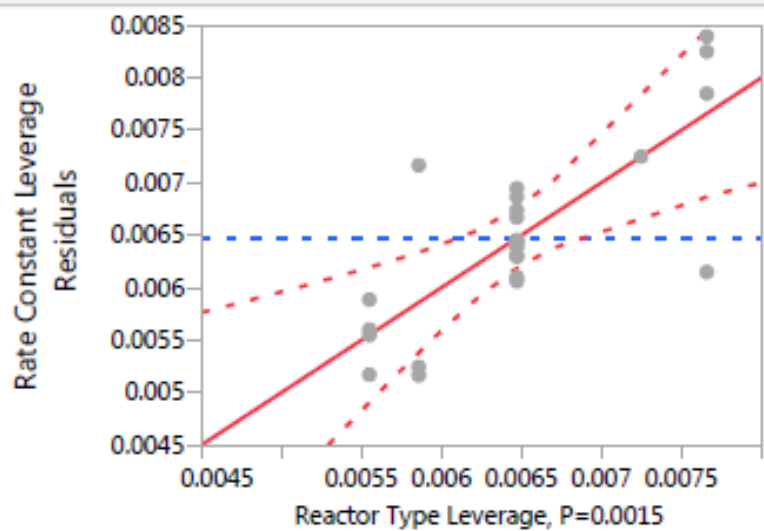
Least Squares Means Table

Level	Least Sq Mean	Std Error	Mean
Med	0.00702000	0.00032847	0.007318
Steel	0.00521833	0.00037929	0.005837
Thick	0.00660900	0.00065695	0.007167
Thin	0.00491025	0.00032847	0.005771

Response Rate Constant

Reactor Type

LS Means Plot
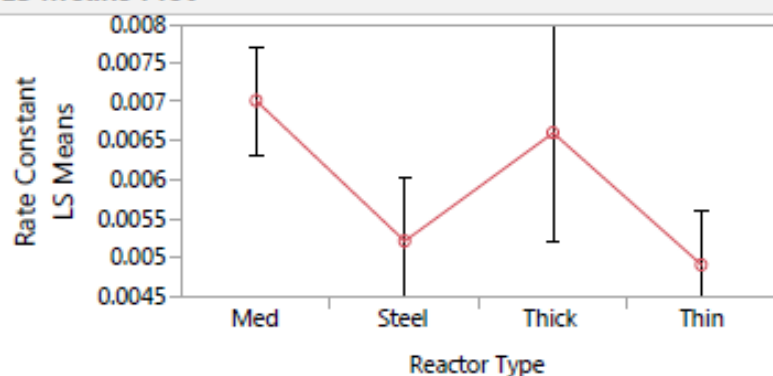
LSMeans Differences Tukey HSD

α= 0.050   Q= 2.86102

	LSMean[j]			
Mean[i]-Mean[j]	Med	Steel	Thick	Thin
Std Err Dif				
Lower CL Dif				
Upper CL Dif				
Med	0	0.0018	0.00041	0.00211
	0	0.0005	0.00073	0.00046
	0	0.00037	-0.0017	0.00078
	0	0.00324	0.00251	0.00344
Steel	-0.0018	0	-0.0014	0.00031
	0.0005	0	0.00076	0.0005
	-0.0032	0	-0.0036	-0.0011
	-0.0004	0	0.00078	0.00174
Thick	-0.0004	0.00139	0	0.0017
	0.00073	0.00076	0	0.00073
	-0.0025	-0.0008	0	-0.0004
	0.00169	0.00356	0	0.0038
Thin	-0.0021	-0.0003	-0.0017	0
	0.00046	0.0005	0.00073	0
	-0.0034	-0.0017	-0.0038	0
	-0.0008	0.00113	0.0004	0

Level		Least Sq Mean
Med	A	0.00702000
Thick	A B	0.00660900
Steel	B	0.00521833
Thin	B	0.00491025

Levels not connected by same letter are significantly different.

Swirl*Reactor Type

Response Rate Constant

Swirl*Reactor Type

Leverage Plot
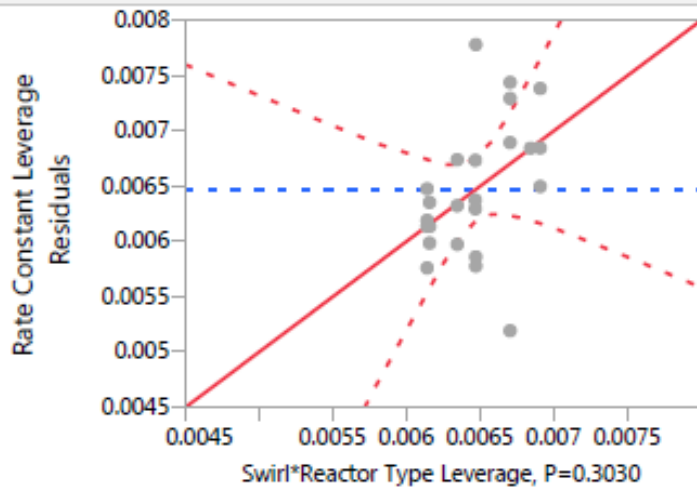
Least Squares Means Table

Level	Least Sq Mean	Std Error
0,Med	0.00702000	0.00032847
0,Steel	0.00521833	0.00037929
0,Thick	0.00660900	0.00065695
0,Thin	0.00491025	0.00032847
1,Med	0.00771567	0.00037929
1,Steel	0.00645633	0.00037929
1,Thick	0.00735300	0.00037929
1,Thin	0.00691967	0.00037929

LS Means Plot

LSMeans Differences Tukey HSD

α= 0.050   Q= 3.46215

Response Rate Constant

Swirl*Reactor Type

LSMeans Differences Tukey HSD

			LSMean[j]					
Mean[i]-Mean[j] Std Err Dif Lower CL Dif Upper CL Dif	0,Med	0,Steel	0,Thick	0,Thin	1,Med	1,Steel	1,Thick	1,Thin
0,Med	0	0.0018	0.00041	0.00211	-0.0007	0.00056	-0.0003	0.0001
	0	0.0005	0.00073	0.00046	0.0005	0.0005	0.0005	0.0005
	0	6.45e-5	-0.0021	0.0005	-0.0024	-0.0012	-0.0021	-0.0016
	0	0.00354	0.00295	0.00372	0.00104	0.0023	0.0014	0.00184
0,Steel	-0.0018	0	-0.0014	0.00031	-0.0025	-0.0012	-0.0021	-0.0017
	0.0005	0	0.00076	0.0005	0.00054	0.00054	0.00054	0.00054
	-0.0035	0	-0.004	-0.0014	-0.0044	-0.0031	-0.004	-0.0036
	-0.0001	0	0.00124	0.00205	-0.0006	0.00062	-0.0003	0.00016
0,Thick	-0.0004	0.00139	0	0.0017	-0.0011	0.00015	-0.0007	-0.0003
	0.00073	0.00076	0	0.00073	0.00076	0.00076	0.00076	0.00076
	-0.003	-0.0012	0	-0.0008	-0.0037	-0.0025	-0.0034	-0.0029
	0.00213	0.00402	0	0.00424	0.00152	0.00278	0.00188	0.00232
0,Thin	-0.0021	-0.0003	-0.0017	0	-0.0028	-0.0015	-0.0024	-0.002
	0.00046	0.0005	0.00073	0	0.0005	0.0005	0.0005	0.0005
	-0.0037	-0.002	-0.0042	0	-0.0045	-0.0033	-0.0042	-0.0037
	-0.0005	0.00143	0.00084	0	-0.0011	0.00019	-0.0007	-0.0003
1,Med	0.0007	0.0025	0.00111	0.00281	0	0.00126	0.00036	0.0008
	0.0005	0.00054	0.00076	0.0005	0	0.00054	0.00054	0.00054
	-0.001	0.00064	-0.0015	0.00107	0	-0.0006	-0.0015	-0.0011
	0.00243	0.00435	0.00373	0.00454	0	0.00312	0.00222	0.00265
1,Steel	-0.0006	0.00124	-0.0002	0.00155	-0.0013	0	-0.0009	-0.0005
	0.0005	0.00054	0.00076	0.0005	0.00054	0	0.00054	0.00054
	-0.0023	-0.0006	-0.0028	-0.0002	-0.0031	0	-0.0028	-0.0023
	0.00117	0.0031	0.00247	0.00328	0.0006	0	0.00096	0.00139
1,Thick	0.00033	0.00213	0.00074	0.00244	-0.0004	0.0009	0	0.00043
	0.0005	0.00054	0.00076	0.0005	0.00054	0.00054	0	0.00054
	-0.0014	0.00028	-0.0019	0.00071	-0.0022	-0.001	0	-0.0014
	0.00207	0.00399	0.00337	0.00418	0.00149	0.00275	0	0.00229
1,Thin	-0.0001	0.0017	0.00031	0.00201	-0.0008	0.00046	-0.0004	0
	0.0005	0.00054	0.00076	0.0005	0.00054	0.00054	0.00054	0
	-0.0018	-0.0002	-0.0023	0.00027	-0.0027	-0.0014	-0.0023	0
	0.00164	0.00356	0.00294	0.00375	0.00106	0.00232	0.00142	0

Response Rate Constant

Swirl*Reactor Type

LSMeans Differences Tukey HSD

Level				Least Sq Mean
1,Med	A			0.00771567
1,Thick	A			0.00735300
0,Med	A			0.00702000
1,Thin	A	B		0.00691967
0,Thick	A	B	C	0.00660900
1,Steel	A	B	C	0.00645633
0,Steel		B	C	0.00521833
0,Thin			C	0.00491025

Levels not connected by same letter are significantly different.

Response Rate Constant

Whole Model

Actual by Predicted Plot

Rate Constant Predicted P=0.0409 RSq=0.55
RMSE=0.0027
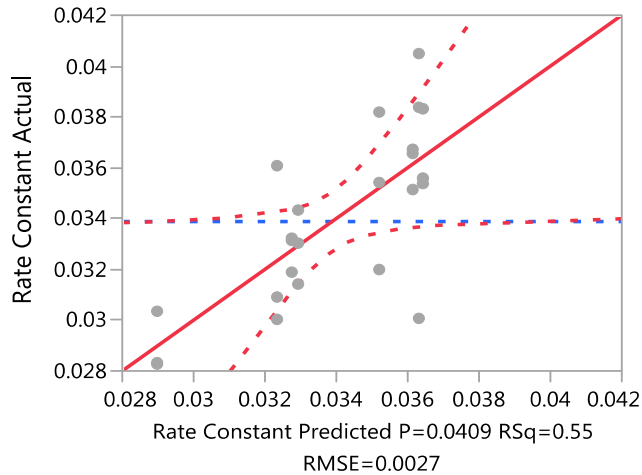
Summary of Fit

RSquare	0.551977
RSquare Adj	0.355967
Root Mean Square Error	0.002698
Mean of Response	0.033885
Observations (or Sum Wgts)	24

Analysis of Variance

Source	DF	Sum of Squares	Mean Square	F Ratio
Model	7	0.00014347	0.000020	2.8161
Error	16	0.00011645	7.278e-6	Prob > F
C. Total	23	0.00025992		0.0409*

Parameter Estimates

Term	Estimate	Std Error	t Ratio	Prob>|t|
Intercept	0.03507	0.000779	45.03	<.0001*
Swirl[1-0]	-0.002371	0.001101	-2.15	0.0470*
Reactor Type[Med]	0.0013567	0.001349	1.01	0.3295
Reactor Type[Steel]	0.00013	0.001349	0.10	0.9244
Reactor Type[Thick]	-0.00273	0.001349	-2.02	0.0600
Swirl[1-0]*Reactor Type[Med]	-0.001306	0.001908	-0.68	0.5034
Swirl[1-0]*Reactor Type[Steel]	0.0000975	0.001908	0.05	0.9599
Swirl[1-0]*Reactor Type[Thick]	0.0061708	0.001908	3.23	0.0052*

Effect Tests

Source	Nparm	DF	Sum of Squares	F Ratio	Prob > F
Swirl	1	1	0.00003373	4.6337	0.0470*
Reactor Type	3	3	0.00003257	1.4916	0.2547
Swirl*Reactor Type	3	3	0.00009663	4.4256	0.0190*

Response Rate Constant

Whole Model

Residual by Predicted Plot
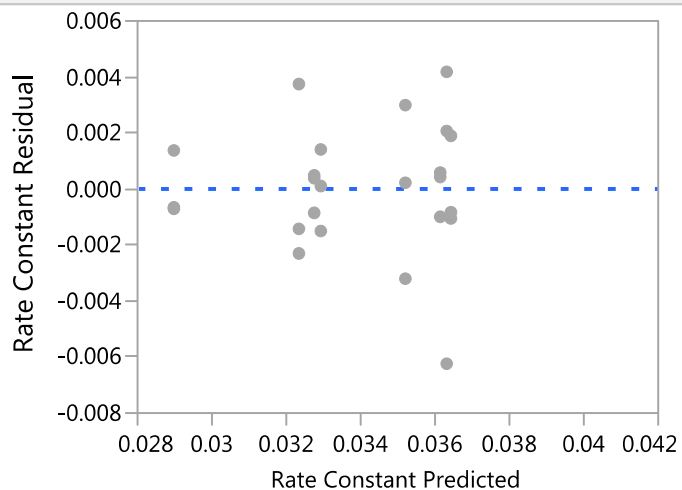
Swirl
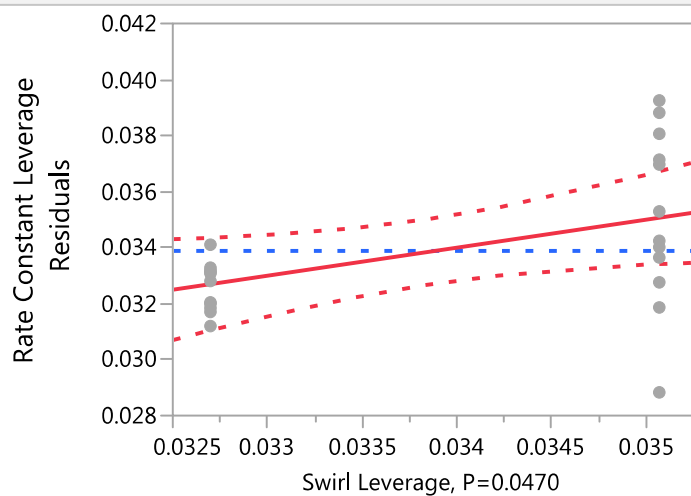
Leverage Plot

Least Squares Means Table

Level	Least Sq Mean	Std Error	Mean
0	0.03507000	0.00077879	0.035070
1	0.03269917	0.00077879	0.032699

Response Rate Constant
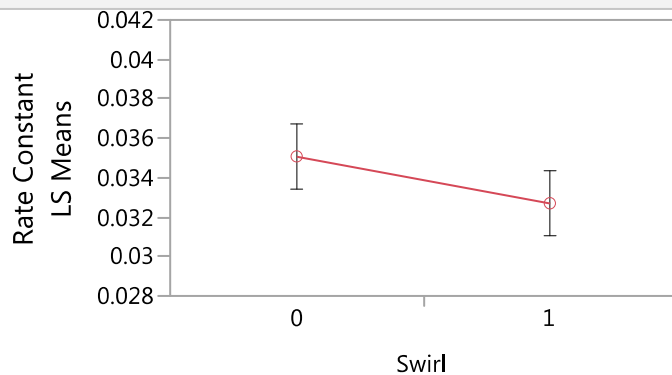
Swirl

LS Means Plot

Reactor Type

Leverage Plot
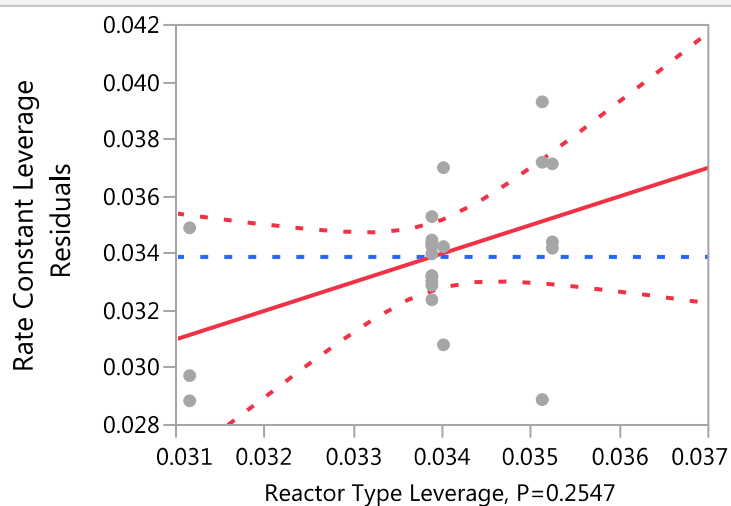
Least Squares Means Table

Level	Least Sq Mean	Std Error	Mean
Med	0.03642667	0.00155758	0.034588
Steel	0.03520000	0.00155758	0.034063
Thick	0.03234000	0.00155758	0.034240
Thin	0.03631333	0.00155758	0.032647

Response Rate Constant

Reactor Type

LS Means Plot

LSMeans Differences Tukey HSD

α= 0.050   Q= 2.86102

LSMean[j]

Mean[i]-Mean[j] Std Err Dif Lower CL Dif Upper CL Dif	Med	Steel	Thick	Thin
Med	0	0.00123	0.00409	0.00011
	0	0.0022	0.0022	0.0022
	0	-0.0051	-0.0022	-0.0062
	0	0.00753	0.01039	0.00642
Steel	-0.0012	0	0.00286	-0.0011
	0.0022	0	0.0022	0.0022
	-0.0075	0	-0.0034	-0.0074
	0.00508	0	0.00916	0.00519
Thick	-0.0041	-0.0029	0	-0.004
	0.0022	0.0022	0	0.0022
	-0.0104	-0.0092	0	-0.0103
	0.00222	0.00344	0	0.00233
Thin	-0.0001	0.00111	0.00397	0
	0.0022	0.0022	0.0022	0
	-0.0064	-0.0052	-0.0023	0
	0.00619	0.00742	0.01028	0

Level		Least Sq Mean
Med	A	0.03642667
Thin	A	0.03631333
Steel	A	0.03520000
Thick	A	0.03234000

Levels not connected by same letter are significantly different.

Response Rate Constant

Swirl*Reactor Type

Leverage Plot

Swirl*Reactor Type Leverage, P=0.0190
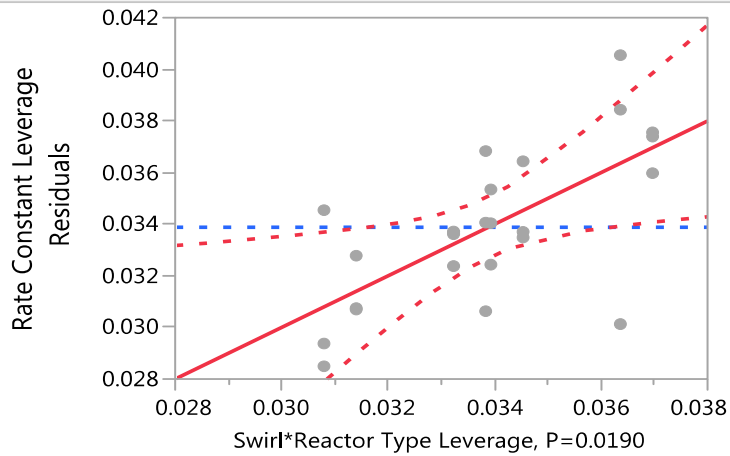
Least Squares Means Table

Level	Least Sq Mean	Std Error
0,Med	0.03642667	0.00155758
0,Steel	0.03520000	0.00155758
0,Thick	0.03234000	0.00155758
0,Thin	0.03631333	0.00155758
1,Med	0.03275000	0.00155758
1,Steel	0.03292667	0.00155758
1,Thick	0.03614000	0.00155758
1,Thin	0.02898000	0.00155758

LS Means Plot

LSMeans Differences Tukey HSD

α= 0.050   Q= 3.46215

Response Rate Constant

Swirl*Reactor Type

LSMeans Differences Tukey HSD

				LSMean[j]				
Mean[i]-Mean[j] Std Err Dif Lower CL Dif Upper CL Dif	0,Med	0,Steel	0,Thick	0,Thin	1,Med	1,Steel	1,Thick	1,Thin
0,Med	0	0.00123	0.00409	0.00011	0.00368	0.0035	0.00029	0.00745
	0	0.0022	0.0022	0.0022	0.0022	0.0022	0.0022	0.0022
	0	-0.0064	-0.0035	-0.0075	-0.0039	-0.0041	-0.0073	-0.0002
	0	0.00885	0.01171	0.00774	0.0113	0.01113	0.00791	0.01507
0,Steel	-0.0012	0	0.00286	-0.0011	0.00245	0.00227	-0.0009	0.00622
	0.0022	0	0.0022	0.0022	0.0022	0.0022	0.0022	0.0022
	-0.0089	0	-0.0048	-0.0087	-0.0052	-0.0054	-0.0086	-0.0014
	0.0064	0	0.01049	0.00651	0.01008	0.0099	0.00669	0.01385
0,Thick	-0.0041	-0.0029	0	-0.004	-0.0004	-0.0006	-0.0038	0.00336
	0.0022	0.0022	0	0.0022	0.0022	0.0022	0.0022	0.0022
	-0.0117	-0.0105	0	-0.0116	-0.008	-0.0082	-0.0114	-0.0043
	0.00354	0.00477	0	0.00365	0.00722	0.00704	0.00383	0.01099
0,Thin	-0.0001	0.00111	0.00397	0	0.00356	0.00339	0.00017	0.00733
	0.0022	0.0022	0.0022	0	0.0022	0.0022	0.0022	0.0022
	-0.0077	-0.0065	-0.0037	0	-0.0041	-0.0042	-0.0075	-0.0003
	0.00751	0.00874	0.0116	0	0.01119	0.01101	0.0078	0.01496
1,Med	-0.0037	-0.0024	0.00041	-0.0036	0	-0.0002	-0.0034	0.00377
	0.0022	0.0022	0.0022	0.0022	0	0.0022	0.0022	0.0022
	-0.0113	-0.0101	-0.0072	-0.0112	0	-0.0078	-0.011	-0.0039
	0.00395	0.00518	0.00804	0.00406	0	0.00745	0.00424	0.0114
1,Steel	-0.0035	-0.0023	0.00059	-0.0034	0.00018	0	-0.0032	0.00395
	0.0022	0.0022	0.0022	0.0022	0.0022	0	0.0022	0.0022
	-0.0111	-0.0099	-0.007	-0.011	-0.0074	0	-0.0108	-0.0037
	0.00413	0.00535	0.00821	0.00424	0.0078	0	0.00441	0.01157
1,Thick	-0.0003	0.00094	0.0038	-0.0002	0.00339	0.00321	0	0.00716
	0.0022	0.0022	0.0022	0.0022	0.0022	0.0022	0	0.0022
	-0.0079	-0.0067	-0.0038	-0.0078	-0.0042	-0.0044	0	-0.0005
	0.00734	0.00857	0.01143	0.00745	0.01102	0.01084	0	0.01479
1,Thin	-0.0074	-0.0062	-0.0034	-0.0073	-0.0038	-0.0039	-0.0072	0
	0.0022	0.0022	0.0022	0.0022	0.0022	0.0022	0.0022	0
	-0.0151	-0.0138	-0.011	-0.015	-0.0114	-0.0116	-0.0148	0
	0.00018	0.00141	0.00427	0.00029	0.00386	0.00368	0.00047	0

Level		Least Sq Mean
0,Med	A	0.03642667
0,Thin	A	0.03631333
1,Thick	A	0.03614000
0,Steel	A	0.03520000
1,Steel	A	0.03292667
1,Med	A	0.03275000
0,Thick	A	0.03234000
1,Thin	A	0.02898000

Levels not connected by same letter are significantly different.

Bibliography

Bates, Christopher. "Ultra Violet Light Emitting Diode Optical Power Characterization." Air Force Institute of Technology, 2014

Bennett, A. (2008). Drinking water: Pathogen removal from water–technologies and techniques. Filtration & Separation, 45(10), 14-16.

Block, S. S. (2001). *Disinfection, Sterilization, and Preservation*. Lippincott Williams & Wilkins.

Bowker, C., Sain, A., Shatalov, M., & Ducoste, J. (2011). Microbial UV fluence-response assessment using a novel UV-LED collimated beam system. *Water research*, *45*(5).

CamelBak | ALL CLEAR UV Microbiological Water Purification Device. (2010). Retrieved October 14, 2015, from http://shop.camelbak.com/all-clear-bottle/d/1208

Cargill, K. L., Pyle, B. H., Sauer, R. L., & McFeters, G. A. (1992). Effects of culture conditions and biofilm formation on the iodine susceptibility of Legionella pneumophila. *Canadian Journal of Microbiology*, *38*(5), 423-429.

CAWST Biosand Filter Construction Manual | WASH Education and Training Resources. (2012). Retrieved December 8, 2015, from http://resources.cawst.org/package/biosand-filter-construction-manual_en

Chatterly, C. and Linden, K. (2010). "Demonstration and evaluation of germicidal UV-LEDs for point-of-use water disinfection." *J. Water Health, 8(3), 479-486.*

Chlorine Disinfection Timetable - Pools & Hot Tubs - Healthy Swimming & Recreational Water - Healthy Water |CDC (2010). Retrieved October 5, 2015, from http://www.cdc.gov/healthywater/swimming/pools/chlorine-disinfection-timetable.html

COMSOL®, Multiphysics Cyclopedia. (2015). Retrieved February 02, 2016, from https://www.comsol.com/multiphysics/navier-stokes-equations

Coblentz, W.W., & Stair. (1929) Reflecting power of beryllium, chromium, and several other metals. *Bureau of Standards Research Paper, 39, 12.*

Curtis, R. (1998, March). The Backpacker's Field Manual. Retrieved from http://www.princeton.edu/~oa/manual/index.html

Disinfection By-Products | The Safe Water System | CDC. (2014). Retrieved October 14, 2015, from http://www.cdc.gov/safewater/chlorination-byproducts.html#four

Duckworth, K. L. (2014). *Ultraviolet light emitting diode use in advanced oxidation processes*. Air Force Institute of Technology

Downes A, Blunt TP. (1877)"The influence of light upon the development of bacteria". Nature; 16:218.

Edberg, S. C., Rice, E. W., Karlin, R. J., & Allen, M. J. (2000). Escherichia coli: the best biological drinking water indicator for public health protection. *Symposium Series (Society for Applied Microbiology)*, (29), 106S–116S.

Fyda, S. Godby, N. Almquist, C. Harper, W. Miller, M. (2015). Investigation of the Use of Ultraviolet Light Emitting Diodes in Water Treatment Systems. Air Force Institute of Technology

Haitz's law. (2007). *Nature Photonics*, *1*(1), 23–23. http://doi.org/10.1038/nphoton.2006.78

Holonyak Jr, N., & Bevacqua, S. F. (1962). Coherent (visible) light emission from Ga (As1−xPx) junctions. *Applied Physics Letters*, *1*(4), 82-83.

Jenny, R. M., Jasper, M. N., Simmons, O. D., Shatalov, M., & Ducoste, J. J. (2015). Heuristic optimization of a continuous flow point-of-use UV-LED disinfection reactor using computational fluid dynamics. *Water research*, *83*, 310-318.

Kovac, J., Peternai, L., & Lengyel, O. (2003). Advanced light emitting diodes structures for optoelectronic applications. *Thin Solid Films*, *433*(1), 22–26.

Lara, H. H., Ayala-Nuñez, N. V., Ixtepan-Turrent, L., & Rodriguez-Padilla, C. (2010). Mode of antiviral action of silver nanoparticles against HIV-1. *Journal of Nanobiotechnology*, *8*, 1. http://doi.org/10.1186/1477-3155-8-1

LG Innotek. (n.d). UV LED - LED – Products. Retrieved August 20, 2015, from http://www.lginnotek.com/products/led_uvled.jsp

Linden, K. G. (1998). UV acceptance. *Civil Engineering*, *68*(3), 58.

Lorch, W. 1987. Handbook of Water Purification 2nd Edition. Ellis Horwood Limited, Chichester, United Kingdom.

Mudimbi, P. M. (2015). Pulsed Ultraviolet Light Emitting Diodes for Advanced Oxidation of Tartrazine. Air Force Institute of Technology.

Murakami, K., Taguchi, T., & Yoshino, M. (2000, June). White illumination characteristics of ZnS-based phosphor materials excited by InGaN-based ultraviolet light-emitting diode. In *Photonics Taiwan* (pp. 112-119). International Society for Optics and Photonics.

Muramoto, Yoshihiko, Masahiro Kimura, and Suguru Nouda. "Development and future of ultraviolet light-emitting diodes: UV-LED will replace the UV lamp." *Semiconductor Science and Technology* 29.8 (2014): 84004-84011.

Nakamura, S., Mukai, T., & Senoh, M. (1994). Candela-class high-brightness InGaN/AlGaN double-heterostructure blue-light-emitting diodes. *Applied Physics Letters*, *64*(13), 1687–1689.

New York Department of Health, Center for Environmental Health. . "Boil Water Response-Information for the Public Health Professional". (2011, August). Retrieved from https://www.health.ny.gov/environmental/water/drinking/boilwater/response_information_public_health_professional.htm

Percival, Steven L., Marylynn V. Yates, David Williams, Rachel Chalmers, and Nicholas Gray. *Microbiology of Waterborne Diseases: Microbiological Aspects and Risks*. Academic Press, 2013.

Pontius, F. (2003). *Drinking Water Regulation and Health*. John Wiley & Sons.

Richwine, J. P. (2014) Modeling Ultraviolet Light Emitting Diode Energy Propigation in Reactor Vessels. Air Force Institute of Technology

Rook JJ. Formation of haloforms during chlorination of natural waters. Water Treatment Examination. 1974; 23:234-243.

Ryer, A., & Light, V. (1997). Light measurement handbook.

Scott, R.W. (2015). The Use of Ultra-Violet Light Emitting Diodes in an Advanced Oxidation Process With Brilliant Blue FCF as an Indicator. Air Force Institute of Technology

Shao, F. (2014). Toxicity of silver nanoparticles on virus. *J Mater Environ. Sci*, *5*(2), 587-590.

Tuncel, A. T., Ruppert, T., Wang, B.-T., Okun, J. G., Kölker, S., Morath, M. A., & Sauer, S. W. (2015). Maleic Acid – but Not Structurally Related Methylmalonic Acid – Interrupts Energy Metabolism by Impaired Calcium Homeostasis. *PLOS ONE*, *10*(6), e0128770. http://doi.org/10.1371/journal.pone.0128770

TB MED 577, Sanitary Control and Surveillance of Field Water Supplies, May 2010

Slow Sand Filtration | The Safe Water System | CDC. (2014) Retrieved December 8, 2015, from http://www.cdc.gov/safewater/sand-filtration.html

Spencer, M. J. (2014). *Design considerations for a water treatment system utilizing ultra-violet light emitting diodes*. Air Force Institute of Technology

Teng, W., Shan, Z., Teng, X., Guan, H., Li, Y., Teng, D., … Li, C. (2006). Effect of iodine intake on thyroid diseases in China. *The New England Journal of Medicine*, *354*(26), 2783–2793. http://doi.org/10.1056/NEJMoa054022

Tran, Tho. "Comparison of Continuous Versus Pulsed Ultraviolet Light Emitting Diode Use in Water Disinfection on Bacillus Globigii Spores." Draft. Air Force Institute of Technology, 2014.

WATER IS LIFE. (2014). Drinkable Book. Retrieved October 20, 2015, from http://www.waterislife.com/clean-water/new-technology?gclid=Cj0KEQjwqZKxBRDBkNmLt9DejNgBEiQAq8XWPgJRGCK3aas9t47oxUy11AEsEdBoztP9I5m2nSt-ZSwaAueH8P8HAQ

Weidner, V. R., & Hsia, J. J. (1981). Reflection properties of pressed polytetrafluoroethylene powder. *JOSA*, *71*(7), 856-861.

Whitby, G. E., & Scheible, O. K. (2004). The history of UV and wastewater. *IUVA News*, *6*(3), 15–26.

World Health Organization (Ed.). (2011). *Guidelines for drinking-water quality* (4th ed). Geneva: World Health Organization.

Vestergaard, 2014. About Lifestraw®. Retrieved from http://www.buylifestraw.com/en/about

US EPA, O. (n.d.). Revised Total Coliform Rule And Total Coliform Rule [Policies and Guidance]. Retrieved January 29, 2016, from http://www.epa.gov/dwreginfo/revised-total-coliform-rule-and-total-coliform-rule

US. EPA. Office of Water. Ultraviolet Disinfection Guidance Manual for the Final Long Term 2 Enhanced Surface Water Treatment Rule. Washington, DC: U.S. Environmental Protection Agency, Office of Water, 2006. EPA 815-R-06-007. Nov. 2006

US. EPA Water Treatability Database. (2015). Retrieved December 10, 2015, from http://iaspub.epa.gov/tdb/pages/treatment/treatmentOverview.do

1. REPORT DATE (DD-MM-YYYY) 24-03-2016	2. REPORT TYPE Master's Thesis	3. DATES COVERED (From – To) October 2014 – March 2016
TITLE AND SUBTITLE Material and Design Considerations for a Portable Ultra-Violet (UV) Light Emitting Diode (LED) Water Purification Device		**5a. CONTRACT NUMBER**
		5b. GRANT NUMBER
		5c. PROGRAM ELEMENT NUMBER
6. AUTHOR (S) Gallucci, Drew D., Captain, USAF		**5d. PROJECT NUMBER**
		5e. TASK NUMBER
		5f. WORK UNIT NUMBER
7. PERFORMING ORGANIZATION NAMES (S) AND ADDRESS (S) Air Force Institute of Technology Graduate School of Engineering and Management (AFIT/ENY) 2950 Hobson Way, Building 640 WPAFB OH 45433-8865		**8. PERFORMING ORGANIZATION REPORT NUMBER** AFIT-ENV-16-M-152
9. SPONSORING/MONITORING AGENCY NAME (S) AND ADDRESS (ES) US Environmental Protection Agency 25 W. Martin Luther King Dr. Mailstop NG-16 Cincinnati, OH 45268 Matthew Magnuson, (513) 569-7321, magnuson.matthew@epa.gov		**10. SPONSOR/MONITOR'S ACRONYM (S)** US EPA/NHSRC
		11. SPONSOR/MONITOR'S REPORT NUMBER (S)

12. DISTRIBUTION/AVAILABILITY STATEMENT DISTRUBTION STATEMENT A. APPROVED FOR PUBLIC RELEASE; DISTRIBUTION UNLIMITED.

13. SUPPLEMENTARY NOTES This material is declared a work of the U.S. Government and is not subject to copyright protection in the United States.

14. ABSTRACT

Department of Defense personnel deploy to austere environments where clean water is not readily available. Ultraviolet (UV) radiation through the use of light emitting diodes (LEDs) in a portable device offers a potential method for expedient water treatment. This research studied the application of one diode, low power, UV LEDs and nine diode, high power, UV LEDs within a portable steel reactor and Teflon reactors of three different wall thicknesses. Reactor efficiency was determined through measuring and comparing the rate constants for Advanced Oxidation of hydrogen peroxide with yellow Tartrazine as a witness dye. Experiments conducted with low power UV LEDs indicate that the medium thickness reactor has a statistically significant higher rate constant than the steel and thin cylinder reactors. All high power UV LED tests had rate constants ten times higher than the low UV LEDs, but exhibited no significant difference between materials or thicknesses. Additionally, this research examined the microorganism inactivation in the optimum reactor by exposing E. Coli to UV radiation. The experiments demonstrated complete reduction of E. Coli at a flow rate up to 15 mL/min, and a 2-Log reduction at 20 mL/min, thus demonstrating proof of concept for future portable UV LED disinfection units.

15. SUBJECT TERMS Ultra-Violet LED, Water Treatment, Chemical Decomposition, Advanced Oxidation

16. SECURITY CLASSIFICATION OF:			**17. LIMITATION OF ABSTRACT**	**18. NUMBER OF PAGES**	**19a. NAME OF RESPONSIBLE PERSON** Dr. Michael E. Miller, AFIT/ENV
a. REPORT U	**b. ABSTRACT** U	**c. THIS PAGE** U	UU	125	**19b. TELEPHONE NUMBER** (Include area code) (937) 785-3636, ext. 4651 (Michael.Miller@afit.edu)